Aus der Medizinischen Klinik und Poliklinik IV der Ludwig-Maximilians-Universität München

Direktor: Prof. Dr. med. Martin Reincke

Molecular mechanisms of tissue injury induced by crystalline particles of different sizes and shapes

Dissertation

zum Erwerb des Doktorgrades der Humanbiologie

an der Medizinischen Fakultät der

Ludwig-Maximilians-Universität zu München

vorgelegt von

Mohammad Mohsen Honarpisheh

aus Shiraz Iran

2020

Mit Genehmigung der Medizinischen Fakultät
der Ludwig-Maximilians-Universität München

Berichterstatter:	Prof. Dr. med. Hans-Joachim Anders
Mitberichterstatter:	Prof. Dr. rer. nat. kirsten Lauber
	Prof. Dr. Markus Rentsch
Mitbetreuung durch den promovierten Mitarbeiter:	Priv. Doz. Dr. Shrikant Ramesh Mulay
Dekan:	Prof. Dr. med. dent. Reinhard Hickel
Tag der mündlichen Prüfung:	16.10.2020

LMU LUDWIG-MAXIMILIANS-UNIVERSITÄT MÜNCHEN

Dean's Office
Faculty of Medicine

MWRS

Affidavit

Honarpisheh, Mohammad Mohsen

Surname, first name

Street

Zip code, town

Country

I hereby declare, that the submitted thesis entitled

Molecular mechanisms of tissue injury induced by crystalline particles of different sizes and shapes

is my own work. I have only used the sources indicated and have not made unauthorised use of services of a third party. Where the work of others has been quoted or reproduced, the source is always given.

I further declare that the submitted thesis or parts thereof have not been presented as part of an examination degree to any other university.

Munich, 22.10.2020

Place, date

Honarpisheh, Mohammad Mohsen

Signature doctoral candidate

Contents

List of Abbreviations

AKI	Acute kidney injury
ACMV	Apoptotic subcellular microvesicles
ASC	Apoptosis-associated speck-like protein containing a CARD
CaP	Calcium phosphate
CaOx	Calcium oxalate
CKD	Chronic kidney disease
COPD	Chronic obstructive pulmonary disease
CytD	Cytochalasin D
CsA	Cyclosporin A
CPPD	Calcium pyrophosphate dihydrate
CYPD	Cyclophilin D
DAMPs	Danger-associated molecular patterns
DISC	Death-inducing signaling complex
DCFDA	2',7'–dichlorofluorescin diacetate
2,8-DHA	2,8-dihydroxyadenine
ELISA	Enzyme-linked immunosorbent assay
FADD	Fas-associated protein with death domain
FACS	Fluorescence-activated cell sorting
FDA	Food and Drug Administration
GPX4	Glutathione peroxidase 4
GSDMD	Gasdermin-D
GSH	Glutathione
HA	Hydroxyapatite
IL-1β	Interleukin 1 beta
IL18	Interleukin 18

IFN	Interferon
IRI	Ischaemia-reperfusion injury
LPS	Lipopolysaccharide
MLKL	Mixed lineage kinase domain-like
MPT-RN	Mitochondrial permeability transition-regulated necrosis
MOMP	Mitochondrial outer membrane permeabilization
MSU	Monosodium urate
MFI	Mean fluorescence intensity
Nec1	Necrostatin-1
NLRP3	NLR family pyrin domain containing 3
NSA	Necrosulphonamide
NFκB	Nuclear factor kappa-light-chain-enhancer of activated B cells
PM	Particulate matter
PARP1	Poly(ADP-Ribose) Polymerase 1
PAS	Periodic acid–schiff
PPIF	Peptidylprolyl isomerase F
pTECs	Primary tubular epithelial cells
PAS	Periodic acid-Schiff
PI	Propidium iodide
ROS	Reactive oxygen species
RIPK1/3	Receptor-interacting serine/threonine-protein kinase 1/3
SMA	Smooth muscle actin
TNF	Tumor necrosis factor
TRADD	TNF receptor-associated death domain
TNFR1/2	Tumor necrosis factor receptor 1/2
TiO2	Titanium dioxide
TAK1	Transforming growth factor-β-activated kinase 1

TLR	Toll-like receptor
TMRE	Tetramethylrhodamine ethyl ester
VDAC	Voltage-dependent anion channels
WHO	World health organization

1. Introduction

1.1. Crystallopathies

Deposits of crystals in the body can lead to tissue injury and even organ failure. The term crystals refers to solid materials composed of atoms, molecules, or irons. However, in living organisms, the formation of crystals can also result in aggregation of atoms and ions, which in turn can built more complex structures like bones, teeth, and shells. Sometimes the formation of crystals could lead to injury. For instance, crystals sticking together can form poly-crystalline masses up to calculi, leading to kidney damage. The supersaturation of calcium oxalate (CaOx) or calcium phosphate (CaP) inside the tubular compartment of the kidney can result in the formation of kidney stone, which manifest as nephrocalcinosis tubular injury and chronic kidney disease (CKD) (Table 1).[4] Many studies have shown an increase in the prevalence and incidence of nephrolithiasis over the last several decades. Kidney stones disease affects all populations, with a prevalence of around 15% worldwide.[5] The aggregation of cholesterol crystals inside arteries' walls can form a plaque resulting in atherosclerosis and cardiovascular diseases.[6] The clinical manifestations involve ischemic stroke, myocardial infarction, cholesterol embolism, and peripheral arterial disease.[7] The mortality rate of cardiovascular diseases is 17.9 million each year [8], according to World Health Organization (WHO). Smoking is the most significant risk for chronic obstructive pulmonary disease (COPD). Smoking a cigarette exposes the human respiratory tract to between 15,000 and 40,000 μg particulate matter (PM)[9], resulting in oxidative stress and tissue injury. Cigarette smoking is considered as air pollution and responsible for 480,000 deaths per year in the United States, according to the WHO. In addition, other environmental and occupational air pollutions are associated with PM exposure to the human body. For example, silicosis is an occupational lung disease, which is caused by inhalation of crystalline silica particles leading to lung injury. Coal workers' pneumoconiosis is associated with prolonged exposure to the coal dust, diesel exhaust particulate matters are composed of carbonaceous combustion could increase the risk of lung cancer [10], and burning of biomass is associated with an acute respiratory infections.[11] According to the Nations Environment Programme (UNEP) web site, outdoor air pollution is responsible for 25% of all deaths, disease from lung cancer is 17% of all deaths, disease from an acute lower respiratory infection is 16% of all deaths, disease from stroke 15% of all deaths, and disease from ischaemic heart disease 8% of all deaths and disease from chronic obstructive pulmonary disease.[12] A study describes that inhaling particulate air pollution could result in

brain tissue damage in children.[13] According to the WHO air quality database, 97% of cities in low-and middle-income countries with a population of more than 100,000 do not meet the air quality guidelines. For example, Delhi, India, and Cairo, Egypt have the worst PM10 pollution levels. Also, Argentina, Brazil, China, Mexico, and Turkey are in the top ten list of the most-polluted countries. The air pollution in Tehran (the capital city of Iran) and Shiraz (one of the big cities in Iran) is above the threshold provided by the WHO air quality guidelines and are thought to cause 28,079 deaths per year in both cities. Therefore, there is an urgent medical need to find better therapies for crystal-related diseases. This requires to first identifying the molecular mechanisms of crystal or crystalline particle-related diseases. The crystal-related diseases can be found in table 1.

1.1.1. Crystal or crystalline particles related to kidney diseases

The deposition of crystalline particles into the kidney can be divided into three types. Cholesterol crystals deposit into renal vascular or vascular calcification (Type 1), deposition of crystalline particles such as CaP, myoglobin, and cysteine inside or outside of tubular cells lead to tubular injury (Type 2) and deposition of crystal particles like CaOx and MSU into ureter cause urolithiasis or kidney stones (Type 3).[14] Type 1 crystalline nephropathy is associated with renal cholesterol embolism.[14] The source of cholesterol crystals are atherosclerotic plaques, which can rupture spontaneously upon trauma or during anticoagulation therapy.[15] Different organs can be affected by cholesterol embolism such as the kidneys, gastrointestinal tract, skin, skeletal muscles, and brain.[14,15] Cholesterol crystals can directly induce cell death in renal epithelial tubular cells by activating RIPK3 and MLKL.[16,1] In addition, they can trigger inflammation. For example, macrophages take up cholesterol crystals and activate the NLRP3 inflammasome, which leads to the release of IL-1β and other cytokines. Type 2 crystalline nephropathy mainly relates to tubular injury, which can present as acute kidney injury (AKI) or CKD. AKI is a result of acute supersaturation, which induces a sudden crystal formation leading to acute crystal-induced tubular cell injury, inflammation, and kidney failure.[14] However, mild supersaturation can cause crystal formation over long periods, which can result in tissue remodelling, tubule obstruction, and CKD. For instance, in monoclonal gammopathies, the immunoglobulin light chains form crystals in the lumen of the proximal tubules depending on their physicochemical properties.[17]

Table 1: Crystal or crystalline particle-related diseases

Crystalline particles	Disorder	Clinical manifestation
Intrinsic inorganic crystals		
Brushite	Cholecystolithiasis/docholithiasis	Renal colic
Calcium carbonate	Cholecystolithiasis/docholithiasis Nephrolithiasis/urolithiasis	Biliary colic Renal colic
Calcium-oxalate monohydrate (whewellite)/ Calcium-oxalate dihydrate (weddellite)	Nephrolithiasis/urolithiasis Acute oxalate nephropathy Polyethelene glycol poisoning Dietary oxalosis: Black tea, star fruit, rhubarb, vitamin C, nuts Bariatric surgery-/short bowl-related Chronic oxalate nephropathy Primary hyperoxaluria	Renal colic Acute kidney injury Acute kidney injury Acute kidney injury, renal colic Acute kidney injury, renal colic Chronic kidney disease CKD, organ oxalosis
Calcium pyrophosphate /Calcium phosphate	Pseudogout, chondrocalcinosis, Hemochromatosis, hyperparathyroidism, Vascular calcification, calciphylaxis Warfarin calcification Dent`s disease, Nephrocalcinosis	Acute monarthritis, periarthritis, bursitis Tissue ischemia, ischemic necrosis Tissue ischemia, ischemic necrosis Nephrocalcinosis
Intrinsic organic crystals or microparticles		
Adenine	Adenine phosphoribosyltransferase deficiency	Nephrolithiasis/urolithiasis, renal colic, chronic kidney disease
Amyloid	Amyloid-β in Alzheimer disease Amylin in diabetes	Dementia Hyperglycemia
Bile pigment	Cholecysto-/docholithiasis Cholecysto-/docholithiasis	Biliary colic, pancreatitis Acute kidney injury
Cholesterol	Atherosclerosis Cholesterol embolism Nonalcoholic steatohepatitis Cholesteryl ester storage disease Cholesterol granuloma Cholecysto-/docholithiasis	Tissue ischemia, ischemic necrosis Ischemic necrosis Acute lipotoxic liver disease Chronic lipotoxic live disease Bone lesions Biliary colic
Cystine	Cystinosis	CKD, urolithiasis, extrarenal
Light chains	Myeloma cast nephropathy Crystalloglobulinemia Light chain Fanconi syndrome Crystal-storing histiocytosis Fibrillary glomerulonephritis Immunotactoid glomerulopathy	Acute kidney injury Thrombotic microangiopathy Renal tubulopathy, CKD Renal tubulopathy, CKD Proteinuria, CKD Proteinuria, CKD
MSU	Gout Nephrolithiasis or urolithiasis Urate nephropathy	Acute monoarthritis, bursitis, chronic tophous gout Renal colic Acute kidney injury
Myoglobin	Myoglobin cast nephropathy	Acute kidney injury
Uromodulin	Cast nephropathies	Acute kidney injury
Extrinsic crystals or particulates		
Asbestos	Lung asbestosis, malignancy	Pulmonary fibrosis, mesothelioma
Drugs(acyclovir,methotrexate, indinavir, sulfadiazine)	Drug-related kidney injury	Acute kidney injury, renal colic
Hemozoin	Malaria	Hemolysis, SIRS
Implants, implant debris particles	Implant-related injury	Monarthritis, aseptic osteolysis, foreign body reactions
Occupational dusts: silica, asbestos, cotton, charcoal…	Acute dust-induced lung injury Pneumoconiosis (silicosis, asbestosis, anthracosis)	Dust-induced respiratory failure Lung fibrosis
Tobacco smoke particulates	Smoking-related COPD, emphysema	Chronic respiratory distress
Air pollutants	Smog-related asthma, pneumonitis, COPD	Acute respiratory distress

CKD: chronic kidney disease, COPD: chronic obstructive pulmonary disease, SIRS: systemic inflammatory response syndrome. Adapted from Mulay, *et. al.*[4]

Deposition of β-sheets and amyloid fibrils can lead to nephrotic syndrome[17,18]. In contrast, during tumor lysis syndrome, uric acid is released from dying cells and MSU crystals deposit and obstruct the tubular lumen.[14]CKD is associated with genetic disorders, which often lead to the synthesis of different minerals such as brushite, CaCO3, CaOx, CaP, hydroxyapatite (HA), struvite uric acid and metabolites wherein the concentrations of such particles can reach supersaturation point leading to crystallization of crystalline particles.[14] A rare genetic disease with deficiency of adenine phosphoribosyl transferase leads to 2,8-dihydroxyadenine (2,8-DHA) nephropathy, where 2,8-DHA crystals form inside the renal tubules. An adenine-enriched diet leads to 2,8-DHA nephropathy in an animal model resulting in inflammation and kidney injury.[19] Crystalline CKD refers to nephrocalcinosis.

Type 3 crystalline nephropathy is associated with nephrolithiasis, ureterolithiasis or cystolithiasis. There are different factors involved in urolithiasis such as hereditary metabolic diseases related to higher production of cysteine, uric acid, or oxalate. Around 80% of all kidney stones are made of calcium stones.[20] Calcium stones consist of 50% of CaOx, 5% of CaP and 45% of a mixture of CaOx and CaP.[21,22] There are two types of CaOx crystals, CaOx monohydrate (COM, whewellite, $CaC_2O_4 \cdot H_2O$) and CaOx dihydrate (COD, weddellite, $CaC_2O_4 \cdot 2H_2O$).[23] Around 60% of the CaOx mixture account for both types.[23] However, CaOx monohydrate is more stable than CaOx dehydrates and COM is also more observed in patients.[22] Many factors are involved in CaOx stone formation, i.e., hypercystinuria, hypercalciuria, hyperoxaluria, hyperuricosuria, hypocitraturia, hypomagnesuria.[24] Clinical manifestations such as gouty arthritis and uric acid kidney stones are associated with hyperuricemia.[24] CaOx formation occurs mostly at a urinary pH of 5.0 to 6.5, while the urinary pH to form CaP stones is more than 7.[24] The prevalence of urolithiasis in the US population is 11%.[25] Moreover, mutations in the genome that encode for mineral or metabolite transporters proteins develop supersaturation of minerals or metabolites in the urine.[26] Another cause of urolithiasis is a diet rich in fructose or oxalate with low fluid intake, which can promote small crystals as well as stone formation.[27,28] Stones are normally present in the renal pelvis, which can cause obstructing urinary outflow leading to kidney injury.[25] Renal colic occurs as a result of sudden-onset pain in the flank or inguinal region.[29] Oliguria can be present if both urinary tracts are affected.[29] Elimination of the stone or stone passage decreases pressure and pain, and removal of such calculus can cause mucosal injury. However, renal colic is not related to long-term urinary tract dysfunction except that chronic obstruction causes obstructive nephropathy and nephron loss. The diseases associated with Type 1, 2 and 3 can be found in table 2.

Table 2: Crystal or crystalline-induced kidney diseases

Type	Renal damage	Disease	Crystal (source of crystal-forming factor)
Type 1 (vascular)	AKI CKD	Cholesterol embolism atherosclerotic renal artery stenosis	Cholesterol Cholesterol, apatite, CaP
Type 2 (tubular)	AKI	Diet-induced crystal nephropathy	CaOx monohydrate (whewellite) CaOx monohydrate (whewellite) CaP,CaOx, and vitamin C
		Drug-induced crystal nephropathy tumor lysis syndrome Drug-induced crystalluria Acute phosphate nephropathy	Uric acid Drug crystals CaP
		Enteric crystal nephropathy	CaOx monohydrate (whewellite) (bariatric surgery, IBD,celiac disease)
		Short bowel syndrome	CaOx dihydrate (weddellite)
		Myogen crystal nephropathy	Myoglobin (rhabdomyolysis)
		Bilirubin crystal nephropathy (bile cast nephropathy)	Bilirubin crystal nephropathy (bile cast nephropathy)
		Paraprotein-induced crystal nephropathy (light-chain cast nephropathy)	Monoclonal light chains
	CKD	CAKUT Genetic forms of RTA	Brushite, CaCO3, CaOx, CaP, hydroxyapatite, struvite
		Genetic forms of hyperuricosuria Primary hyperoxaluria	Uric acid CaOx monohydrate (whewellite), CaOx dehydrate (weddellite)
		Cystinosis APRT deficiency	Cystine Adenine
		Genetic diseases that cause nephrocalcinosis Dent disease, Lowe syndrome, idiopathic infantile Hypercalcemia and hypercalciuria	CaP, calcium pyrophosphate
		Diet- or drug-induced crystal nephropathy	Uric acid (diets rich in sodium, fructose, sucrose)
		Tophaceous gout	Uric acid (diets low in potassium, calcium, phytate, fluid administration as part of Mesoamerican nephropathy treatment)
		Immunoglobulin-induced crystal nephropathies light-chain cast nephropathy, proximal tubulopathy with or without Fanconi syndrome, crystalglobulinemia, crystal-storing histiocytosis	Monoclonal light chains
		Chronic glomerular crystal nephropathies Cryoglobulinemia Crystalglobulinemia Cystinosis	Monoclonal and polyclonal IgG Monoclonal light chains Cystine
Type 3 (urolithiasis)	Colic	Monogenic crystal nephropathies (CAKUT) Genetic forms of RTA	Brushite, CaCO3, CaOx, CaP, hydroxyapatite, struvite
		Primary hyperoxaluria	CaOx monohydrate (whewellite), CaOx dehydrate (weddellite)
		Cystinosis	

		APRT deficiency Genetic forms of hyperuricosuria and hypercalciuria	Cysteine Adenine Uric acid, CaOx, CaP
		diet- or drug-induced crystal nephropathy Hyperuricosuric syndromes Drug crystalluria	CaOx, CaP (diets rich in oxalate, sodium, fructose, vitamin C, sucrose; diets low in potassium, calcium, phytate) Uric acid Drug crystals
		Enteric oxalosis Short bowel syndrome	CaOx monohydrate (whewellite) CaOx dihydrate (weddellite) (bariatric surgery, IBD, celiac disease

AKI: acute kidney injury, **APRT**: adenine phosphoribosyl transferase, **CaCO3**: calcium carbonate, **CAKUT**: congenital anomalies of the kidney and the urinary tract, **CaOx**: calcium oxalate, **CaP**: calcium phosphate, **CKD**: chronic kidney disease, **IBD**: inflammatory bowel disease, **RTA**: renal tubular acidosis. Adapted from Mulay, *et. al.*[14]

1.1.2. Source of crystals

Crystallization can occur in different parts of the body.[4,30] MSU crystals are the result of the crystallization of uric acid within joints, presenting as gouty arthritis.[30] Kidney stone formation is due to the urinary supersaturation of calcium oxalate.[31] On the other hand, crystalline particles can enter the body from the outside. Silicosis is a work-related lung disease caused by inhalation of crystalline silica particles.[32] Silica particles accumulate within the alveolar sacs and ducts in the lungs, which lead to the formation of nodular lesions and fibrosis.[33] Silica dust can be found in soil, mortar, plaster, and shingles. They are produced during cutting, breaking, crushing, drilling, and grinding. TiO2 particles are in a nanometer size of around 20 to 100 nm. They are widely used in cosmetic products like sunscreen, in which TiO2 blocks UV radiation according to the "EU Health scientific committee." Ultrafine TiO2 is also used in paints, plastics, cement, windows, tiles, and other products for UV absorption and photocatalytic sterilizing properties. Ultrafine TiO2 is considered as an occupational carcinogen, which has been shown to increase the risk for lung cancer in an animal model. TiO2 is also widely used in medicine, agriculture, building and food.[34] The toxicity of TiO2 depends on the size, shape, aggregation and surface charge.[35,36] It has been shown that TiO2 can affect cell cycle, constriction of nuclear membranes and apoptosis.[37,38] TiO2 can be absorbed by inhalation, skin and injection and can be found in different organs such as lung, kidney, alimentary tract, liver, heart, spleen and cardiac muscle.[36,39,34]

1.1.3. Crystalline particles induce inflammation

The first evidence that macrophages were able to phagocytose particles such as silica, MSU crystal particles, and HA was first documented by electron microscopy about 40 years ago.[40,41] It has been shown, that crystals cannot be digested by macrophages but rather cause lysosomal damage, inflammation, and autophagy,[42,4] whereas calculi, stones or implants are too big to be phagocytosed by the macrophages. As a consequence, they form a specific structure known as foreign-body giant cells, whereby two or more macrophages fuse together and try to engulf or cover such large particles.[4] Recent studies showed that various crystals or crystalline particles such as MSU, CaOx, TiO2, asbestos, CPPD, HA, cholesterol, and alum crystals induce NLRP3 inflammasome activation and secretion of IL-1β and IL18 in macrophages .[43,44,33,45,46,47] To activate the NLRP3 inflammasome complex, two signals are needed: The first signal (signal 1) is mediated through damage-associated molecular patterns (DAMPs) or cytokines that increase NLRP3 and pro-IL-1β expression level mediated via the nuclear factor-κB (NF-κB) pathway. The second signal (signal 2) including crystals or crystalline particles, triggers the assembly of the inflammasome complex including NLRP3, ASC, and pro-caspase-1. These processes lead to the activation of pro-caspase 1 and activate caspase 1, the process of pro-IL-1β and pro-IL18 to mature IL-1β and IL18. Then, mature IL-1β or IL18 are secreted into the extracellular compartment and induce inflammation.[48] The mechanisms of inflammasome activation upon crystals or crystalline particles uptake encompass lysosomal damage, phagolysosomal rupture and the release of cathepsin B [49,50,51], followed by cathepsin B activating NLRP3, an effect that can be blocked with the cathepsin B inhibitor CA-074-Me.[52,53] However, *cathepsin B*-deficient primary macrophages show no or less effect on inhibiting NLRP3 activation and IL-1β production on stimulated macrophages or dendritic cells in response to hemozoin, MSU, alum, and silica.[54] This observation suggests that CA-074-Me can block other cathepsin proteins. Indeed, Orlowski, *et al.* showed that multiple cathepsins can activate NLRP3 and induce IL-1β or IL18 release.[55] A role for cathepsin on NLRP3 inflammasome formation and activation as well as potassium efflux has been demonstrated in response to various crystal or crystalline particles. Muñoz-Planillo, *et al.* showed that macrophages exposed to CPPD and silica particles cause potassium efflux leading to NLRP3 and inflammasome activation.[56] Interestingly, activated caspase 1 can cleave gasdermin-D (GSDMD) and produce N-terminal GSDMD leading to the activation of the regulated necrosis cell death pathway known as pyroptosis, followed by the release of DAMPs into the extracellular compartment. IL-1β/IL18 and pyroptosis contribute to the auto-amplification loop

of necroinflammation that mediates renal injury.[49] Interestingly, crystalline particles can induce inflammation independent of phagocytosis, whereby crystals interact with the cell membrane without internalization and sufficiently induce NLRP3-dependent ion influx.[33]

1.1.4. Crystalline particles induce cell death

Several studies suggested that crystals induce apoptosis, a predominant form of cell death dependent on the activity of caspases.[57,58,59] For example, IYER, *et al*. showed that silica induces apoptosis in human macrophages. In this study, the authors used only cytosolic histone-bound DNA fragments as a cell death ELISA assays to show apoptosis and Z-Val-Ala-Asp-fluoromethyl ketone have been used as caspase 1 inhibitor.[60] Meanwhile, caspase 1 is well-known to induce pyroptosis upon inflammasome activation in macrophages. In another study, Refsnes M, *et al*. showed by using the fluorescence activated cell sorting (FACS) that mineral particles of different physical-chemical properties induce apoptosis in alveolar macrophages.[57] Our group showed for the first time that crystals or crystalline particles can activate the necroptosis pathway directly via RIPK1, RIPK3, and MLKL proteins.[16] In this study, Mulay SR, *et al*. reported that CaOx, MSU, CPPD, and cystine have cytotoxic effects on mouse and human tubular epithelial cells as well as primary human synovial fibroblasts. Cells exposed to crystal particles induce phosphorylation of Ripk1, then phosphorylated Ripk1 triggers Ripk3 phosphorylation with subsequent phosphorylated Ripk3 induced Mlkl phosphorylation and oligomerization. As a result, phosphorylated Mlkl translocates into the plasma membrane and cell rupture occurs. During this process, cytokines and chemokines are released that trigger inflammation in the organ. Interestingly, blocking the main proteins involved in the necroptosis pathway such as RIPK1, RIPK3, and MLKL with chemicals or using a genetic approach showed a protective effect on renal epithelial tubular cells and fibroblasts. Surprisingly, ZVAD-FMK alone, a pan-caspase inhibitor, had no protective effect on cells exposed to crystal particles. These results suggest that caspase-dependent pathways such as apoptosis or pyroptosis are not involved in crystal or crystalline particles cytotoxicity. Interestingly, mice deficient in the two core proteins of the necroptosis pathway Ripk3 or Mlkl developed less severe oxalate crystal-induced acute kidney injury compared to wild-type mice.[16] In addition, human progenitor cells exposed to CaOx, MSU, CPPD, and cystine showed protective effect when RIPK1 or MLKL were inhibited using chemical inhibitor. This discovery shed new insight into the cytotoxic effects of crystal particles. Interestingly, tumor necrosis factor receptor 1 (*Tnfr1)* and*Tnfr2*-deficient mice showed less injury in oxalate-induced kidney injury. Yet, the exact mechanism of how crystals bind to TNFR receptors or how crystals

activate TNFR receptors is still uncertain. A further study from our group demonstrated that necroptosis is the predominant cell death pathway in neutrophils exposed to crystal or crystalline particles. Desai J, *et al.* reported that RIPK3 and MLKL are needed in neutrophils stimulated with MSU, CaOx, silica, CaP crystal to release extracellular trap-like chromatin.[61] Neutrophil necroptosis was limited when RIPK1, RIPK3, and MLKL were blocked using chemical inhibitors. The *in-vivo* model of gout-like tophus formation that involves suicidal NETosis similar to gouty arthritis showed less tophus formation in *Ripk3*-and *Mlkl*-deficient mice.[61,62] These results demonstrate that RIPK3 and MLKL are required for neutrophil cell death exposed to crystal or crystalline particles. However, both studies showed partial effects on crystal or crystalline particles cytotoxicity when necroptosis was blocked. These data suggest the involvement of other cell death pathways.

Another critical aspect of crystal or crystalline particles-related diseases is the origin of crystal particles. As mentioned earlier, crystals or crystalline particles can form inside the body, such as CaOx crystal particles or enter the body from the outside, such as silica particles. For a better understanding of the molecular mechanisms in each cell death pathway, the details of each pathway are presented.

1.2. Cell death pathways

Cell death refers to a highly complex biological event, which is crucial in many processes such as infection, immune system development, tissue homeostasis, and removal of damaged cells.[63,64] Traditionally, it was believed that cell death is divided into two main pathways, apoptosis known as programmed cell death, characterized by Kerr, *et al.* for the first time in 1972 [65] and necrosis previously known as un-programmed cell death.[66] These two pathways differ by morphological changes. For example, apoptosis defined by shrinking of the cells, plasma membrane blebbing, condensation of the nucleus, and internucleosomal DNA fragmentation. The dead cells are packaged into an apoptotic body, which is engulfed and removed by phagocytes.[67] Apoptosis is considered as non-immunogenic cell death due to the formation of apoptotic bodies, which do not release DAMPs as danger signals. The initiation of apoptosis can be divided into an intrinsic or an extrinsic pathway. Both pathways involve caspase enzymes to execute cell death. However, necrotic cell death characterized by plasma membrane loss, random DNA degradation and DAMPs release, which results in strong immune responses.[68] Necrotic cell death is considered as an accidental event without including any molecular mechanism opposite to apoptosis. However, for the first time, Laster, *et al.* in 1988 reported that tumor necrosis factor (TNF) can induce necrotic and apoptotic cell death.[69] Later

on, between 1992 to 1998, more studies reported that necrotic cell death can be regulated. For example, mitochondrial ROS requires a cytotoxic response to TNF in L929 (murine fibroblast) cells.[70] However, the mechanism of regulated necrosis were not well understood until 2000, when Holler, *et al.* reported a non-apoptotic cell death pathway in primary T cells. This pathway is independent of caspase enzyme activity but dependents on the FADD (FAS-associated protein with a death domain) protein, known as RIPK1, and its enzyme activity.[71] In the following years, several studies referring to necrosis as programed cell death. In 2005, Degterev, *et al.* discovered a small chemical molecule known as necrostatin-1 (Nec1), which could potentially block programmed cell death independent of caspases activity in different cell types. They named this form necroptosis as a non-apoptotic type of programmed cell death.[72] Nec1 can block RIP kinases protein, which is a crucial element in the necroptosis pathway.[73] The programmed cell death topic became highly interesting and kept on growing. Meanwhile, many different non-apoptotic pathways were defined, including necroptosis, ferroptosis, pyroptosis, MPT, and parthanatos (Figure 1).

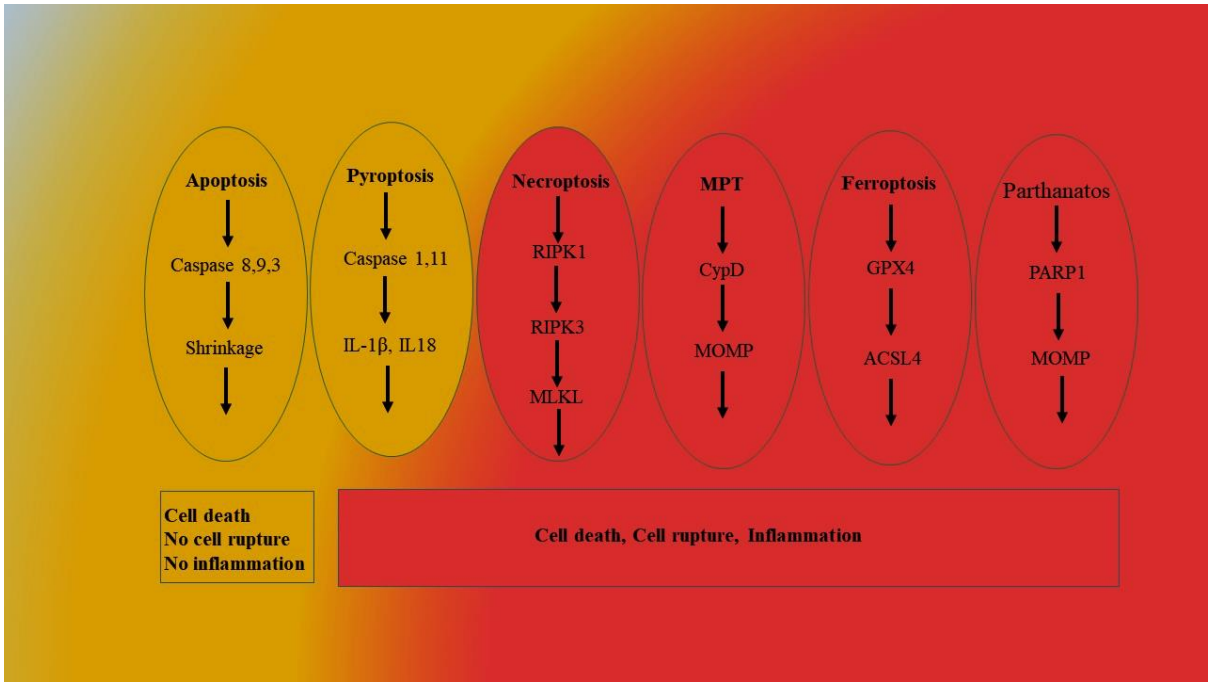

Figure1: Apoptosis and pyroptosis pathways are dependent on caspases activity. Apoptosis cell death does not lead to inflammation (non-immunogenic), while pyroptosis is highly immunogenic due to the release of IL-1β and IL18. Necroptosis, MPT, ferroptosis, and parthanatos are independent of caspases activity. **IL-1β**: interleukin 1 beta, **IL18**: interleukin 18, **MPT**: mitochondrial membrane permeability transition.

1.2.1. Apoptosis

As mentioned earlier, the apoptosis pathway was the first described programmed cell death by Kerr, *et al.* in 1972.[65] The morphological hallmarks of apoptosis include cytoplasmic shrinkage, chromatin condensation, nuclear fragmentation as well as plasma membrane blebbing, which form the apoptotic body. Caspase proteins are involved in apoptosis activation and execution. Caspase proteins exist in their inactivated form, and upon induction, each caspase can cleave the other caspase protein at the identical sequence, which results in protease cascade activation. In humans, 11 caspases (1-11 and 14) have been identified.[74,75] Caspases categorize in two groups based on their functions: 1. Initiator of apoptosis include caspases 2, 8, 9, 10, and 12. Caspases 1, 5, and 11 initiate apoptosis through inflammation pathways. 2. Effectors of apoptosis include caspases 3, 6, and 7. Both intrinsic and extrinsic pathways can induce caspase proteins depending on different signals. DNA damage, ROS production, microtubular changes, endoplasmic reticulum stress and mitotic defects trigger intrinsic pathway.[76,77] Mitochondrial outer membrane potential (MOMP) controls the intrinsic pathway of apoptosis.[78,79] The BCL-2 family controls MOMP. Upon activation of MOMP, different proteins such as cytochrome c are released into the cytoplasm and activate caspase proteins. Cytochrome c induces caspase 3 activation through the apoptosome complex to contain cytochrome c/Apaf-1/caspase-9 [80]. Cytochrome c directly binds to the C-terminal of Apaf-1 protein and facilitates the association of dATP with Apaf-1 which results in exposing of its N-terminal CARD, which can recruit and activate caspase 9 through CARD-CARD interaction.[81] Activated caspase 9 induces caspase 3 as an effector mediator in apoptosis cell death.[82] However, the extrinsic apoptosis signalling pathway involves the transmembrane receptor known as death receptor.[83] Death receptors are involved in the TNF receptor gene superfamily.[83] TNF receptor family members have similar cysteine-rich extracellular domains as well as cytoplasmic domain around 80 amino acids known as the death domain.[84] The death domain plays a crucial role in transferring signals from the cell surface into the intracellular pathways. Some different receptors and ligands have been identified, such as TNF-α/TNFR1, Apo3L/DR3, Apo2L/DR4, FasL/FasR and Apo2L/DR5.[84,85,86,87,88] Upon binding of the TNF ligand to TNFR1, adapter proteins such as Fas-associated death domain (FADD) and TNF receptor-associated death domain (TRADD) are recruited.[89] Pro-caspases 8 and 10 can bind to these adaptor proteins, which results in the formation of the death-inducing signaling complex (DISC), complex I and complex II.[90,91] FAS ligand and TRAILR receptors can stabilize the receptor homotrimers to trigger a configurational change on intracellular tails that facilitate the

death domain (DD)-dependent association of the adapter FADD.[92,93] Then, FADD activates DISK assembly by promoting the death effector domain-dependent recruitment of CASP8 or CASP10 and c-FLIP as multiple isoforms. The extrinsic apoptosis execution can be divided into two different pathways, type I cells (for example, thymocytes and mature lymphocytes) dependent on CASP8 proteolytic, which maturate executioner CASP3 and CASP7. Upon TNF-α stimulation, RIPK1 recruits to complex I, which is independent of TRADD, then RIPK1 is polyubiquitinated with the help of c-IAP1, c-IAP2, and LUBAC.[94,95] These processes can drive inflammation and cell survival by recruitment of TGF-beta activated kinase 1 MAP3K7-binding protein 2 (TAB2), TAB3, and mitogen-activated protein kinase kinase kinase 7 (MAP3K7). In addition, this event can promote mitogen-activated protein kinase (MAPK) or IkB kinase that depend on nuclear factor kappa light chain enhancer of activated B cells (NF-κB) activation,[96,97] and promote survival process. Nonetheless, apoptosis is considered as non-immunogenic pathway and differs from regulated-necrosis.

1.2.2. Necroptosis

The necroptosis pathway is a type of regulated necrosis that is distinct from apoptosis. Activation of necroptosis leads to plasma membrane rupture and induces inflammation [98], which can be triggered by inducing death receptors, including FAS, TNFR1, TNFR2 [99,73], TNF-related apoptosis-inducing ligand receptor 1/2,[71] as well as toll-like receptor (TLR)3 and TLR4.[100,101] At the molecular level, RIPK1, RIPK3, and MLKL proteins drive necroptosis (Figure 2).[102,103] TNFR1 activation leads to induction of NF-kB, which promotes either cell survival or apoptosis or necroptosis depending on the microenvironment, various signals as well as cell types. Apoptosis and necroptosis are highly interlinked on the molecular level (Figure 2A).[63] Interestingly, some of the apoptosis inducer can initiate the necroptosis pathway, typically when casp8 is blocked (Figure 2C). For example, TNF ligand can lead to both apoptosis and necroptosis depending on casp8 activity (Figure 2B-D).[63] On the other hand, casp8 can cleave Ripk1 and therefore limiting necroptosis (Figure 2B)[104]. Other stimuli such as TLR2, 3, 4, 5 and 9, DNA damage and IFN, mitochondrial antiviral signalling protein, retinoic acid-induced gene 1, anti-cancer drugs such as obatoclax, shikonin, and smac mimetic, vaccinia infection, can induce necroptosis through the activation of death receptor-like TNFR, FAS, and TRAILR.[72,71,105] Interestingly, it was reported that ROS production can induce necroptosis through activation of RIPK1 phosphorylation.[106] On the other hand, MLKL activation leads to NLRP3 induction through potassium efflux, recruited ASC, and pro-caspase 1, which results in the formation of the NLRP3 inflammasome and IL-1β release as well as

activation of the pyroptosis pathway.[107] This event occurs in a necroinflammation loop and release of pro-inflammatory cytokines, DAMPs, and histones, which then trigger necroptosis.[108] Many studies showed that RIPK1 and RIPK3 play a crucial role in tissue injury.[109,110] For example, inhibition of Ripk1 with Nec1 can limit the area of infarction in ischaemia-reperfusion injury (IRI) in the brain.[72] In line with previous studies, necroptosis inhibition leads to reduced cardiac as well as kidney IRI.[111,112] In addition, *Ripk3*-deficient mice with transplanted allogeneic kidneys showed less necrosis area and prolong survival in the transplant recipients of the wild-type group.[113] Recent studies showed that crystalline particles such as CaOx, MSU, and silica can induce necroptosis and lead to organ injury.[16,61] Crystal particles can activate RIPK3 and MLKL proteins resulting in renal tubular cell injury. *Ripk3*-and-*Mlkl*-deficient mice presented with less injury in oxalate crystal-induced AKI.[25] However, the exact mechanism of activating necroptosis remains unclear. Accumulating evidence suggest that necroptosis can be used as therapy target in kidney related-diseases. Necroptosis is implicated in several diseases that involve organ injury and inflammation processes such as kidney injury, sepsis, inflammatory bowel disease, neurodegenerative diseases, and atherosclerosis.[108,114] However, other regulated-necrosis pathways including mitochondrial membrane permeability transition-related necrosis (MPT-RN), pyroptosis, and ferroptosis, can also lead to tissue injury and organ injury. However, they induce tissue injury via different molecular mechanisms.

1.1.1. Mitochondrial membrane permeability transition-related necrosis

MPT-RN is a form of cell death associated with permeability changes of the inner mitochondrial membrane, which was first described in 1979.[115] It has been shown that MPT can be induced by a high concentration of mitochondrial Ca2+ and oxidative stress, resulting in necrotic morphology.[115,116,117] Permeability transition pore complex can form between the inner mitochondrial membrane and outer mitochondrial membrane during activation of MPT. The molecular mechanism of MPT relies on a protein known as peptidylprolyl isomerase F (PPIF) (cyclophilin D, CYPD), which has been validated by genetic tools.[118] In addition, blockade of PPIF protein with chemical inhibitors such as cyclosporin A (CsA)[119], sanglifehrin A [120], and JW47[121] prevent MPT-driven necrosis. However, a clinical study in 2015 (the CIRCUS trial) using CsA as intervention showed no cardioprotective effects on patients before percutaneous coronary intervention (PCI) with acute myocardial infarction.[122] Although, a previous study in 2008 showed some protective effect on using CsA.[123]

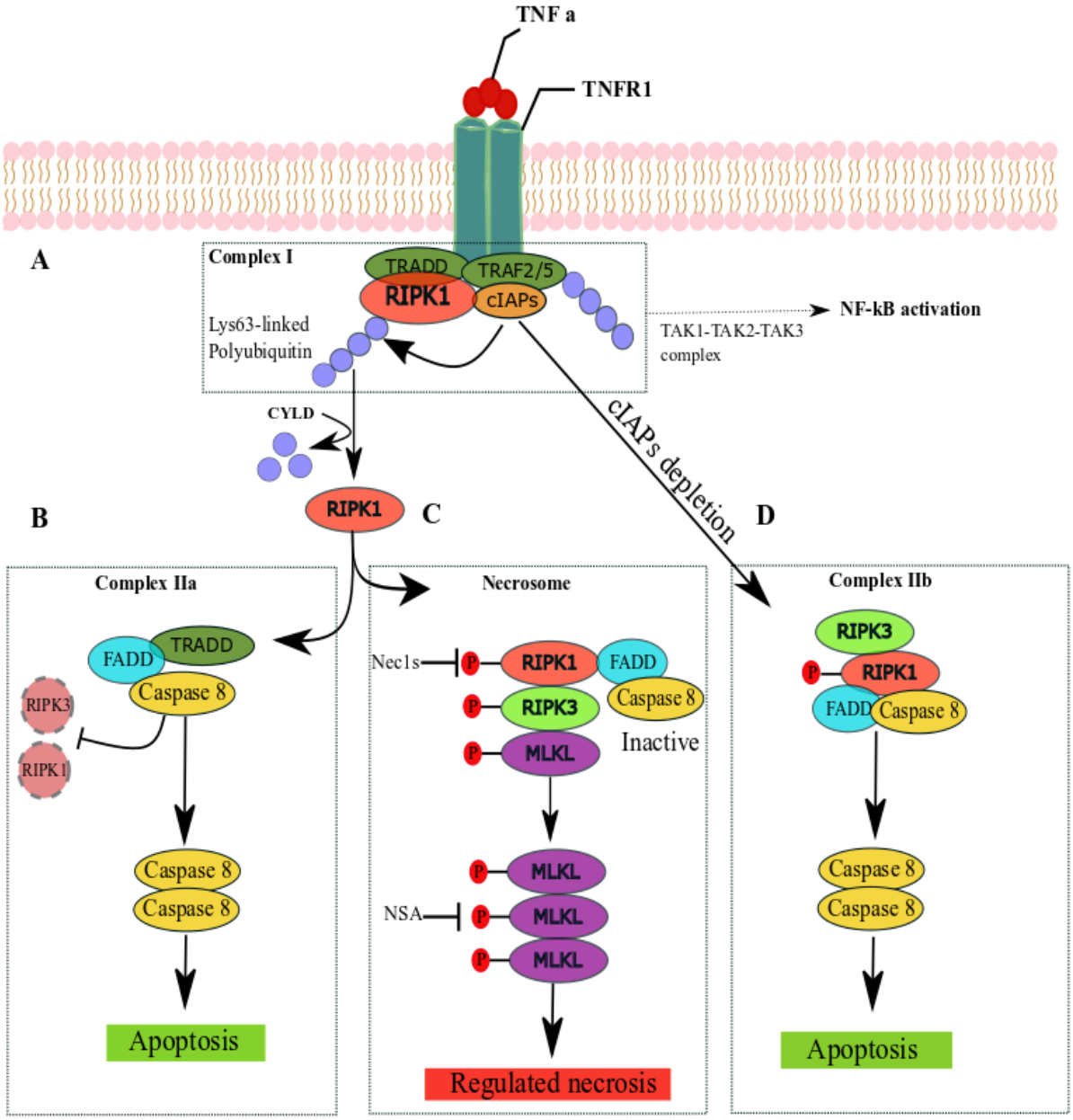

Figure 2. The overview of the necroptosis pathway. A: Upon TNF ligand-TNFR interaction, complex I, including TRADD, TRAF2/5, cIAPs, and RIPK1, is formed. cIAP proteins promote RIPK1 polyubiquitinating, and the complex I leads to activation of the NFKb pathway through TAK1 complex. **B:** Deubiquitinating enzymes like CYLD can remove the Lys63 chain from RIPK1, which recruit TRADD, caspase 8 and FADD and form complex IIa. These two proteins can cleave RIPK1 and RIPK3 resulting in the activation of apoptosis independent of RIPK1. **C:** Inactivation of caspase 8 can lead to RIPK1 phosphorylation, which induces RIPK3 phosphorylation; thus MLKL gets phosphorylated. This complex named necrosome and lead to oligomerization of MLKL. MLKL oligomers translocate into the plasma membrane and activation of necroptosis pathway occurs. **D:** If cIAP proteins get inactivated caspase 8, RIPK1, FADD form a complex IIb, which induces the apoptosis pathway-dependent on RIPK1. **TNF**: tumor necrosis factor, **TNFR**: tumor necrosis factor receptor, **TRADD**: tumor necrosis factor receptor type 1-associated DEATH domain, **TRAF2/5**: TNF receptor-associated factor 2/5, **cIAP**: cellular inhibitor of apoptosis protein, **RIPK1**: receptor-interacting serine/threonine-protein kinase 1, **RIPK3**: receptor-interacting serine/threonine-protein kinase 3, **NFkB**: nuclear factor 'kappa-light-chain-enhancer' of activated B-cells, **TAK1**: transforming growth factor beta-activated kinase 1, **CYLD**: CYLD lysine 63 deubiquitinase, **MLKL**: mixed lineage kinase domain like pseudokinase.

Such contradictory results could be due to using different methods to measure infarct size and specific formulation of CsA, which was used in the CIRCUS trial.[124] *Ppif*-deficient mice were protected from ischemic or toxic acute kidney injury.[111,125] Vaseva AV, *et al.* showed that P53 interacts with Ppif and contributes to mitochondrial pore opening, which leads to cell necrosis in brain injury.[126] However, the exact mechanism is unclear.[127] Another protein involved in the permeability transition pore complex is the voltage-dependent anion channel (VDAC). VDAC protein plays an essential role in controlling the trafficking of metabolites such as ATP, ADP, and respiratory substrates.[128] A recent study identified ANT family genes including Ant1, Ant2, and Ant4 to play an important role in MPT-driven cell death. Surprisingly, the deletion of Ant and Ppif resulted in complete inhibition of MPTP.[129] These results support the "multi-pore model," in which there are two distinct molecular components involved.[129] However, these data need to be validated and confirmed in animal disease models. A relevance in human diseases is still unclear. Interestingly, the MPT pathway seems to be involved in neutrophil activation and to induce NETosis.[130] The inhibition of PPIF by using CsA leads to less ROS production and less NETosis.[130] However, these data need to be confirmed by genetic tools. Interestingly, hyperactivation by poly (ADP-ribose) polymerase 1 (PARP1) can result in MOMP and mitochondrial damage.[131,132] Although, PARP1 activation is associated with parthanatos, a non-apoptotic cell death pathway. The parthanatos pathway is associated with the DNA damage response machinery and it can be induced in response to oxidative stress, hypoxia, hypoglycemia, inflammatory condition, and alkylating DNA damage.[131,133] However, the role of PPIF protein as the main regulator of mitochondrial function has not been described in PARP1 dependent-cell death.

1.1.2. Pyroptosis

Pyroptosis is a caspase-dependent form of regulated necrosis. Cookson and Brennan defined a pro-inflammatory regulated cell death based on caspase 1 activity and first used the term pyroptosis.[134] It was thought that pyroptosis is specific to macrophages or monocytes due to activation of caspase 1.[135,136] A recent study demonstrated that pyroptosis can be induced by caspase 3 [137] and in different cell types such as T lymphocytes[138], neurons[139], and tubular epithelial cells.[140,141] The molecular mechanism of pyroptosis relies on the activation of caspase proteins such as caspase 1, caspase 3, and caspase 11 (murine), caspase 4 (human), and caspase 5, which depends on the stimulus.[142,143] Pyroptosis leads to the secretion of IL-1β and IL18, induce robust pro-inflammatory markers, and, therefore, is considered as high immunogenic cell death pathway.[144,145] Different studies showed that pyroptosis could be triggered via

cytosolic lipopolysaccharides (LPS) as gram-negative bacterial infection through the activation of caspase 11 but independent of caspase 1.[146,147,148,149] The execution of pyroptosis is associated with proteolytic cleavage of GSDMD protein.[150,151] *Gsdmd*-deficient macrophages showed a protective effect upon LPS stimulation. In addition, *Gsdmd*-deficient mice have survived a lethal dose of LPS.[150,151] It has been shown that GSDMD is auto-inhibited through binding of the C-terminal repressor domain to the N-terminal pore-forming domain. Upon activation, caspases can cleave the inter-domain and release GSDMD-N, which translocate to the plasma membrane and bind to phosphoinositides.[152,153] This interaction results in GSDMD-N oligomerization, pore formation, and rapid plasma membrane permeabilization.[152,154] Therefore, the pyroptosis dependent-cell death pathway leads to the release of inflammatory mediators, and inflammation.

1.1.3. Ferroptosis

Ferroptosis is a form of regulated necrosis cell death, which depends on lipid peroxidation followed by ROS generation and iron.[155,156] Yagoda N, *et al*. have identified a chemical compound known as erastin that can induce a form of cell death in resistant RAS-transformed cancer cells.[157] Ferroptosis occurs independent of caspase activity, necrosome formation, PPIF as well as autophagy.[158] Morphological characterization of ferroptosis is associated with necrotic and mitochondrial alteration mainly related to an electron-dense ultrastructure, a decrease in cristae and outer membrane rupture.[117] Ferroptosis is an immunogenic cell death pathway due to the release of DAMPs.[159] The molecular mechanism of ferroptosis relies on a protein known as glutathione peroxidase 4 (GPX4). GPX4 is the main regulator of the ferroptosis pathway by inhibiting lipid peroxidation through promoting glutathione (GSH)-dependent reduction of lipid hydroperoxides to lipid alcohols.[160,161] In line with these findings, erastin induces ferroptosis by indirectly preventing cystine/glutamate antiporter system X_c^-, that results in decreased intracellular cysteine and GSH.[158,161] Therefore, blocking GSH with L-buthionine sulfoximine, the glutamate-cysteine ligase complex is able to trigger ferroptosis -regulated cell death.[160] The Food and Drug Administration (FDA)-approved tyrosine kinase inhibitor sorafenib can persuade ferroptosis through blocking GSH upon system X_c^- inhibition.[162,163] Recently, altretamine has been identified using genome-wide screening as potential inhibitor of GPX4.[164] A large body of evidence suggest that GPX4 pro-survival activity participates in development as well as homeostatic tissue maintenance. *Gpx4*-deficient mice showed embryonic lethality.[165,166] Friedmann Angeli JP, *et al*. demonstrate that inducible *Gpx4*-deficient mice develop acute renal failure.[160] In addition, GPX4 is essential in hepatic

injury[167], neurodegeneration[165], as well as toxic renal injury[168], and Parkinson disease.[169] However, the details of how GPX4 protein contributes to cell death and organ injury is not very well understood.

As mentioned earlier, necroptosis is involved in metabolic crystal particle-induced kidney injury.[25] Many studies have reported that occupational work-related diseases are associated with crystal particles, including silica, nanomaterials, and crystal-related bone remodeling, which can deposit within different parts of the body. However, there are no data available on whether environmental crystals can share the same mechanisms of cell death as metabolic crystal particles or not. In addition, whether crystalline particles can activate another form of regulated necrosis or not is currently not known. Therefore, in this thesis, we intend to answer these questions.

2. Hypotheses

Crystal particles result in clinical complications once they deposit within the human body. Various crystal particles lead to tissue and organ injury, for example, CaOx is involved in nephrolithiasis, oxalate nephropathy, and acute kidney injury, cholesterol can lead to cholesterol embolism and atherosclerosis, MSU is involved in gout. Occupational and air pollution-related diseases like silicosis, asbestosis, pneumoconiosis, smoking-related COPD, and chronic respiratory distress are considered as serious global health problem leading to death of millions of people. There are no effective drugs available to limit the cytotoxic effects of crystal particles directly. We first need to better understand the molecular mechanisms of crystal- or crystalline particle-induced tissue injury. It is still not clear whether environmental particles can activate necroptosis and whether other forms of cell death are involved in crystalline particle-induced tissue and organ injuries.

Therefore, we hypothesized that:

1. Acute tissue injury leading to progressive organ damage is associated with increased expression of necroptosis-related genes

2. Environmental and metabolic crystals, regardless of their shape and size, induce necroptosis in human and mouse renal tubular primary and immortalize cells.

3. Crystalline particles induce MPT as an alternative cell death pathway to drive organ injury.

3. Materials and Methods

3.1. Instruments and Chemicals

3.1.1. Instruments

Balance:	
Analytic Balance, BP 110 S	Sartorius, Göttingen, Germany
Mettler PJ 3000	Mettler-Toledo, Greifensee, Switzerland
Cell Incubator:	
Type B5060 EC-CO_2	Heraeus Sepatech, Munich, Germany
Centrifuges:	
Heraeus, Biofuge primo	Kendro Laboratory Products GmbH, Hanau, Germany
Heraeus, Sepatech Biofuge A	Heraeus Sepatech, Munich, Germany
ELISA-Reader:	
Tecan, GENios Plus	Tecan, Crailsheim, Germany
Fluorescence Microscopes:	
Leica DMi8	Leica Microsystems, Cambridge, UK
Olympus BX50	Olympus Microscopy, Hamburg, Germany
Zeiss Libra 120 TEM	Zeiss, Germany
Electron Microscope:	
JEOL EXII 1200	Jeol, Tokyo, Japan
FEG-SEM Quanta 250	Thermo Fisher Scientific, FEI, Hillsboro, OR
Spectrophotometer:	
Beckman DU® 530	Beckman Coulter, Fullerton, CA, USA
TaqMan Sequence Detection System:	

qRT-PCR syber green LC-480	ROCHE, Mannheim, Germany
Transfection device:	
Neon	Invitrogen, Germany
Other Equipments:	
Nanodrop	PEQLAB Biotechnology GMBH, Erlangen, Germany
Cryostat RM2155	Leica Microsystems, Bensheim, Germany
Cryostat CM 3000	Leica Microsystems, Bensheim, Germany
Microtome HM 340E	Microm, Heidelberg, Germany
pH meter WTW	WTW GmbH, Weilheim, Germany
Thermomixer 5436	Eppendorf, Hamburg, Germany
Vortex Genie 2™	Bender & Hobein AG, Zürich, Switzerland
Water bath HI 1210	Leica Microsystems, Bensheim, Germany
XtremeCT scanner	SCANCOMedical AG, Brüttisellen, Switzerland

3.1.2. Chemical and Reagents

RNeasy mini kit	Qiagen GmbH, Hilden, Germany
RNA isolation kit	Ambion (Ambion, CA, USA)
RT-PCR primers	Metabion, Munich, Germany
ROS assay: DCFDA dye	Sigma lifesciences, Germany
TMRE	Invitrogen, Carlsbad, CA
Epoxy glue	Model 2400; CircuitWorks, Kennesaw, GA
Lysotracker	Abcam, Cambridge, UK
Calcein	Invitrogen, Carlsbad,CA
Propidium iodide	Invitrogen, Carlsbad, CA
Acridine Orange	Sigma lifesciences, Germany

LDH cytotoxicity assay	Roche, Germany
MTT viability assay	Sigma-Aldrich, Steinheim, Germany
Durcupan ACM	Merck Sigma-Aldrich, Darmstadt, Germany
Silver paint	Agar Scientific Ltd, Stansted, UK
Quorum Q150TS	Quorum Technologies, Laughton, UK
GenMute	SignaGen Laboratories, US
TNF-α	Immunotools, Germany
Superscript reverse transcriptase II	Invitrogen, Karlsruhe, Germany
Cell culture:	
DMEM-medium	Biochrom KG, Berlin, Germany
RPMI-1640 medium	GIBCO/Invitrogen, Paisley, Scotland, UK
FCS	Biochrom KG, Berlin, Germany
Dulbecco's PBS (1×)	PAN Laboratories GmbH, Cölbe, Germany
Trypsine/EDTA (1×)	PAN Laboratories GmbH, Cölbe, Germany
Glutamine	PAN Laboratories GmbH, Cölbe, Germany
Penicillin/Streptomycin (100×)	PAN Laboratories GmbH, Cölbe, Germany
Prostaglandin E1	Calbiochem, Darmstadt, Germany
EGF	Sigma-Aldrich, Munich, Germany
I-T-SS	Sigma-Aldrich, Munich, Germany
l-thyroxine	Sigma-Aldrich, Munich, Germany
Hydrocortisone	Sigma-Aldrich, Munich, Germany
Inhibitors	
Nec-1s	Enzo Life Sciences, Lörrach, Germany
Necrosulfanamide	Millipore, Schwalbach, Germany
Pan caspase inhibitor zVAD	Enzo Life Sciences, Lörrach, Germany
CsA	Sigma-Aldrich, Munich, Germany

APDC	Sigma-Aldrich, Munich, Germany
Cytochalasin D	Calbiochem, Darmstadt, Germany
CA074Me	Calbiochem, Darmstadt, Germany
Antibodies:	
Ripk3	Abcam, Cambridge, United Kingdom
Mlkl	Abcam, Cambridge, United Kingdom
SMA	Abcam, Cambridge, United Kingdom
Collagen1α1	DAKO, Hamburg, Germany
Elisa and assay Kits:	
Creatinine FS	DiaSys Diagnostic System, GmBH, Holzheim, Germany
Chemicals:	
Acetone	Merck, Darmstadt, Germany
Bovines Serum Albumin	Roche Diagnostics, Mannheim, Germany
DEPC	Fluka, Buchs, Switzerland
DMSO	Merck, Darmstadt, Germany
EDTA	Calbiochem, SanDiego, USA
Ethanol	Merck, Darmstadt, Germany
Formalin	Merck, Darmstadt, Germany
Hydroxyethyl cellulose	Sigma-Aldrich, Steinheim, Germany
HCl (5N)	Merck, Darmstadt, Germany
Isopropanol	Merck, Darmstadt, Germany
Calcium chloride	Merck, Darmstadt, Germany
Calcium dihydrogenphosphate	Merck, Darmstadt, Germany
Calcium hydroxide	Merck, Darmstadt, Germany
Beta mercaptoethanol	Roth, Karlsruhe, Germany

Sodium acetate	Merck, Darmstadt, Germany
Sodium chloride	Merck, Darmstadt, Germany
Sodium citrate	Merck, Darmstadt, Germany
Sodium dihydrogenphosphate	Merck, Darmstadt, Germany
Penicillin	Sigma, Deisenhofen, Germany
Roti-Aqua-Phenol	Carl Roth GmbH, Karlsruhe, Germany
Streptomycin	Sigma, Deisenhofen, Germany
Crystals:	
Calcium oxalate	Alfa aesar, Karlsruhe, Germany
MSU	Invivogen, Toulouse, France
Calcium phsphate	Chem Cruz
Calcium pyrophosphate dihydrate	Invivogen
Cholesterol	Invivogen, Toulouse, France
Silica	Alfa aesar, Karlsruhe, Germany
TiO2	Io-li-Tec, Germany
Miscellaneous:	
Preseparation Filters	Miltenyl Biotec, Bergish Gladbach, Germany
Needles	BD Drogheda, Ireland
Pipette’s tip 1-1000µL	Eppendorf, Hamburg, Germany
Syringes	Becton Dickinson GmbH, Heidelberg, Germany
Plastic histocasettes	NeoLab, Heidelberg, Germany
Tissue culture dishes Ø 100x20mm	TPP, Trasadingen, Switzerland
Tissue culture dishes Ø 150x20mm	TPP, Trasadingen, Switzerland
Tissue culture dishes Ø 35x10mm	Becton Dickinson, Franklin Lakes, NJ, USA
Tissue culture flasks 150 cm2	TPP, Trasadingen, Switzerland
Tubes 15 and 50 mL	TPP, Trasadingen, Switzerland

Tubes 1.5 and 2 mL	TPP, Trasadingen, Switzerland

All other reagents were of analytical grade and are commercially available from Invitrogen, SIGMA or ROCHE.

3.2. Experimental procedures

3.2.1. Animals

Ppif-deficient mice were obtained from Jackson laboratories (Bar Harbour, USA (Stock no: 009071) and backcrossed to C57BL/6J mice. *Mlkl*-deficient mice were kindly provided by J. Murphy and W. Alexander, WEHI, and Australia.[170] C57BL/6 male mice were purchased from Charles River. All mice were housed in groups of maximum five in filter-top cages with bedding and pulp, 22.2 °C and a 12 hours light/dark cycle, and had free access to food and water ad libitum. Cages, litter, nest lets, houses, food and water were sterilized by autoclaving at 121 °C and 1 bar pressure for 20 minutes. All experiments were done according to the EU directive (2010/63/EU) for animal welfare and German animal protection laws. Honarpisheh M, et al[3], Mulay SR, Honarpisheh MM, et al.[2]

3.2.2. Animal models

Acute oxalate nephropathy:

Ppif-deficient, *Mlkl*-deficient, and C57BL/6J mice were injected intraperitoneally with 100 mg/kg sodium oxalate and received 3% sodium oxalate in drinking water. After 24 hours, the kidneys were harvested to evaluate the extend of kidney injury.[47,16] For the therapeutic purpose, mice received a single injection of either CsA (2 mg/kg i.v., Sigma-Aldrich, Munich, Germany) or Nec1s (1.65 mg/kg i.p., Millipore, Darmstadt, Germany) or a combination of both prior to sodium oxalate injections. Honarpisheh M, et al[3], Mulay SR, Honarpisheh MM, et al.[2]

Chronic oxalate nephropathy:

C57BL/6J mice were fed an oxalate-rich diet that was made by adding 50 µmol/g sodium oxalate to a calcium-free standard chow diet, and mice were sacrificed on day 7, 14 and 21.[171] Honarpisheh M, et al[3]

Acute ischemia-reperfusion injury:

Mice were killed after 24 hours of reperfusion of bilateral pedicle clamping group. The damaged kidneys were harvested for RNA isolation and histology analysis.

Honarpisheh M, et al[3]

Cisplatin-induced nephropathy model:

Mice received a single dose (intraperitoneal injection) of 20 $mgkg^{-1}$ of cisplatin (Sigma-Aldrich), and kidneys were collected after three days for RT-PCR and histology analysis.[172] Honarpisheh M, et al[3]

3.2.3. Transmission Electron Microscopy (TEM)

One drop of crystals suspended in PBS was transferred onto formvar-coated copper grids (Plano, Wetzlar, Germany). The extra liquid was removed after 30 seconds, and grids were allowed to dry. JEOL EXII 1200 TEM was used at 80 kV. KeenViewII (Olympus, Hamburg, Germany) camera was used to capture images and processed using iTEM software package (analySISFive, Olympus, Hamburg, Germany). For kidney tissue and cell processing, small pieces of kidney tissue were fixed in 3% PBS and cells fixed in 3% glutaraldehyde, followed by removal from the plate and centrifuged. 5% low-melting agarose was used to embed the cell pellets. Soerensen's phosphate buffer (0.1 M) was used to wash tissue or gelatined blocks, 17% sucrose buffer and 1% OsO4 were used for post-fixation and dehydration by ethanol series with 30, 50, 70, 90 and 100% for 10 minutes each, which was repeated three times. Epon resin and propylene oxide were used to mix (1:1) dehydrated samples for 1 hour after incubation in propylene oxide for 30 minutes, than embedded in pure Epon. Polymerization was carried out at 90°C for 2 hours. An ultramicrotome with a diamond knife was used to cut thin sections of 70-100 nm. The contrast was increased by staining with 0.5% uranylacetate and 1% lead citrate. Samples were visualized at an acceleration voltage of 60 kV using a Zeiss Leo 906 TEM.[2] This method was carried out in collaboration with Bastian Popper (Biomedical Center, Core Facility Animal Models, Ludwig Maximilian University, Planegg Martinsried, Germany) and Peter Boor (Division of Nephrology, Institute of Pathology, Rheinisch-Westfälische Technische Hochschule University of Aachen, Germany). Mulay SR, Honarpisheh MM, et al.[2]

3.2.4. Serial Block Face Scanning Electron Microscopy

The enhanced staining protocol was used to stain fixed cells. Briefly, Durcupan ACM resin was used to embed the dehydrated and stained specimens, and mixed accordingly as per manufacturers' protocol. Conductive epoxy glue was used to embed the tissue. The tissue was then trimmed to a pyramid, and mounted onto a pin. Silver paint was used to cover the sides of the pyramid and finally Quorum Q150TS was used to coat the whole assembly with platinum. The set of data from SB-EM were collected using FEG-SEM Quanta 250. Afterwards, the

images were processed by cutting the block faces into 30 nm and visualized with a resolution of 22 nm per pixel. An open-source software Microscopy Image Browser was used to process and segment all images. The final visualization of models was performed in Amira (Thermo Fisher Scientific, MA) 31296606.[2] This method was carried out in collaboration with Ilya Belevich, and Eija Jokitalo (Electron Microscopy Unit, Institute of Biotechnology, University of Helsinki, Helsinki, Finland). Mulay SR, Honarpisheh MM, et al.[2]

3.2.5. Small interfering RNA experiments

Transient transfection was performed in L929 and HK2 cells with 120 nM of siRNA duplexes for PPIF (iBONi siRNA pool, Lot no.: 2017d0119, Riboxx, Radebeul, Germany), MLKL (Ambion, Foster City, CA) and scrambled siRNA (Ambion, Foster City, CA) using Neon electroporation device (Thermofisher, Germany). The parameters used for electroporation were as follow: Voltage: 1400v, with 20ms, pulses. Cells were exposed to 1 mg/ml CaOx crystals, 0.5 mg/ml silica, 0.5 mg/ml MSU, 0.5 mg/ml CPPD, 3 mg/ml cholesterol and 0.5 mg/ml TiO2 for 48 hours post-transfection. Cell death was quantified by PI positivity and LDH assay 24 hours after exposure to crystals. Mulay SR, Honarpisheh MM, et al.[2]

3.2.6. Assessment of renal injury

The 2 µm kidney sections were stained with periodic acid-Schiff (PAS) reagent. Tubular damage was scored by assessing the percentage of necrotic tubules and tubular casts. CaOx crystals and crystal deposit in the kidney were determined using Pizzolato´s staining and assessed as (7, 8, and 45), No deposits = 0 points; crystals in papillary tip = 1 point; crystals in cortical medullary junction = 2 points; crystals in cortex = 3 points. The points were combined if crystals found in multiple areas. Plasma creatinine levels were analyzed using a commercial kit according to the manufacturer's protocol. TUNEL kit was used to analyze dead cells. All assessments were performed in a blind manner. Mulay SR, Honarpisheh MM, et al.[2]

3.2.7. Micro-computed tomography (µCT)

For µCT scanning of PFA-fixed kidneys, a XtremeCT scanner was used. Scans were carried out at 20 µm voxel size with a 70 kV energy set as described previously.[173] Kidney tissues were fixed in vertical (longitudinal) direction. The scan area was changed to include all organs, with a total of 490 slices and 45 minutes scanning. ImageJ software was used to analyze image density and 3D reconstruction. We performed this method in collaboration with Rostyslav

Bilyy (Department of Histology, Cytology, and Embryology, Danylo Halytsky Lviv National Medical University, Lviv, Ukraine). Mulay SR, Honarpisheh MM, et al.[2]

3.3. Cell culture

3.3.1. Cell freezing and thawing

At earlier passages, cells were grown under normal culture conditions and frozen for future use. For freezing cells, cells were detached from the cell culture plates and centrifuged at 1000 rpm for 3 minutes. The cell pellet was resuspended in 90 % FCS and 10 % DMSO by pipetting repeatedly up and down. 1 ml of the cells in freezing media were immediately poured into freezing vials (4^0C) and the cells slowly frozen at -20^0C for 1 hour and then at -80^0C overnight. All cells were transferred into liquid nitrogen on the next day. To thaw cells, a frozen vial was removed from liquid nitrogen and put into water bath at 37^0C. The cells were then put in 5 ml warm complete growth medium and centrifuged. The old medium was removed and fresh medium prior to transfer into a new culture plate. After 24 hours, the old medium was replaced with fresh medium.

3.3.2. Cell culture studies

Primary tubular epithelial cells (pTECs) were freshly isolated from kidney of *Mlkl*- (J. Murphy and W. Alexander, WEHI, Australia[170]), and *Ppif*-deficient mice *(*original strain *Ppiftm1Jmol/J*, Jackson Stock no: 009071) as well as from C57BL/6J (wildtype) mice. All cells were maintained in DMEM/F12 containing 10% fetal calf serum, 1% penicillin-streptomycin, 125 ng/ml prostaglandin E1 , 25 ng/ml EGF, 1.8 µg/ml l-thyroxine, 3.38 ng/ml hydrocortisone and 2.5 mg/ml of insulin transferrin-sodium selenite supplement (I-T-SS). RPMI and DMEM/F12 were used to maintain human kidney cells (HK2) and L929 respectively, including fetal calf serum, 1% penicillin-streptomycin. Peter Nelson and Bruno Luckow, LMU Munich, Germany, kindly provided HK2 and L929 cells, respectively. All cells were cultured under standard conditions (incubator at 370 C, 5% CO2), followed by stimulation with various crystals such as CaOx (1 mg/ml, 1-2 µm size, silica (0.5 mg/ml, 1-5 µM size), MSU (1 mg/ml, 25-125 nm size,), CPPD (0.5 mg/ml, 25-125 nm size), and TiO2 (0.5 mg/ml, 80 nm size). For treatment experiments, cells were pre-treated with MPT inhibitor CsA (0.5 and 1 µm), mitochondrial ROS inhibitor (2R, 4R)-4-aminopyrrolidine-2, 4-dicarboxylate (APDC) (100 and 200 µM), cytochalasin D (CytD) (5 and 10 µM) as phagocytosis (actin-polymerization)

inhibitor, and cathepsin inhibitor CA074Me (10 and 20 μM) for 30 minutes prior to stimulation with crystals. The tetramethylrhodamine ethyl ester (TMRE), lysotracker (Abcam, Cambridge, UK), and the 2', 7'–dichlorofluorescin diacetate (DCFDA) dyes used to evaluate MOMP and ROS production. We used necrosulfonamide (NSA) (5 or 10 μM), dabrafenib (10 μM) or Nec1s (100 μM) as necroptosis inhibitor. Propidium iodide (PI) was used to quantify dead cells and calcein to evaluate live cells according to the manufacturer's protocol. We used a Leica fluorescence microscope (Leica, Wetzlar, Germany) to detect positive fluorescence signals and ImageJ software (USA) to analyze and quantified them. We used the Lactate dehydrogenase (LDH) cell cytotoxicity assay (Roche, Mannheim, Germany) to evaluate cell death in the cell culture supernatants by detecting LDH that was released from dying cells. LDH assay was carried out according to the manufacturer's protocol. Honarpisheh M, et al.[1], Mulay SR, Honarpisheh MM, et al.[2]

3.3.3. Cell death quantification using multi-parameter flow cytometry

HK2 cells were stimulated with various crystals for 24 hours to induced cell death. Cell death was characterized by analyzing different parameters such as size, granularity, phosphatidylserine exposure, plasma membrane integrity, mitochondrial membrane potential, and DNA content[174]. Stimulated cells were harvested and incubated with 400 µl freshly prepared four-color staining solution , which contained 1.8 µg/ml AxA5-FITC, 100 ng/ml PI and 10 nM DiIC1 (5), and 1ng/ml Hoechst 33342 in Ringer's solution for 30 minutes at room temperature. FACSCantoII flow cytometer (BD, Germany) was used to performed flow cytometry experiments. We used FlowJo software (USA) for analyzing the data. Cells were classified according to their position in the forward scatter (FSc; size) versus side scatter (SSc; granularity) dot plot and their staining analyzed as previously described [16]. Briefly, primary necrosis was considered when cells expressed annexinV-FITC+, PI high, DilC1 (5) low, for secondary necrosis, cells expressed annexinV-FITC+, PIlow, DilC1 (5) low-int and for apoptosis cells were annexinV-FITC+, PI−, DilC1 (5) int-high. We recorded 100000 events to assure an equal number of cells. The gating strategy considered as sideward scatter vs. forward scatter and annexinV vs. PI staining. annexinV/PI staining was used to detect different cell populations, then characterized using the DilC1 (5) and Hoechst 33342 dyes. Honarpisheh M, et al.[1]

3.3.4. Histopathology

The kidney tissues from mice were harvested, fixed in 4% formalin and embedded in paraffin. 4 µm sections were stained for haematoxylin and eosin (H&E) and periodic acid–Schiff (PAS). The area of necrotic and tubular casts was evaluated by scoring tubular injury as mentioned above. The primary antibodies RIPK3, MLKL and SMA were used for immunostaining. Mulay SR, Honarpisheh MM, et al.[2]

3.4. RNA analysis

3.4.1. RNA isolation from murine solid organs and cells

We preserved organs in RNA-later immediately after isolation and stored them at -20 °C until RNA isolation. RNA was isolated using a commercial kit. Briefly, 30 mg tissue was homogenized using a blade homogenizer for 30 seconds in lysis buffer (600 µl) containing β-mercaptoethanol (10 µl/ml). The homogenized tissues were centrifuged at 6000 rpm for 5 minutes and 350 µl of supernatants were transferred into fresh RNAas and DNAas free tubes. For cells, media was removed and the cells were harvested using 350 µl lysis buffer with β-mercaptoethanol (10 µl/ml). We used 70% ethanol to mix either lysed cells or homogenized tissues, and loaded them on a RNA column before processing for RNA isolation as per manufacturer's instruction. The purified RNAs were measured and stored at -80 ^{0}C. Honarpisheh M, et al.[3]

3.4.2. Quantification and purity check of RNA samples

The Nanodrop was used to quantify extracted RNA samples. The ratio of 260 nm and 280 nm was considered for RNA purity, which indicates contamination of proteins in the RNA samples. Samples with only a ratio of 1.8 or more were considered to have a good quality. Honarpisheh M, et al.[3]

3.4.3. cDNA conversion

The superscript reverse transcriptase II used for cDNA synthesis. Isolated RNAs were diluted in ultra-pure (RNAs and DNAs free) water to get a final concentration of 1 µg/15µl. We prepared the cDNA conversion reaction by mixing 9 µl 5x buffer , 1 µl 25 mM dNTP mixture, 2 µl 0.1 M DTT, 1 µl 40U/ µl RNAsin , 0.5 µl hexanucleotide, 1 µl of superscript or ultrapure water in the case of the control cDNA (RT minus). The diluted RNAs (1µg) were added to the 13.9 µl master mix reaction and incubated at 42^{0}C for 1 hours and 30 minutes on a thermal

shaker. After incubation, converted cDNAs were stored at 20^0C until usage. We prepared cDNA samples (1:10) for real-time RT-PCR. In short, 10 µl SYBR green master mix, 0.6 µl forward primer and 0.6 µl of reverse primer, which are specific for the target gene, 0.16 µl Taq polymerase and 6.64 µl distilled water mixed with 2µl diluted cDNA samples. Honarpisheh M, et al.[3]

3.4.4. Real-time PCR

We used a SYBR green dye assay (SYBR Green I 96 protocol LC480 Roche) for RT-PCR. Light Cycler 480 was used to the quantification of real-time PCR. Amplification steps included the initiation phase (95 °C), annealing phase (60 °C) and amplification phase (72 °C) with a repetition of 45 times. The primer-blast online tool (NCBI) was used to designed specific primers for genes of interest. In addition, Primers-BLAST tool (NCBI) was used to check specificity of genes. The lengths of product PCR were between 80 to 130 pb. All primers were purchased from Metabion, Martinsried, Germany and are listed in table 3. Distilled water was used as negative control. The efficiency was achieved using the Light Cycler 480 according to the standard curves describing the PCR efficiencies of the gene and the reference gene [ratio = E target Δ CP target (control-sample) / E ref Δ CP ref (control − sample)]. Crossing points (Cp) between 5 and 40 cycles were considered positive signals. Honarpisheh M, et al.[3] The melting curves were analyzed for each sample to detect unspecific products and primer dimers. Honarpisheh M, et al.[3]

3.5. Statistical analysis

To check for normal distribution of the dataset, the Shapiro-Wilk Normal distribution test, the Levene homoscedasticity test and the Grubb outlier test were applied. Student's t-test was only used for the comparison of two normally distributed datasets. Alternatively, in the case of two non-normally distributed datasets, the Wilcoxon-Mann-Whitney test was used. For more than two datasets, the normally distributed and homoscedastic datasets were evaluated by using one-way analysis of variance (ANOVA) with Tukey's post-test. In the case of heteroscedasticity, the post-hoc Games Howell test was used. In case of, two parameters with multiple groups, two-way ANOVA with Bonferroni's comparison post-hoc test was carried out. All statistical analyses were performed using GraphPad Prism 7 (CA, USA). Unless otherwise indicated, data are presented as mean values ± standard error of the mean (SEM). Differences were considered significant if $p<0.05$; non-significant differences (ns) are indicated accordingly. Sample sizes were indicated in each corresponding figure legend.

Table: 3. Oligonucleotide primer sequences used in the study

Gene	**Sequence**		**Accession number**
Mouse			
Tnfr1	Forward:	GTGCGTCCCTTGCAGCCACT	NM_0116094
	Reverse:	GCAACAGCACCGCAGTAGCTGA	
Ripk1	Forward:	GACTGTGTACCCTTACCTCCGA	NM_009068
	Reverse:	CACTGCGATCATTCTCGTCCTG	
Ripk3	Forward:	GAAGACACGGCACTCCTTGGTA	NM_019955
	Reverse:	CTTGAGGCAGTAGTTCTTGGTGG	
Mlkl	Forward:	CTGAGGGAACTGCTGGATAGAG	NM_001310613
	Reverse:	CGAGGAAACTGGAGCTGCTGAT	
Casp8	Forward:	ATGGCTACGGTGAAGAACTGC	NM_009812
	Reverse:	TAGTTCACGCCAGTCAGG	
Fadd	Forward:	CACACAATGTCAAATGCCACCTG	NM_01017
	Reverse:	TGCGCCGACACGATCTACTGC	
Ciap1/2	Forward:	GGACATTAGGAGTCTTCCCACAG	NM_007464
	Reverse:	GAACACGATGGATACCTCTCGG	
Gpx4	Forward:	CCTCTGCTGCAAGAGCCTCCC	NM_001037741
	Reverse:	CTTATCCAGGCAGACCATGTGC	
Ppif (CypD)	Forward:	GGACGCTTGAAAATGTAGAGGTG	NM_026352
	Reverse:	GGATGACTGTCACCAGAGCCAT	
Casp1	Forward:	TCAGCTCCATCAGCTGAAAC	NM_009807
	Reverse:	TGGAAATGTGCCATCTTCTTT	
Nlrp3	Forward:	TCACAACTCGCCCAAGGAGGAA	NM_145827
	Reverse:	AAGAGACCACGGCAGAAGCTAG	
Parp1	Forward:	CTCTCCCAGAACAAGGACGAAG	NM_007415
	Reverse:	CCGCTTTCACTTCCTCCATCTTC	

Tnfr1: Tumor necrosis factor receptor 1, **Ripk1**: receptor-interacting serine/threonine-protein kinase 1, **Ripk3**: receptor-interacting serine/threonine-protein kinase 3, **Mlkl**: mixed lineage kinase domain like pseudokinase, **Casp8**: cysteine-aspartic acid protease 8, **Fadd**: Fas-associated protein with death domain, **Ciap1/2**: cellular inhibitor of apoptosis protein 1, **Gpx4**: glutathione peroxidase 4, **CypD**: cyclophilin D, **Casp1**: cysteine-aspartic acid protease 1, **NLRP3**: nod-like receptor family pyrin domain containing 3, **Parp1**: Poly [ADP-ribose] polymerase 1. Honarpisheh M, et al.[3]

4. Results

4.1. Expression of regulated necrosis-related genes in acute tissue injury

We first sought to determine the expression level of necroptosis- and other regulated-necrosis-related genes in various AKI models such as ischemia-reperfusion injury, acute oxalate nephropathy, and cisplatin nephropathy. We performed histochemistry staining for H&E and PAS to evaluate the extent of injury in our models compared to the baseline level. PAS, H&E staining, and tubular injury score reveal the kidney damage after induction of acute kidney injury in mice (Figure 3A-C). We selected genes that are associated with necroptosis (Tnfr1, Ripk1, Ripk3, *Mlkl*, *Fadd*, and *cIAP-1/2)*, ferroptosis (*Gpx4*), MPT-RN *Ppif* (*CypD*), pyroptosis (Nlrp3 and caspase-1), and parthanatos (Parp1) pathways and performed RT-PCR, to quantify the mRNA expression levels of those genes. We observed high expression levels of necroptosis-related mRNAs such as *Ripk3*, *Mlkl*, and *cIAP-1/2* in all three mouse models of AKI compared to baseline (Figures 4A-B). In addition, *Casp1*, *Nlrp3* mRNAs were highly induced only in IRI and *Tnfr1*, *Casp8* mRNA expression levels were significantly increased only in acute oxalate nephropathy, whereas *Ripk1*, *Casp8*, *Fadd*, *Ppif* (*CypD*), and *Parp1* mRNA levels were significantly down-regulated in cisplatin-induced nephropathy (Figure 3A-B). However, *Gpx4* mRNA expression level did not change in all three acute tissue injury models (Figures 4A-B). Then, we checked the main proteins involved in the necroptosis pathway *Ripk3* and *Mlkl* via immunostaining, and we found that both proteins Ripk3 and Mlkl increased in all three models (Figure 5). Together, these data show that the necroptosis pathway might be involved in all acute kidney injury, whereas the induction of regulated necrosis pathway is highly dependent on the trigger.

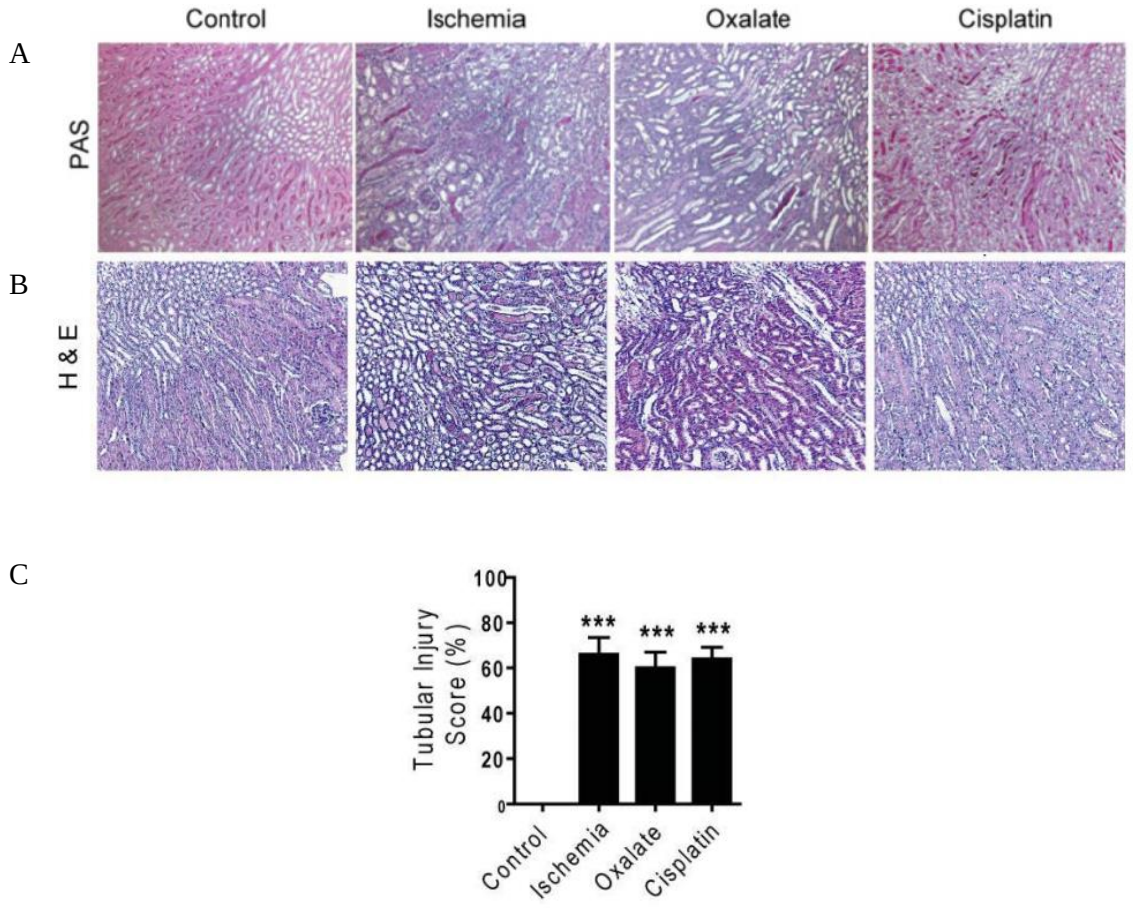

Figure 3. **PAS and H&E staining in acute kidney injury**. Three animal models of acute kidney injury including IRI, oxalate nephropathy, and cisplatin were induced as described in detail in the methods. **(A)** PAS was used to stain kidney sections, Original magnification:×100 **(B)** H&E was used to stain kidney sections. Original magnification: x200. **(C)** Quantification of tubular injury is indicated as percentage. Data presented as means ± SEM. ***P<0.001 either versus control. **PAS**: periodic acid–Schiff, **H&E**: Hematoxylin and eosin.

Honarpisheh M, et al.[3]

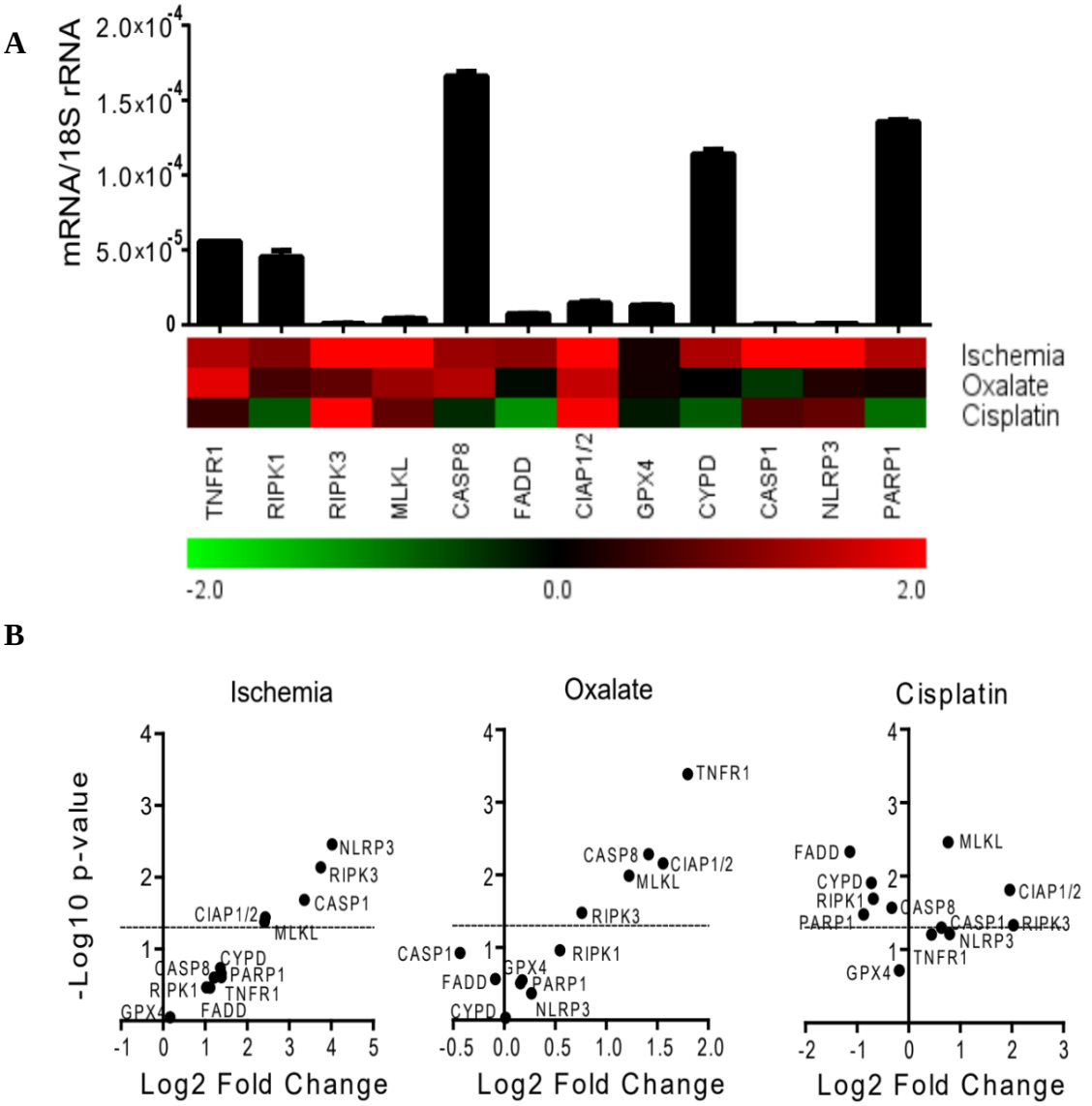

Figure 4. **Expression of necrosis-related mRNA levels in acute kidney injury**. **(A)** Real-time RT-PCR was carried out from the injured kidneys. To normalize the expression level of mRNA 18s rRNA was used as an internal control. The histogram graph shows the level of expression of various genes in the wild-type kidney (control). Data presented as means ± S.E.M. The heatmap shows the relative expression of genes of interest in different models compared with wild-type control group. **(B)** Volcano plots reveal a significant up-regulation and down-regulation of different genes in injured kidneys compared to control kidneys. ***P < 0.05 indicated as statistically significant. Dotted lines represent P = 0.05.

Honarpisheh M, et al.[3]

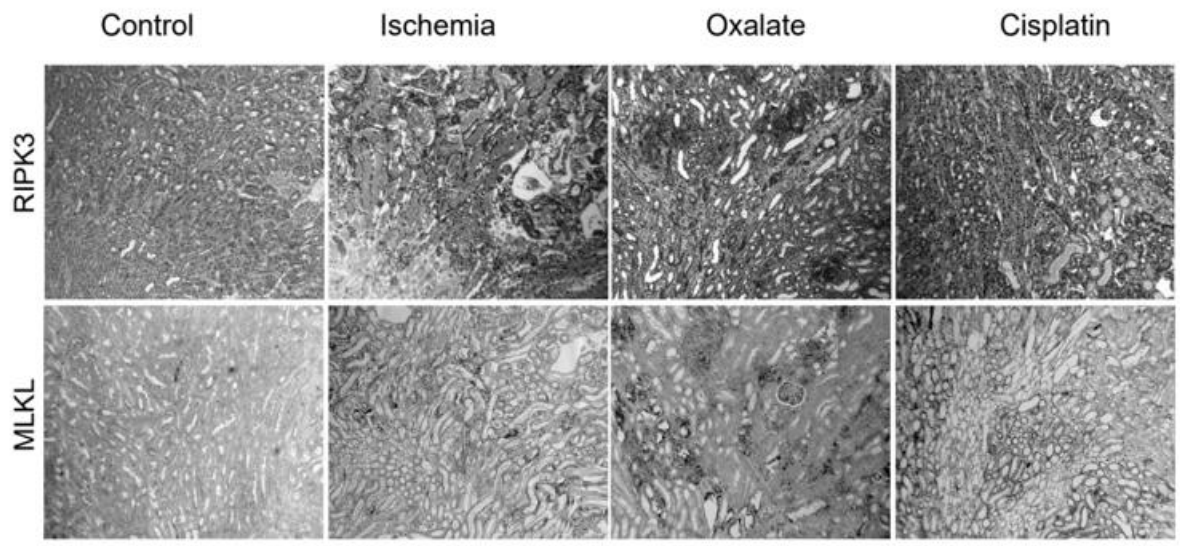

Figure 5. **Increase expression level of Ripk3 and Mlkl in acute organ injury**. Immunostaining of kidney sections from mice with AKI that were stained for RIPK3 and MLKL, Original magnification: ×100. **Ripk3**: receptor interacting serine/threonine kinase 3, **Mlkl:** mixed lineage kinase domain-like pseudokinase.

Honarpisheh M, et al.[3]

4.2. Differential regulation of necrosis-related genes in chronic oxalate nephropathy

Progression of tissue injury leads to chronic tissue remodelling[175, 176] and several inflammatory cells infiltrate into the injury site and promote fibrosis by producing pro-fibrotic proteins.[177,178] To investigate the change in expression levels of regulated necrosis-related genes, we made use of the well-established murine model of chronic oxalate nephropathy.[171] For this, mice were fed an oxalate-rich diet containing 50 μmol/g sodium oxalate in a calcium-free standard chow diet, [171] and sacrificed on day 7, 14 and 21. PAS, alpha-SMA, and collagen 1α1 staining showed progression of kidney damage starting from day 7, which further increased until day 21 (Figure 6A). In addition, tubular injury as the hallmark of kidney damage significantly increased upon feeding mice an oxalate-rich diet at day 7, 14 and 21 (Figure 6B). This was consistent with more fibrotic lesions as indicated by alpha-SMA and collagen 1α1 (Figure 6A).

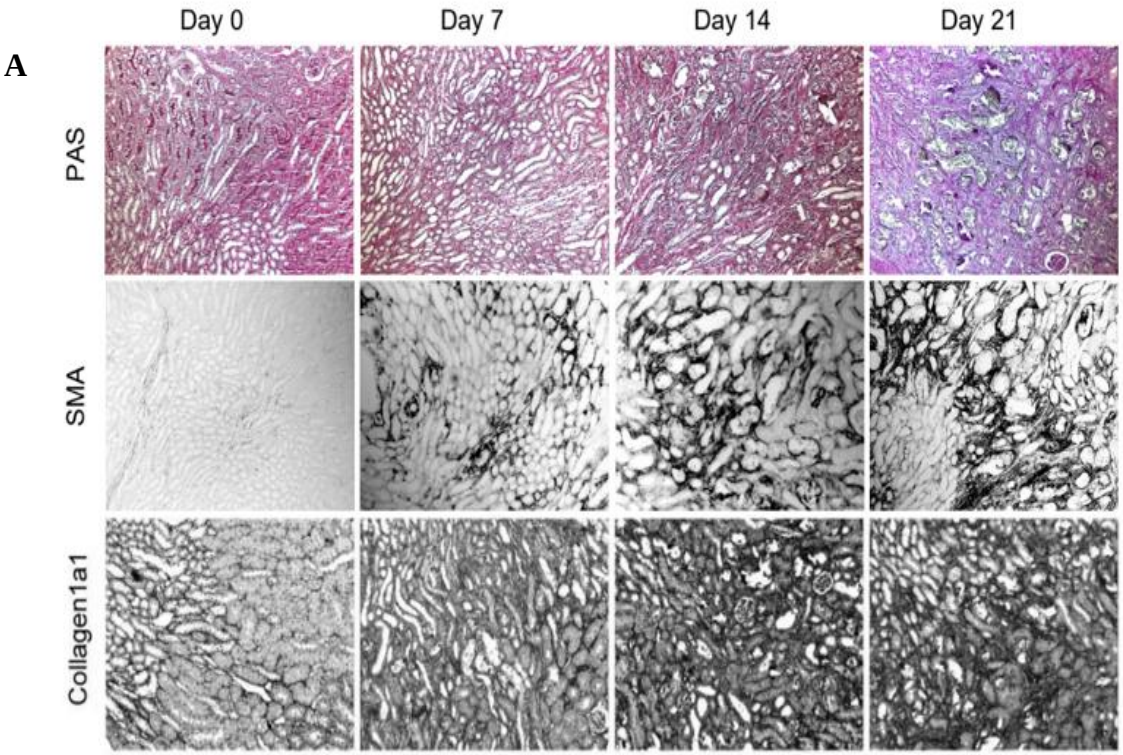

Figure 6. **PAS, H&E and collagen 1a1 staining in chronic oxalate nephropathy. (A)** Representative images of kidney sections stained for PAS, SMA on day 0, 7, 14 and 21. Original magnification: ×100 and collagen 1a1 at day 0, 7, 14 and 21. Original magnification: x200. **(B)** PAS injury score was determined as described in the method and material section. Data presented as means ± SEM. ***P<0.001 either versus day 0. **PAS**: Periodic acid–schiff, H**&E**: hematoxylin and eosin. **SMA**: smooth muscle actin.

Honarpisheh M, et al.[3]

Next, we checked the expression levels of regulated necrosis-related molecules in chronic oxalate nephropathy. As expected, the mRNA as well as protein expression levels of the necroptosis-specific genes Ripk3 and Mlkl significantly increased on day 7 and 14 (Figures 7A-B and 8). Of note, the mRNA and protein expression levels of *Ripk3* were still significantly higher compared to mRNA and protein expression level of *Mlkl* (Figures 7A-B and 8). In addition, the upstream genes of the necroptosis pathway *Tnfr1* and *cIAP1/2* were significantly increased as well as the pyroptosis-related genes *Nlrp3* and *Casp1* during the chronic oxalate nephropathy on day 7, 14 and 21, whereas, *Ripk1*, *Casp8*, *Fadd*, *Gpx4*, *Ppif* (*CypD*), and *Parp1* mRNA expressions significantly decreased (Figures 7-B and 8). Taken together, the data show that necroptosis might be involved in chronic oxalate nephropathy by activating Ripk3 and Mlkl proteins.

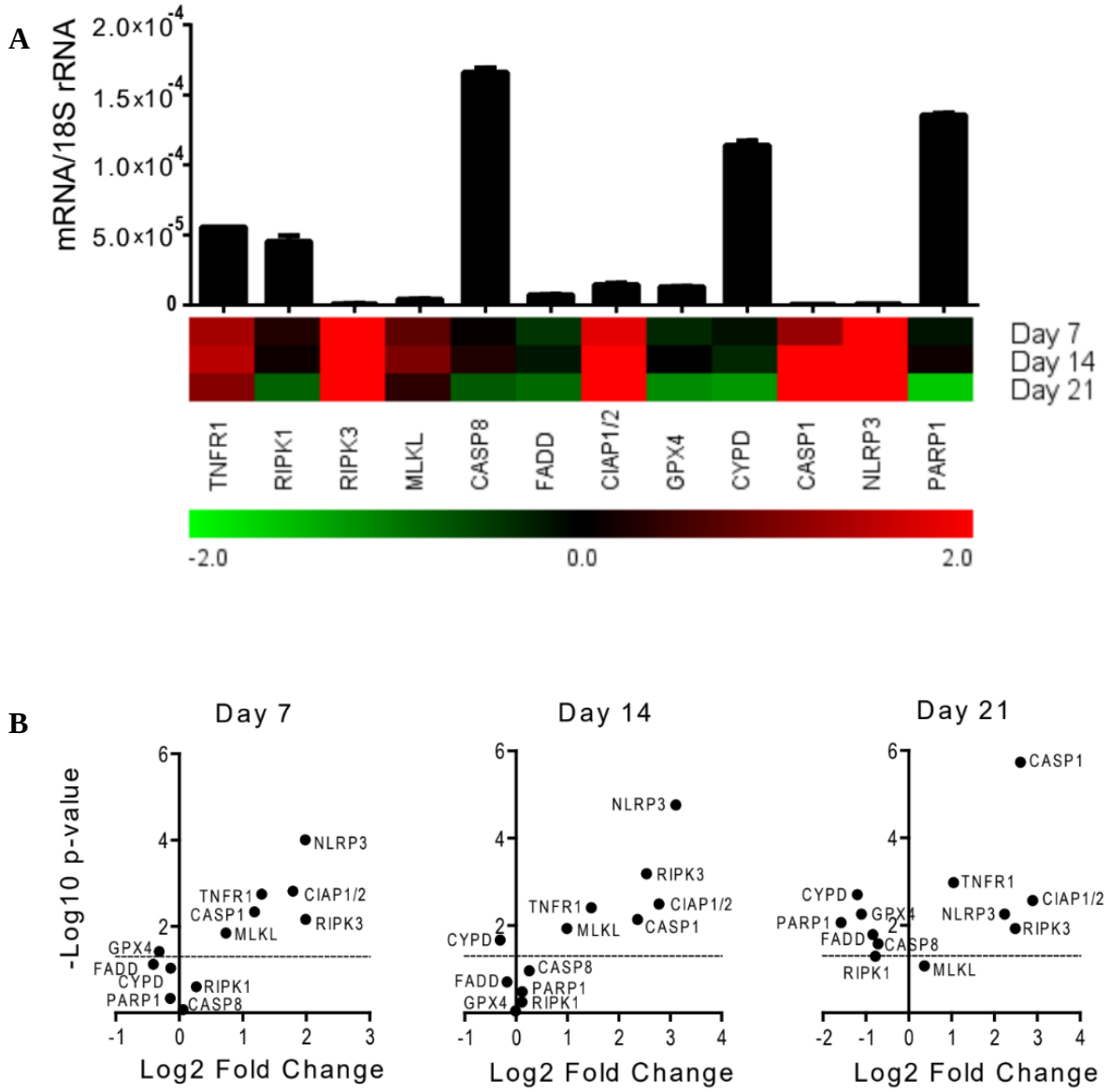

Figure 7. **Expression of necrosis-related mRNA levels in chronic oxalate nephropathy. (A)** RT-PCR was performed on the damaged kidneys at day 0, 7, 14 and 21 and the mRNA expression level normalized to 18s rRNA as an internal control. The bar graph shows the expression levels of various genes of wild-type kidney (control). Data presented as means ± S.E.M. The heatmap shows the expression of mRNA levels at day 7, 14 and 21 compared with day 0. **(B)** Volcano graphs show significant up- and down-regulation of various genes in damaged kidneys at day 7, 14 and 21 compared with day 0. ***P < 0.05 indicated as statistically significant. Dotted lines represent P = 0.05. **RT-PCR**: real-time polymerase chain reaction.

Honarpisheh M, et al.[3]

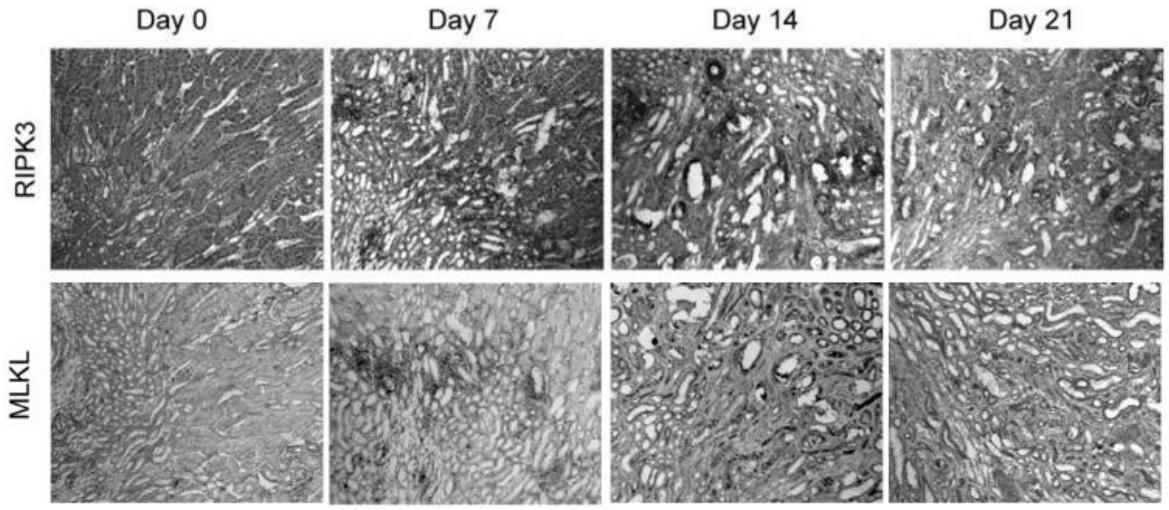

Figure 8. **Increase expression level of Ripk3 and Mlkl proteins in chronic oxalate nephropathy at day 0, 7, 14 and 21.** Kidneys from mice with chronic oxalate nephropathy were harvested and kidney sections stained to determine Ripk3 and Mlkl protein expression level on day 0, 7, 14 and 21. Original magnification: ×100 and collagen1a1 at day 0, 7, 14 and 21. Original magnification: x200. **Ripk3**: Receptor Interacting Serine/Threonine Kinase 3, **Mlkl**: mixed lineage kinase domain-like pseudokinase.

Honarpisheh M, et al.[3]

4.3. Crystalline particles induce cell death in human tubular epithelial cells

Next, we investigated whether metabolic and environmental crystals can induce cell death and whether their specific shape and size have an effect on cell death. To address this issue, we used various environmental and metabolic crystalline particles with different shapes and sizes including, CaP (rhomboid and prism shape, 0.2–1 µm size), silica (sphere shape, 1–1.5 µM size), TiO2 (sphere shape, 80 nm size), cholesterol (rhomboid shape, 0.2–1.5 µm size), CaOx (rhomboid and prism shape, 1–2 µm size), and MSU (needle-like shape, 1–2 µm size). We visualized all crystals by light microscopy and TEM; all crystals had completely different sizes and shapes. As shown in (Figure 9A-B). To check the cytotoxicity of these crystals, HK2 cells were exposed to different concentrations of CaP (0.15, 0.25, 0.5 and 1 mg/ml), silica, TiO2 (0.15, 0.25 and 0.5 mg/ml), cholesterol (1, 2, and 3 mg/ml), CaOx (0.15, 0.25, 0.5 and 1 mg/ml), MSU (0.15, 0.25 and 0.5 mg/ml) for 24 hours. The LDH assay revealed that all crystals were able to induce cell death in a dose-dependent manner (Figure 10). In further experiments, we selected only one concentration of each crystal type for CaP 1mg/ml, TiO2 0.5 mg/ml,

cholesterol 3 mg/ml, CaOx 1 mg/ml, and MSU 0.5 mg/ml, and applied PI (for staining the death cells) and acridine orange (for staining the live cells) staining after 24 hours stimulation to confirm the LDH assay data. Those cells that died upon crystal stimulation were positive for PI (red color) whereas, the live cells were positive for acridine orange (green color) (Figure 11A). Fluorescence imaging revealed that crystals induced an increase in the mean fluorescence intensity (MFI) of PI compared to untreated cells (Figure 11B). Taken together, these data clearly showed that crystals regardless of their sizes and shapes were able to induce cell death in HK2 cells.

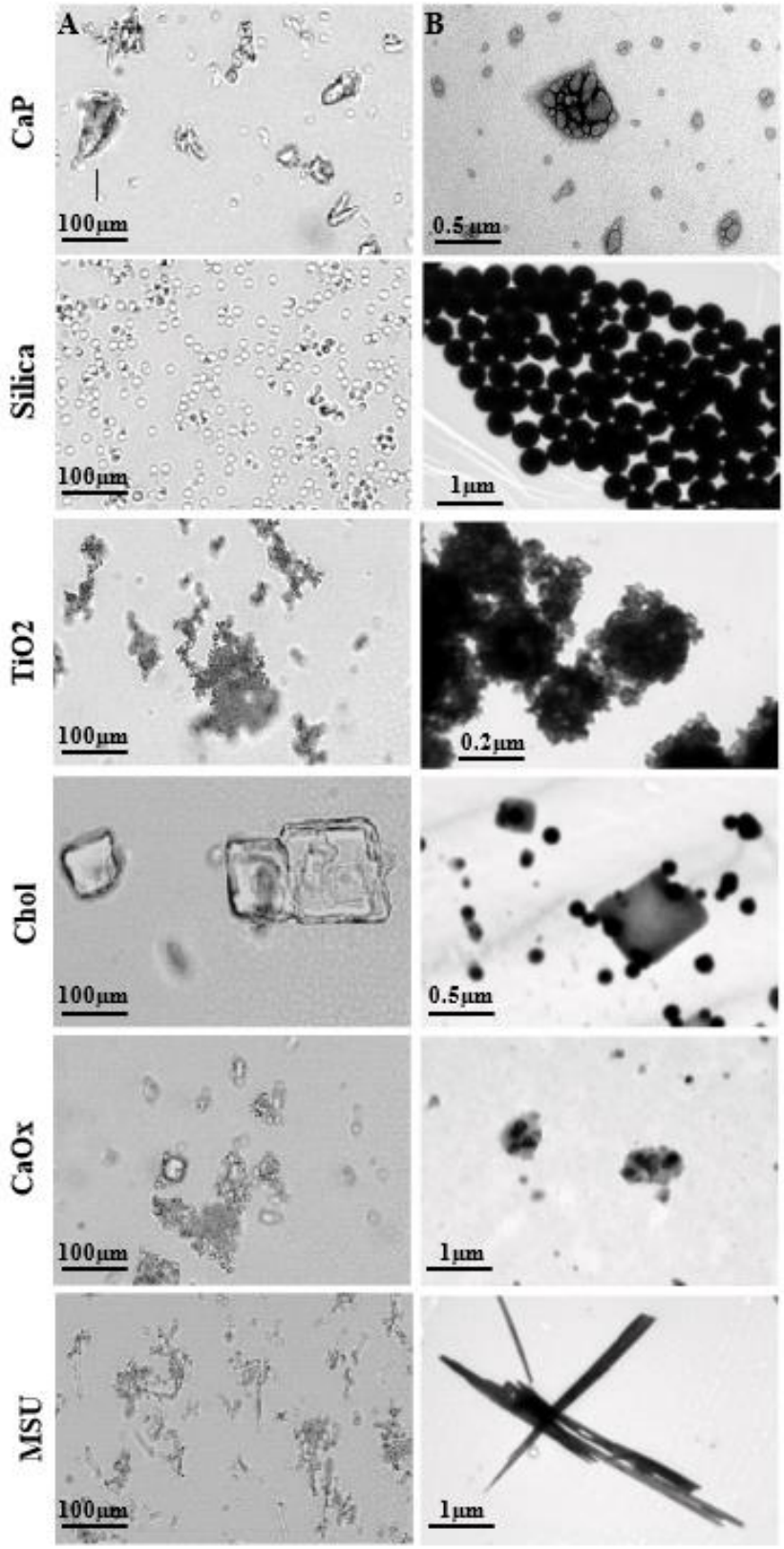

Figure 9. **Light microscopy and transmission electron microscopy of crystalline particles.** (**A**) Light microscopy, and (**B**) TEM was used to show differences in the size and shape of crystals including CaP, silica, cholesterol, and TiO2 nanoparticles. **TEM**: transmission electron microscopy, **CaP**: calcium phosphate, **TiO2**: titanium dioxide.

Honarpisheh M, et al.[1]

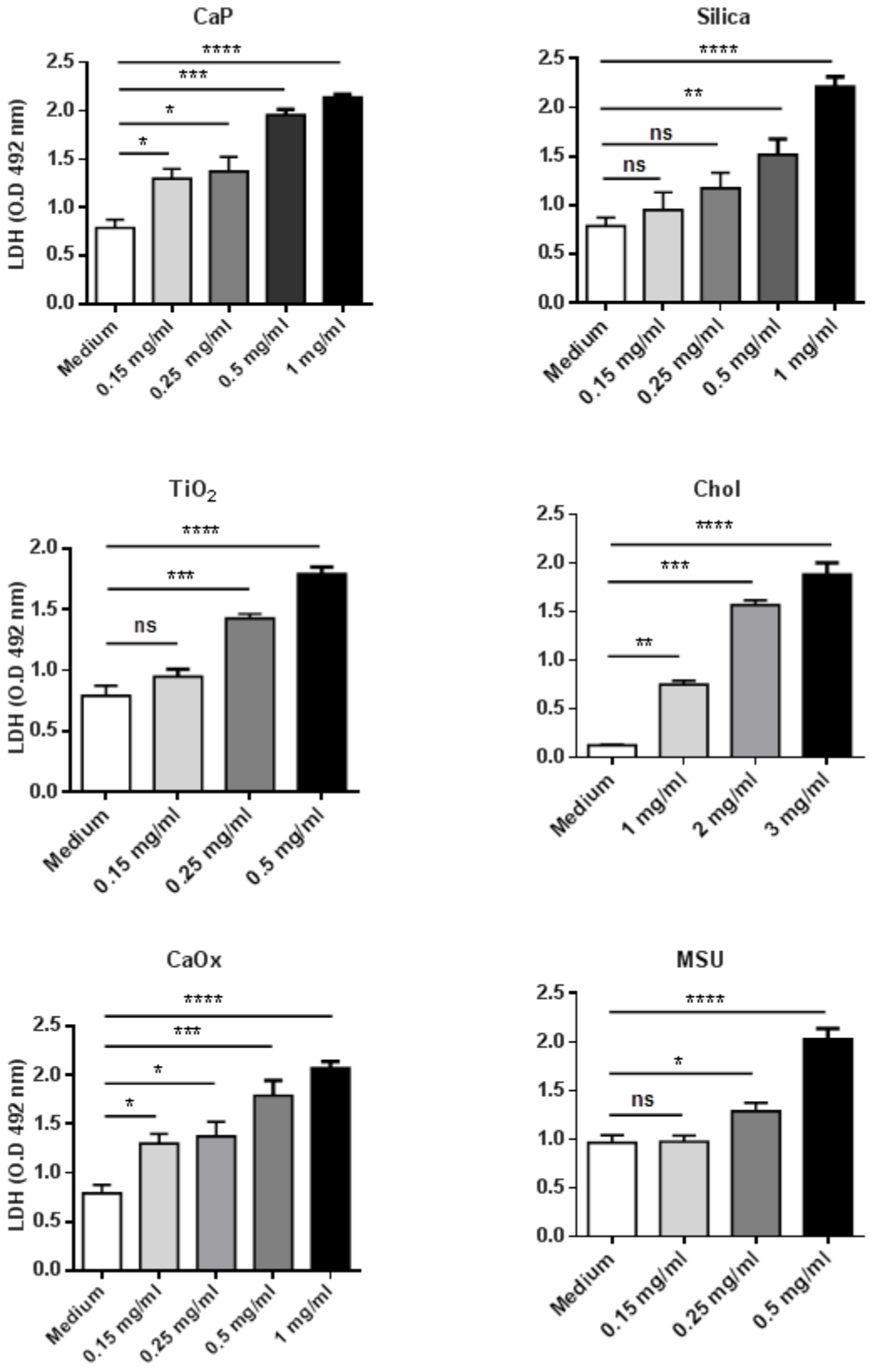

Figure 10. **Crystalline particles induce cell death in HK2 cells.** HK2 cells were stimulated with CaP, silica, TiO2, cholesterol, CaOx, and MSU crystals at various concentrations for 24 hours. The LDH was used to check cytotoxicity of crystals. Data are presented as mean ± SEM from three independent experiments, *p<0.05, *** p<0.001. n.s. = not significant vs vehicle. **LDH**: Lactate dehydrogenase. Honarpisheh M, et al.[1]

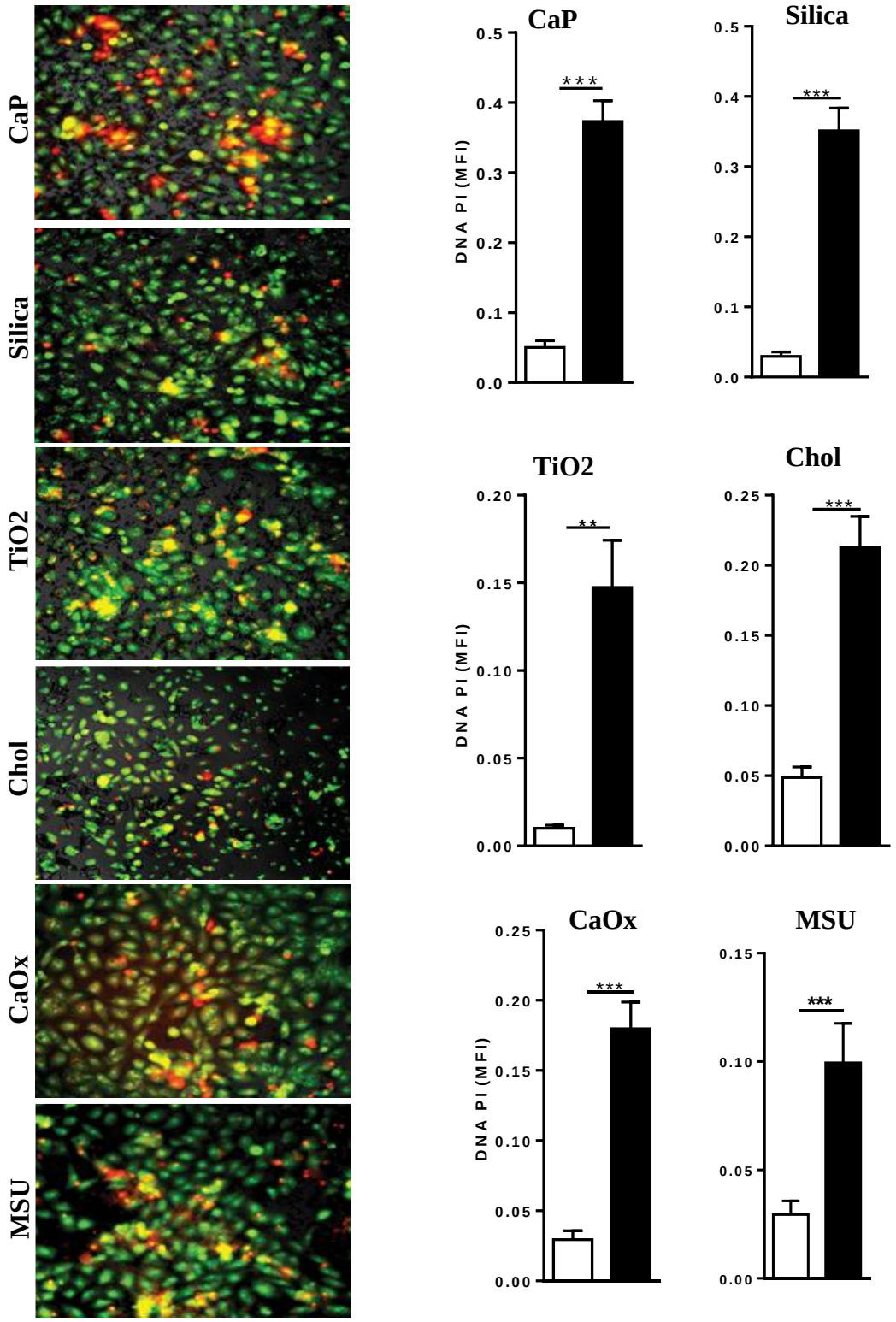

Figure 11. **Crystalline particles induce cytotoxicity in HK2 cells. (A)** HK2 cells were stimulated with 1 mg/ml CaP, 1 mg/ml silica, 0.5 mg/ml TiO2, 3 mg/ml cholesterol, 1 mg/ml CaOx, and 0.5 mg/ml MSU crystals for 24 hours. Cells were stained with PI in red color and acridine orange in green color. **(B)** PI signals were quantified and represented as MFI. Data are presented as mean±SEM from three independent experiments, *p<0.05, *** p<0.001. n.s. = not significant vs vehicle. **CaP**: calcium phosphate, **TiO2:** titanium dioxide**, CaOx**: calcium oxalate,**MSU**: monosodium urate, **PI**: propidium iodide, **MFI**: mean fluorescence intensity.

Honarpisheh M, et al.[1]

4.4. Crystalline particles induce primary necrosis in human tubular epithelial cells

To investigate the mechanism of crystalline particle-induced cell death, we carried out multi-color flow cytometry and determined the type of cell death based on the positivity of hoechst 33342, annexin V-FITC, 1,1′-dioctadecyl-3,3,3′,3′-tetramethyl-indocarbocyanine perchlorate (DiLC1) or PI staining. We found that environmental and metabolic crystalline particles of different sizes and shapes mostly induced primary necrosis (annexinV-FITC+, PI high, DilC1(5)low) in HK2 cells (Figure 12). Secondary necrotic cells were identified as annexinV-FITC+, PI low, DilC1(5)low-int and apoptotic cells as annexinV-FITC+, PI−, DilC1(5)int-high[174] (Figure 12). To investigate the role of apoptosis in crystals induced cell death, we used the pan-caspase inhibitor zVAD-FMK to block apoptosis. As shown in Figure 13, blocking apoptosis with zVAD-FMK did not reduce the PI positive signal in HK2 cells stimulated with crystals (Figure 13). Taken together, we conclude that crystals or crystalline particle-induced cell death mainly involves primary necrosis (necroptosis) and not apoptosis because this crystal-induced cell death was independent of caspase activity.

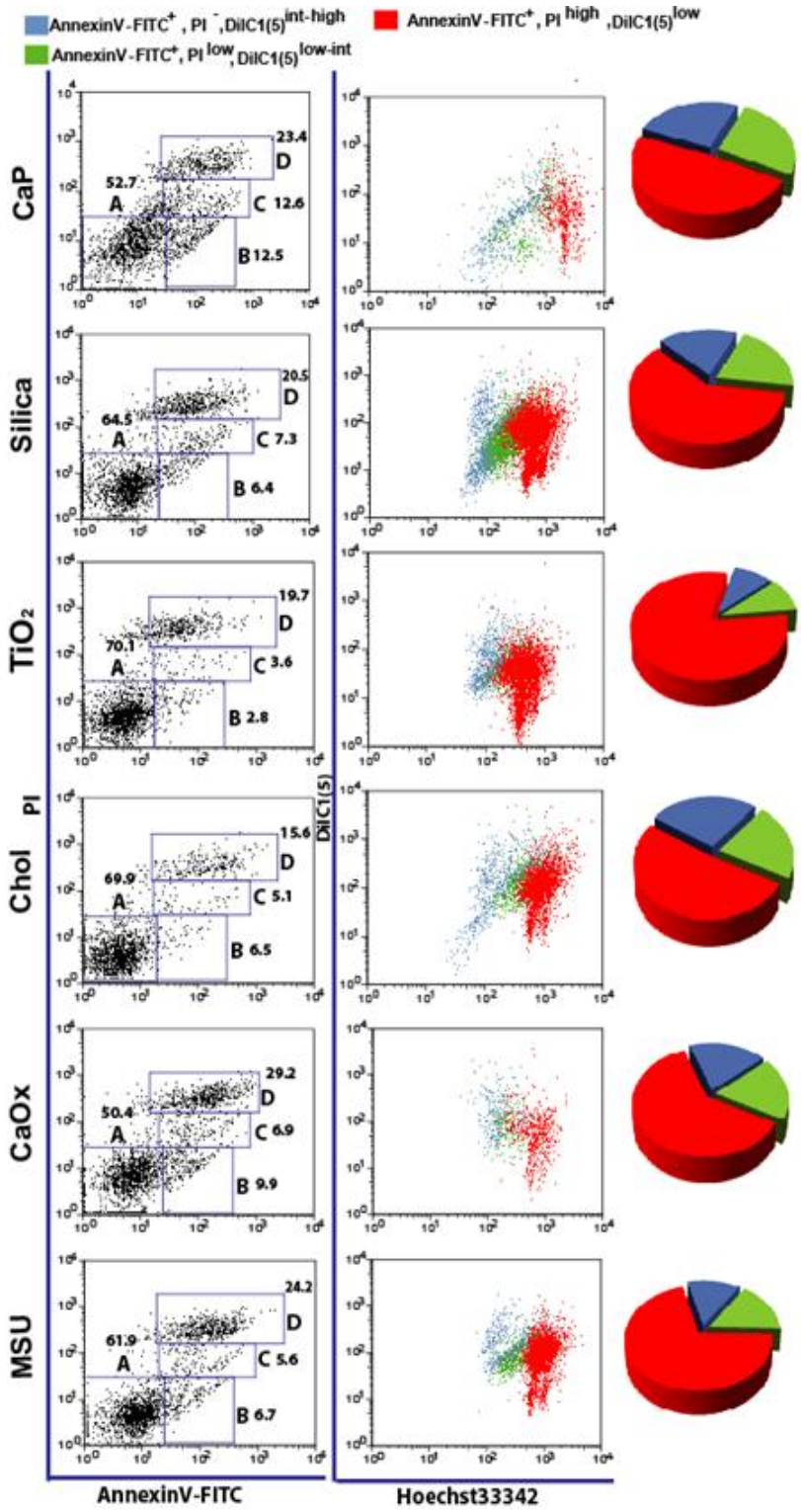

Figure 12.**Crystals induce primary necrosis in HK2 cells**. HK2 cells were stimulated with 1 mg/ml CaP, 1 mg/ml silica, 0.5 mg/ml TiO2, 3 mg/ml cholesterol, 1 mg/ml CaOx, and 0.5 mg/ml MSU crystals for 24 hours. Multicolor FACS was used to determine different types of cell death as described in the material and method section. Analysis revealed primary necrosis as main form of cell death in crystal-induced HK2 cells. Primary necrotic cells were identified as annexinV-FITC+, PI high, DilC1 (5) low, and secondary necrotic cells as annexinV-FITC+, PI low, DilC1(5)low-int, and apoptosis: annexinV-FITC+, PI−, DilC1(5)int-high. **CaP**: calcium phosphate, **TiO2:** titanium dioxide**, CaOx**:calcium oxalate, **MSU**: monosodium urate, **FITC**: fluorescein isothiocyanate, **PI**: propidium iodide, **DilC1(5)**: 1,1′,3,3,3′,3′-hexamethylindodicarbo - cyanine iodide. Honarpisheh M, et al.[1]

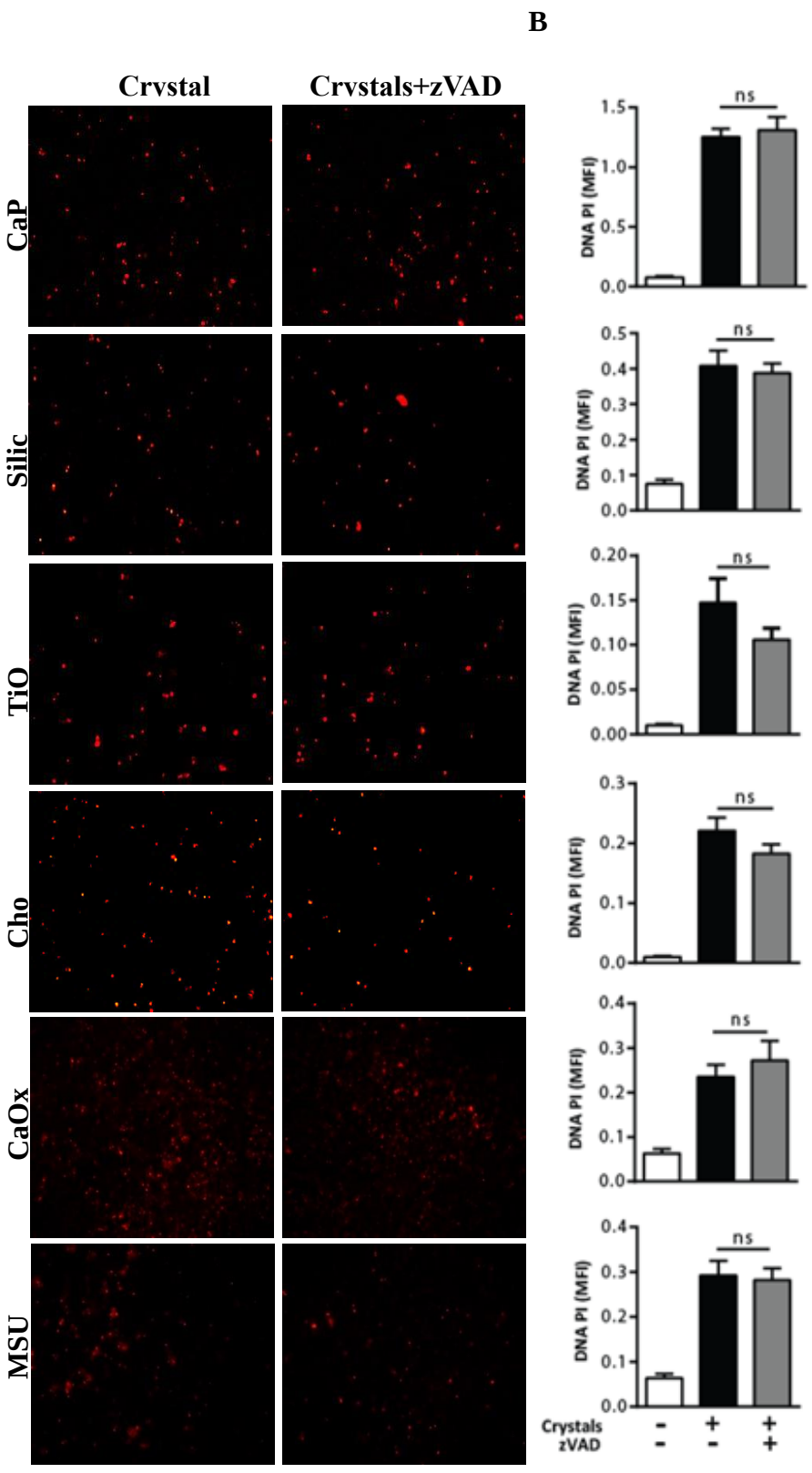

Figure 13. **Cell death analysis of HK2 cells expose to crystalline particles in presence or absence of zVAD. (A)** HK2 cells were pretreated with zVAD-FMK, a pan-caspase inhibitor (10 µl) for 30 minutes prior to stimulation with 1 mg/ml CaP, 1 mg/ml silica, 0.5 mg/ml TiO2, 3 mg/ml cholesterol, 1 mg/ml CaOx, and 0.5 mg/ml MSU crystals for 24 hours. Cells were stained with PI. **(B)** PI was quantified and represented as MFI with ImageJ software. Data are presented as mean ± SEM from three independent experiments, *p<0.05, *** p<0.001. n.s. = not significant vs vehicle.

CaP: calcium phosphate, **TiO2:** titanium dioxide**, CaOx**: calcium oxalate, MSU: monosodium urate, **PI**: propidium iodide. **MFI**: mean fluorescence intensity.

Honarpisheh M, et al.[1]

4.5. Necroptosis inhibition with chemical inhibitors of RIPK1, RIPK3, and MLKL reduce crystal-induced cell necrosis

To confirm the involvement of the necroptosis pathway in crystal-induced cell death we used the RIPK1 inhibitor Nec1s, the RIPK3 inhibitor dabrafenib and the MLKL inhibitor NSA. HK2 cells were pre-treated with Nec1s (100 µM), dabrafenib (10 µM) and NSA (5 and 10 µM) 30 minutes prior stimulation with different crystals, including CaP (1 mg/ml), silica (1 mg/ml), TiO2 (0.5 mg/ml), cholesterol (3 mg/ml), CaOx (1 mg/ml), and MSU (0.5 mg/ml) for up to 24 hours. Cell death was analysed via PI and acridine orange staining (Figure 14A-B and 15A-B). Stimulation of HK2 cells with crystals resulted in an increased PI positivity (Figure 14A-B and15A-B), a cytotoxic effect that was significantly reduced in the presence of the inhibitorsNec1s, dabrafenib and NSA. In addition, we also checked for cellular toxicity of crystals in HK2 cells using the LDH assay. To do so, HK2 cells were pre-treated with Nec1s (100 µM), dabrafenib (10 µM), and NSA (5 and 10 µM) prior to stimulation with crystals for 24 hours and supernatants were collected. The results showed that all three necroptosis inhibitor reduced the LDH signals compared with vehicle-treated crystal-stimulated HK2 cells (Figure 16A-B).

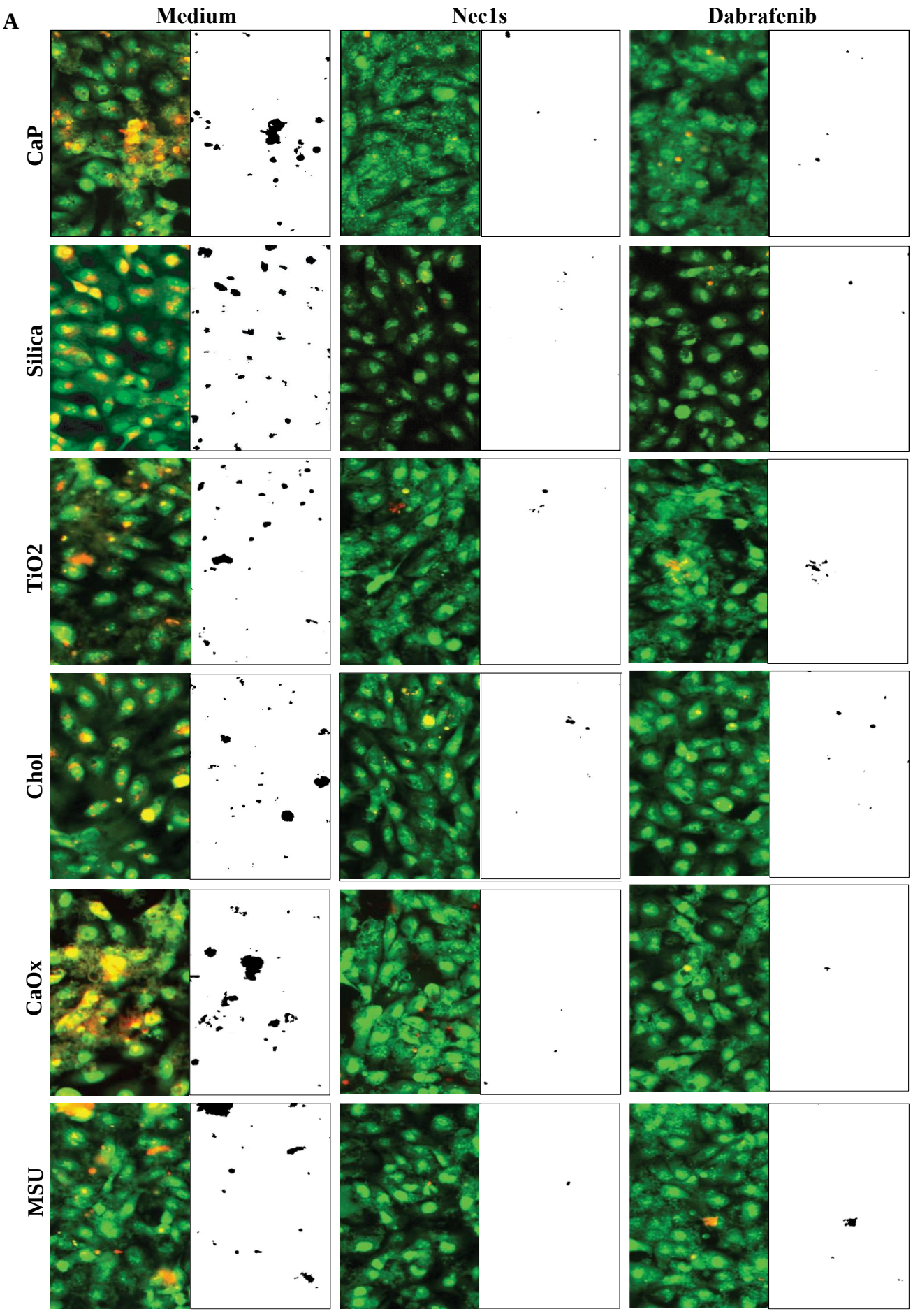
A
Medium
Nec1s
Dabrafenib
CaP
Silica
TiO2
Chol
CaOx
MSU

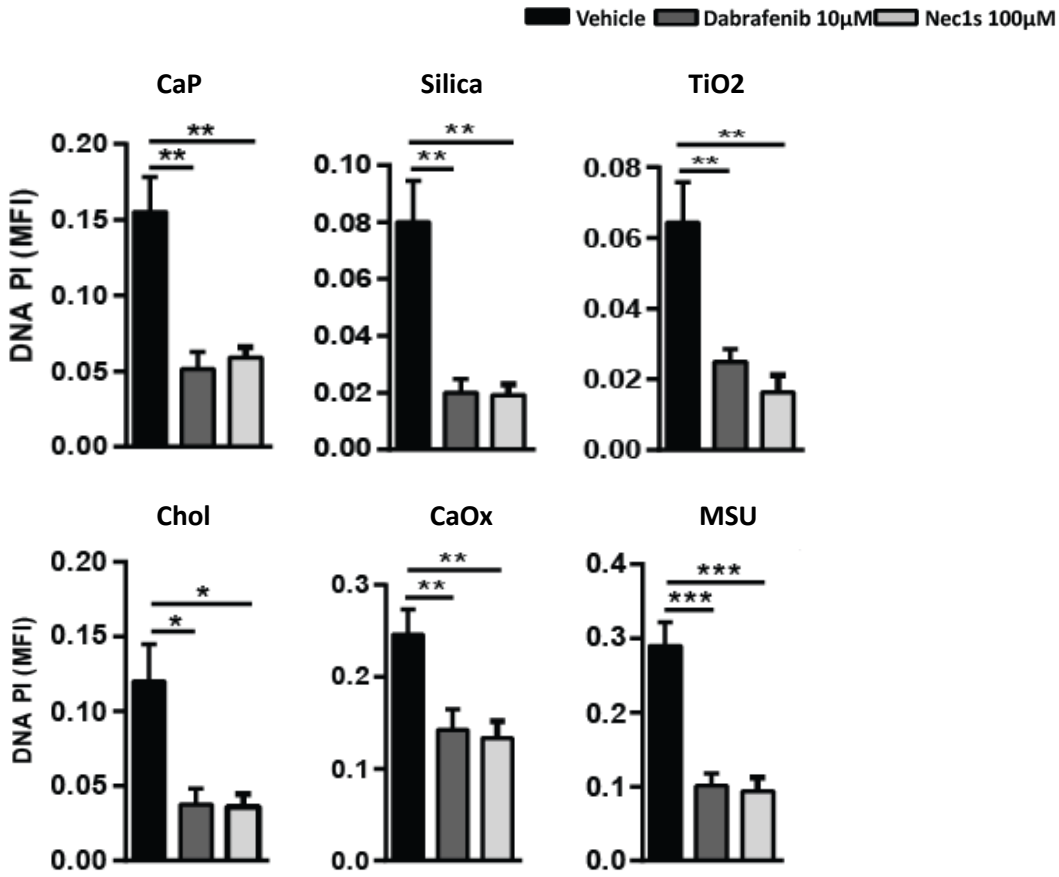

Figure 14. **Necroptosis inhibitors reduce cell death in HK2 cell in presence of crystalline particles. (A)** HK2 cells were pretreated with Nec1s (100 µM), dabrafenib (10 µM) for 30 minutes prior to stimulation with 1 mg/ml CaP, 1 mg/ml silica, 0.5 mg/ml TiO2, 3 mg/ml cholesterol, 1 mg/ml CaOx, and 0.5 mg/ml MSU crystals for 24 hours. After stimulation, cells were stained with PI in red color and acridine orange in green color. Images were taken from the PI staining and converted into black and white using ImageJ software. **(B)** PI quantification is presented as MFI. Data are expressed as mean ± SEM from three independent experiments, *p<0.05, *** p<0.001. n.s. = not significant vs vehicle. **CaP**: calcium phosphate, **TiO2:** titanium dioxide**, CaOx**: calcium oxalate, MSU: monosodium urate, **PI**: propidium iodide. **MFI**: mean fluorescence intensity, **Nec1s:** Necrostatin-1s.

Honarpisheh M, et al.[1]

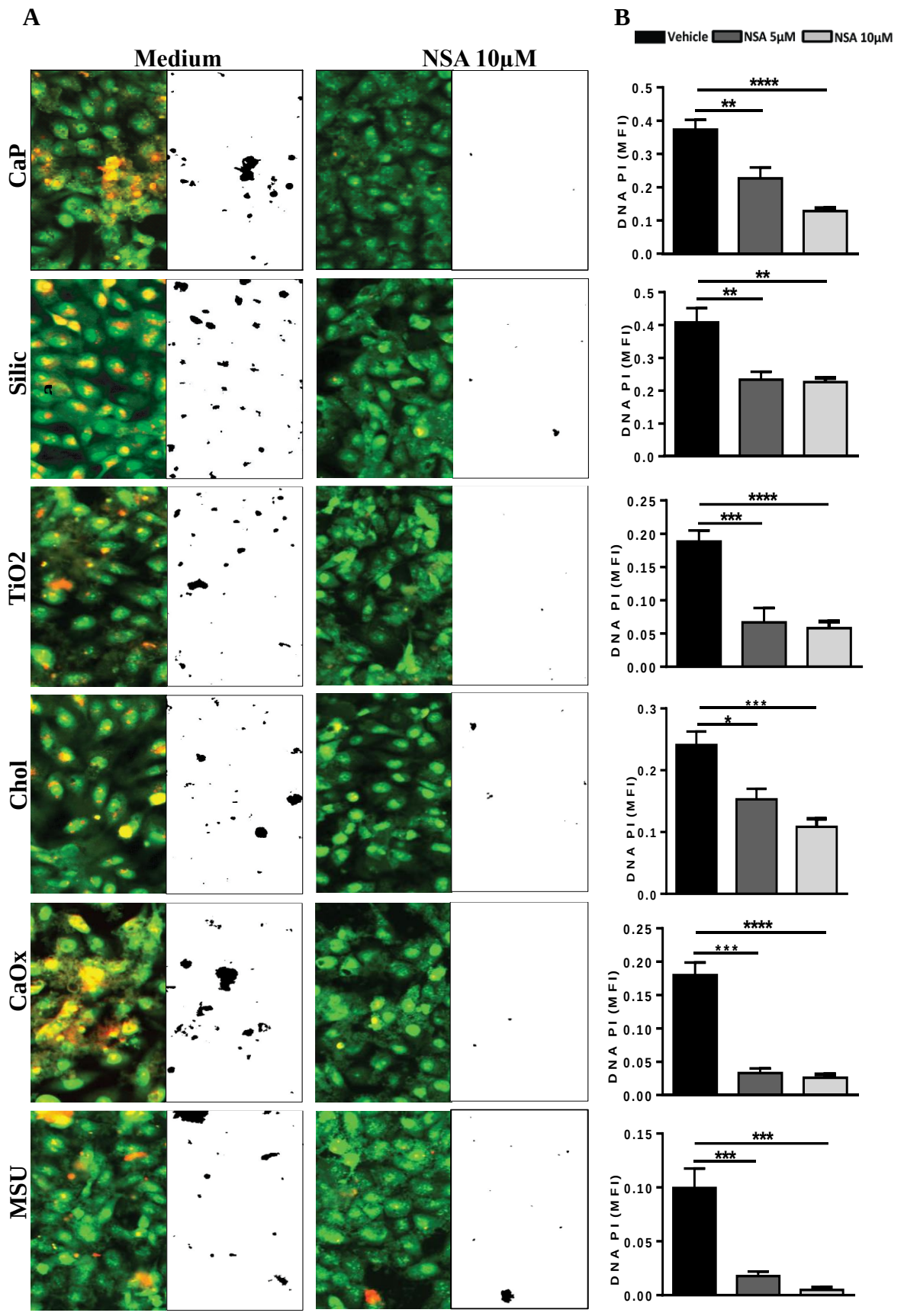
A
Medium
NSA 10µM
CaP
Silic
TiO2
Chol
CaOx
MSU
B
Vehicle
NSA 5µM
NSA 10µM
DNA PI (MFI)
****
**
**
**
****
***
***
*
****
***
***
***

Figure 15. **MLKL inhibitor (NSA) decrease cell death in HK2 cells. (A)** HK2 cells were pretreated with NSA (5 μM and 10 μM) 30 minutes prior to stimulation with 1 mg/ml CaP, 1 mg/ml silica, 0.5 mg/ml TiO2, 3 mg/ml cholesterol, 1 mg/ml CaOx, and 0.5 mg/ml MSU crystals for 24 hours. Cells were stained with PI in red color and acridine orange in green color. Images collected from PI staining were converted into black and white using ImageJ software. **(B)** PI quantification is presented as MFI. Data are expressed as mean ± SEM from three independent experiments, *p<0.05, *** p<0.001. n.s. = not significant vs vehicle. **CaP**: calcium phosphate, **TiO2:** titanium dioxide**, CaOx**: calcium oxalate, **MSU**: monosodium urate, **PI**: propidium iodide. **MFI**: mean fluorescence intensity, **NSA**: necrosulfonamide.

Honarpisheh M, et al.[1]

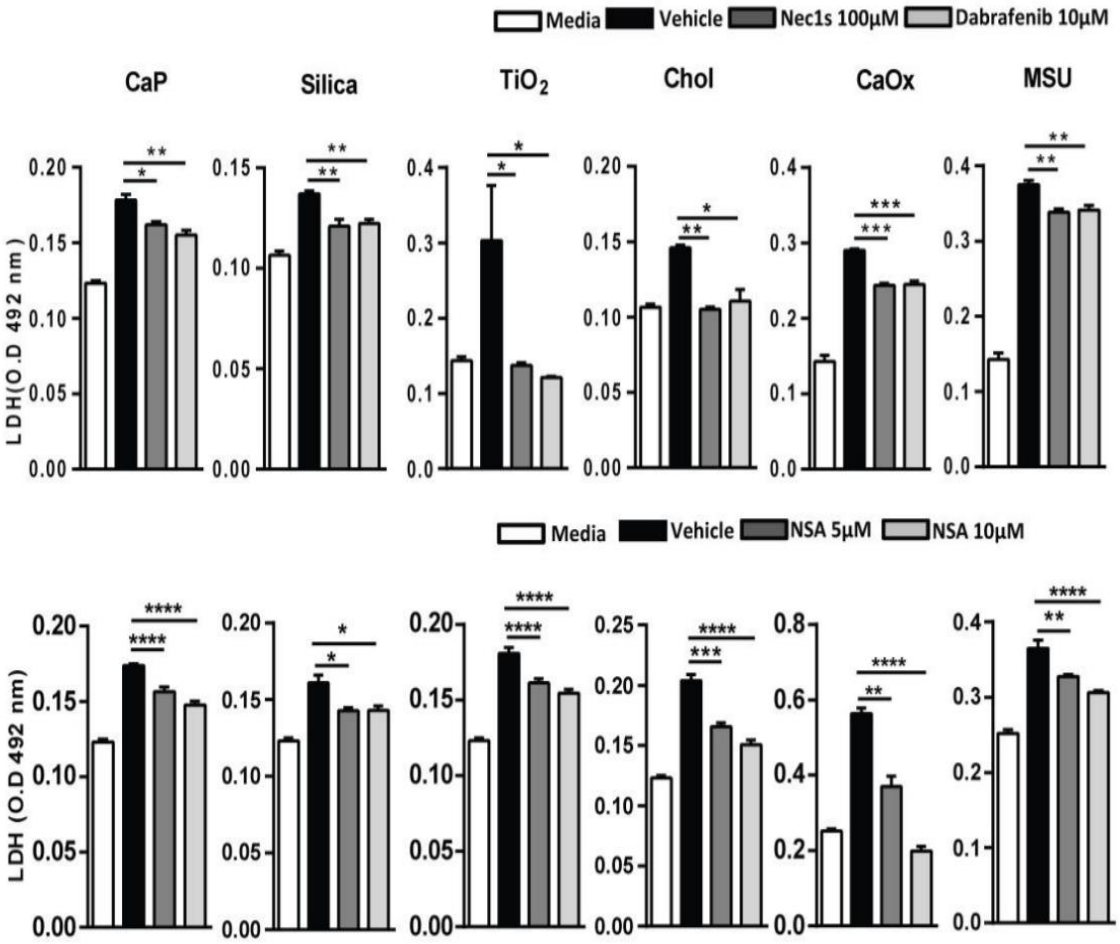

Figure 16. **MLKL inhibitor (NSA) decrease cell death in HK2 cells.** HK2 cells were pretreated with Nec1s (100 μM), dabrafenib (10 μM) or NSA (5 μM and 10 μM) for 30 minutes prior to stimulation with 1 mg/ml CaP, 1 mg/ml silica, 0.5 mg/ml TiO2, 3 mg/ml cholesterol, 1 mg/ml CaOx, and 0.5 mg/ml MSU crystals for 24 hours. LDH assay was used to analyze cell death after 24 hours by quantifying the LDH release in cell culture supernatants. Data are presented as mean ± SEM from three independent experiments, *p<0.05, *** p<0.001. n.s. = not significant vs vehicle. **CaP**: calcium phosphate, **TiO2:** titanium dioxide**, CaOx**: calcium oxalate, **MSU**: monosodium urate, **PI**: propidium iodide. **MFI**: mean fluorescence intensity, **NSA**: necrosulfonamide, **Nec1s**: necrostatin-1s, **LDH**: lactate dehydrogenase

Honarpisheh M, et al.[1]

4.6. *RIPK3* knock-down or *Mlkl* deficiency reduce cytotoxicity of crystalline particles in human and mouse tubular epithelial cells

In addition, we applied a genetic approach to further validate our results, because of potential off-target effects of the chemical necroptosis inhibitors. To address this issue, we knocked down *RIPK3* using siRNA with a Neon electroporation system. HK2 cells were transfected with 120 nm of siRNA against the *RIPK3* or scramble control group for 48 hours. The electroporation parameters were optimized for HK2 as described in the method and material section and the transfection efficacy was evaluated using RT-PCR for *RIPK3* mRNA levels (Figure 17). After optimization, transfected HK2 cells were stiumulated with 1 mg/ml CaP, 1 mg/ml silica, mg/ml TiO2 0.5, 3 mg/ml cholesterol, 1 mg/ml CaOx, and 0.5 mg/ml MSU crystals, and cell death determined by quantification of PI positivity and LDH assay. As expected, the number of PI positive HK2 cells and LDH levels were reduced in transfected HK2 cells with siRNA-*Ripk3* compared to scramble siRNA upon stimulation with various crystal types (Figure 18A-C).

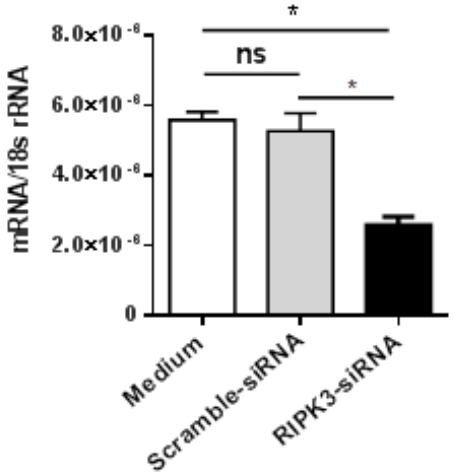

Figure 17. **siRNA against *RIPK3* decrease *RIPK3* mRNA level in HK2.** Transfection of HK2 cells was carried out using 120 nm of siRNA against *RIPK3* or scramble group for 48 hours. The efficiency of siRNA was checked by RT-PCR for *RIPK3*. Data are expressed as mean ± SEM from three independent experiments, *p<0.05, *** p<0.001. n.s. = not significant vs vehicle. **RIPK3**: receptor interacting serine/threonine kinase 3.

Honarpisheh M, et al.[1]

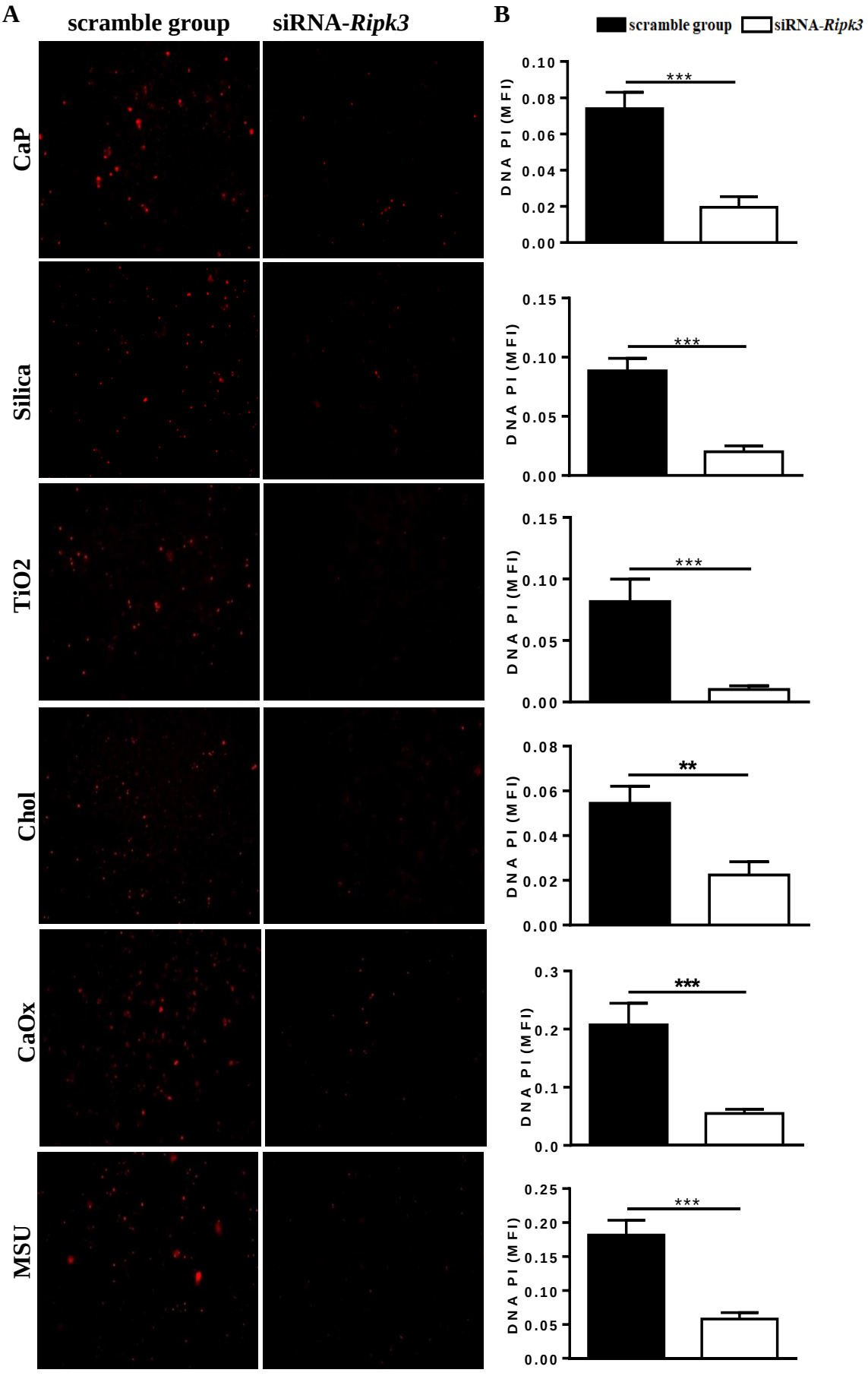
A
scramble group
siRNA-Ripk3
CaP
Silica
TiO2
Chol
CaOx
MSU
B
scramble group
siRNA-Ripk3
DNA PI (MFI)
0.10
0.08
0.06
0.04
0.02
0.00
***
DNA PI (MFI)
0.15
0.10
0.05
0.00
***
DNA PI (MFI)
0.15
0.10
0.05
0.00
***
DNA PI (MFI)
0.08
0.06
0.04
0.02
0.00
**
DNA PI (MFI)
0.3
0.2
0.1
0.0
***
DNA PI (MFI)
0.25
0.20
0.15
0.10
0.05
0.00
***

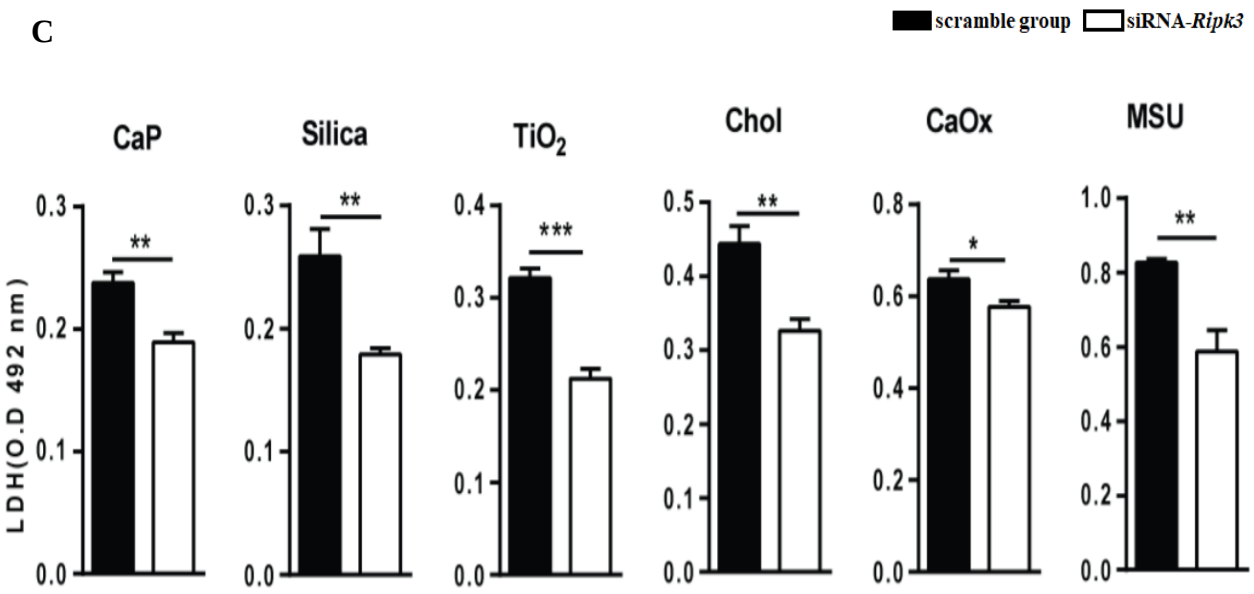

Figure 18. **siRNA against *RIPK3* reduce cytotoxic effect of crystalline particles in HK2 cells (A)** Transfected HK2 cells with siRNA-*RIPK3* were stimulated with 1 mg/ml CaP, 1 mg/ml silica, 0.5 mg/ml TiO2, 3 mg/ml cholesterol, 1 mg/ml CaOx, and mg/ml MSU 0.5 crystals for 24 hours. Cells were stained with PI **(B)** and the PI positive signals quantified by ImageJ. **(C)** LDH release was measured in cell culture supernatants. Data are expressed as mean ± SEM from three independent experiments, *p<0.05, *** p<0.001. n.s. = not significant vs vehicle. **CaP**: calcium phosphate, **TiO2:** titanium dioxide**, CaOx**: calcium oxalate, **MSU**: monosodium urate, **PI**: propidium iodide. **MFI**: mean fluorescence intensity.

Honarpisheh M, et al.[1]

In addition, we used *Mlkl*- deficient primary tubular epithelial cells to confirm the role of Mlkl in crystal-induced cell death. To do so, *Mlkl*- deficient primary tubular epithelial cells were stimulated with 1 mg/ml CaP crystals, 1 mg/ml silica, 0.5 mg/ml TiO2, 3 mg/ml cholesterol, 1 mg/ml CaOx, and 0.5 mg/ml MSU for 24 hours, and cell death was visualized and quantified by PI positive signal and LDH assay. We found that primary tubular epithelial cells isolated from *Mlkl*-deficient mice were protected from crystal- induced cell death regardless of sizes, shapes and origin of the particles (environmental or metabolic) (Figures 19A-B and 20). Interestingly, we saw different trends of protection between crystalline particles, which suggest the possible impact of particle types, different sizes and specific-shapes on regulated cell death. Taken together, we conclude that crystal-induced cell death involves necroptosis and that blocking Ripk1, Ripk3, and Mlkl consistently abrogates the cytotoxic effect of environmental or metabolic crystalline particles, whereas inhibiting apoptosis had no effect (Figure 13A-B).

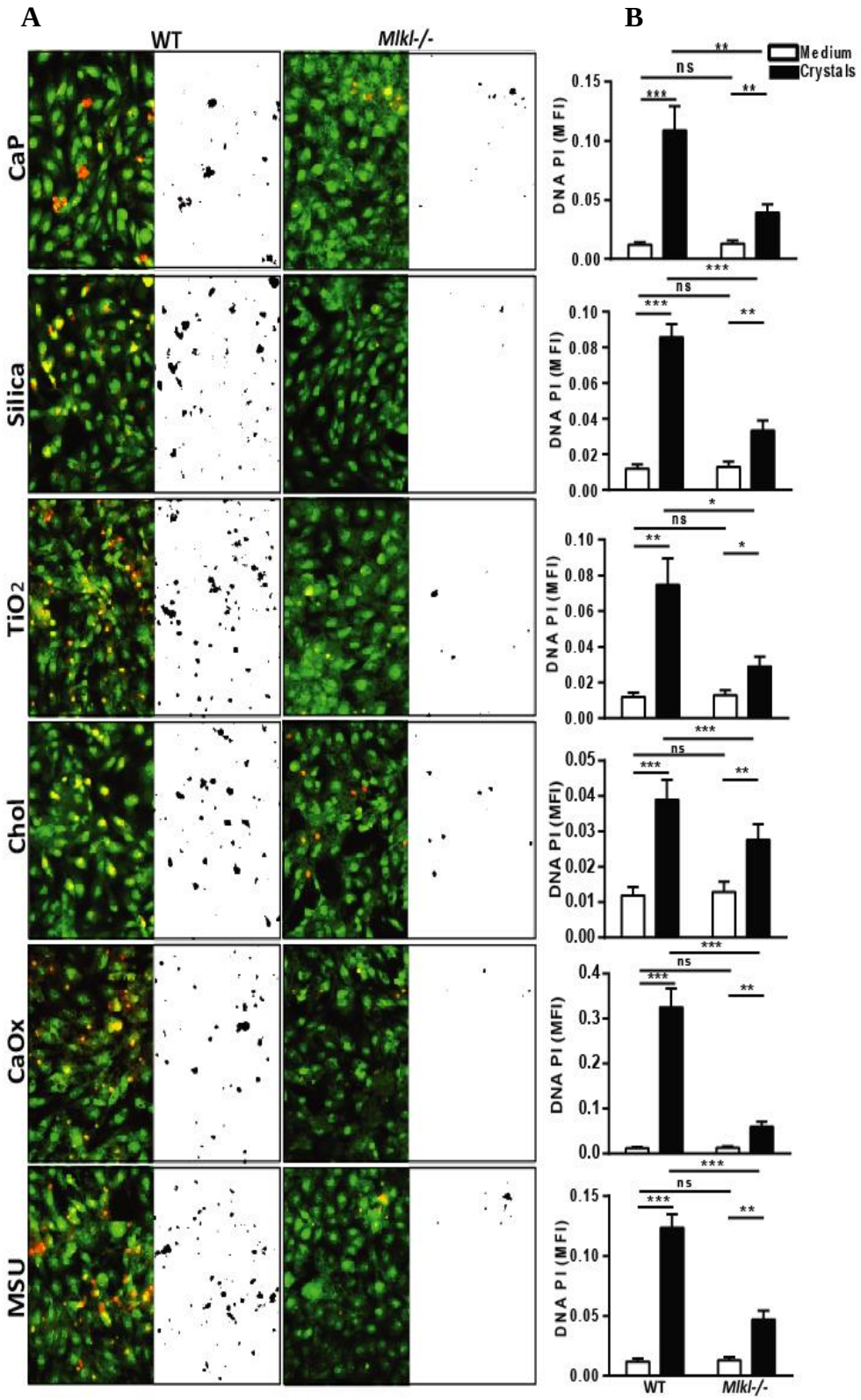

Figure 19. ***Mlkl*-deficient cells reduce cytotoxic effect of crystalline particles in primary tubular epithelial cells. (A)** Freshly isolated pTECs from *Mlkl*-deficient and wild-type mice were stimulated with 1 mg/ml CaP, 1 mg/ml silica, 0.5 mg/ml TiO2, 3 mg/ml cholesterol, 1 mg/ml CaOx, and 0.5 mg/ml MSU crystals for 24 hours. The stimulated as well as untreated cells were stained with PI in red color and acridine orange in green color. The images collected were also visualized in black and white using ImageJ software. **(B)** The PI signals were quantified and represent as MFI. Data are presented as mean±SEM from three independent experiments, *p<0.05, *** p<0.001. n.s. = not significant vs vehicle.

CaP: calcium phosphate, **TiO2:** titanium dioxide**, CaOx**: calcium oxalate, **MSU**: monosodium urate, **PI**: propidium iodide, **MFI**: mean fluorescence intensity. Honarpisheh M, et al.[1]

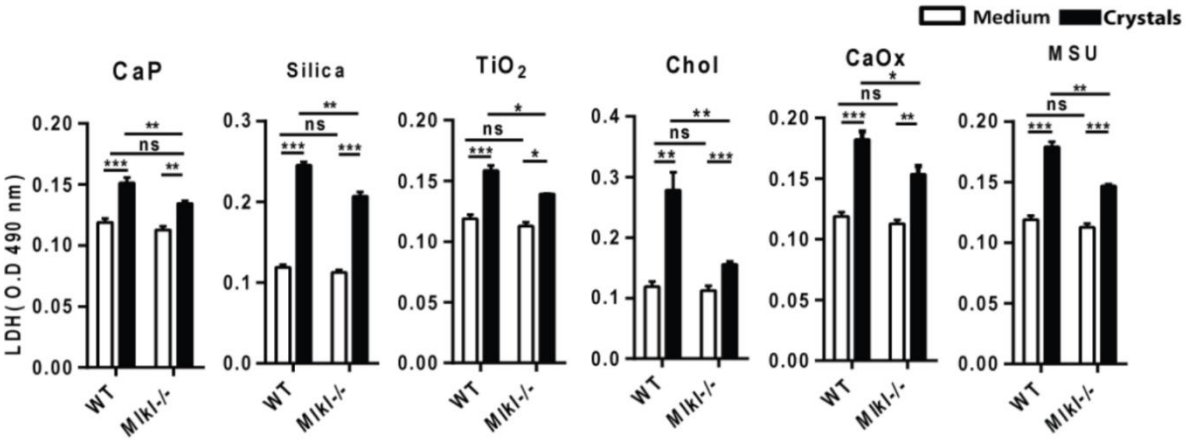

Figure 20. **Exposure of *Mlkl*-deficient cells to crystalline particles**. Freshly isolated pTECs from wild-type and *Mlkl*-deficient mice were stimulated with 1 mg/ml CaP, 1 mg/ml silica, 0.5 mg/ml TiO2, 3 mg/ml cholesterol, 1 mg/ml CaOx, and 0.5 mg/ml MSU crystals for 24 hours LDH assay was used to analyze cell death after 24 hours. Data are presented as mean ± SEM from three independent experiments, *p<0.05, *** p<0.001. n.s. = not significant vs vehicle. **CaP**: calcium phosphate, **TiO2:** titanium dioxide**, CaOx**: calcium oxalate, **MSU**: monosodium urate, **PI**: propidium iodide, **MFI**: mean fluorescence intensity.

Honarpisheh M, et al.[1]

4.7. Phagocytosis precedes crystalline particle-induced cell death

It has been shown that CaOx crystals can be internalized by renal tubular kidney cells via phagocytosis.[179] We speculate that same process might also be the case for other environmental or metabolic crystalline particles, and subsequently leading to cell death. To check this concept, we used CytD an actin polymerization inhibitor to block phagocytosis. HK2 cells were pre-treated with CytD (10µM) for 30 minutes before exposing them to CaP, silica, TiO2, cholesterol, CaOx and MSU. Cell death was quantified using PI staining. Interestingly, we observed that the cytotoxicity of crystalline particles was significantly reduced upon pretreatment with CytD (Figure 21A-B). These results indicate that the internalization of crystalline particles is essential to activate the necroptosis pathway and subsequently leading to cell death.

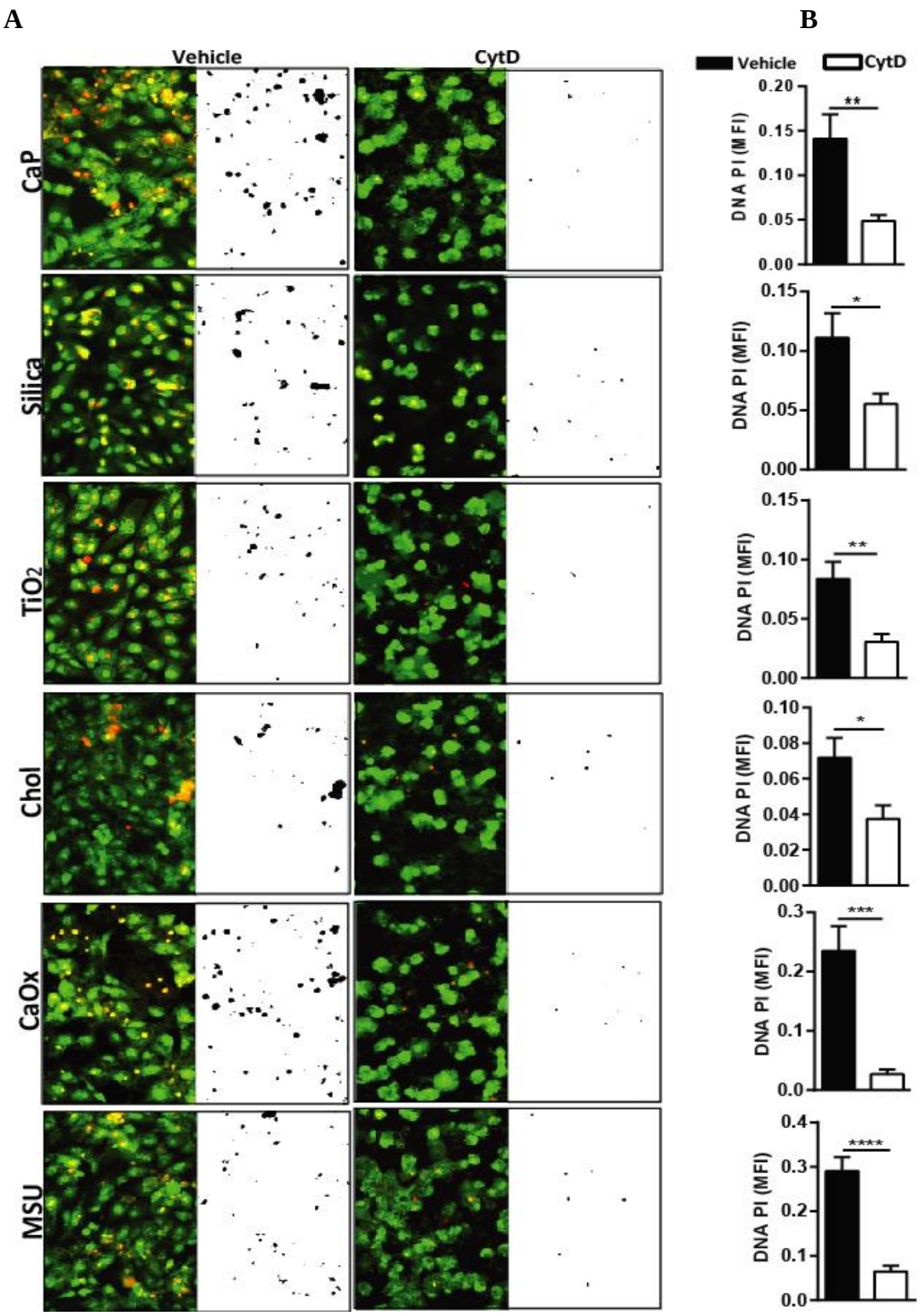
A
B
Vehicle
CytD
CaP
Silica
TiO2
Chol
CaOx
MSU
DNA PI (MFI)
0.20
0.15
0.10
0.05
0.00
**
*
**
*
***
****
0.08
0.06
0.04
0.02
0.3
0.2
0.1
0.0
0.4

Figure 21. **Cell death analysis of the HK2 cells in the presence or absence of a phagocytosis inhibitor.** HK2 cells were pre-treated with the phagocytosis inhibitor Cyt D (10 µM) 30 minutes prior to stimulation with 1 mg/ml CaP, 1 mg/ml silica, 0.5 mg/ml TiO2, 3 mg/ml cholesterol, 1 mg/ml CaOx, and 0.5 mg/ml MSU crystals for 24 hours. **(A)** Cells were stained with PI in red color and acridine orange in green colour. Images collected from PI staining were converted into black and white using ImageJ software. **(B)** PI signals were quantified and represent as MFI. Data are presented as mean ± SEM from three independent experiments, *p<0.05, **** p<0.001. n.s. = not significant vs vehicle. **CaP**: calcium phosphate, **TiO2:** titanium dioxide**, CaOx**: calcium oxalate, **MSU**: monosodium urate, **PI**: propidium iodide. **MFI**: mean fluorescence intensity. **CytD**. cytochalasin D.

Honarpisheh M, et al.[1]

4.8. Mitochondrial damage upon the crystals stimulation

Inhibiting necroptosis either with pharmaceutical inhibitors or using genetic approach did not completely protect the cells from crystal-induced cytotoxicity. These observations led us to ask the question whether another caspase-independent cell death pathway might be involved in crystal-induced cell and tissue injury or not. Previously, Linkermann *et al.* showed that MPT is involved in renal ischemia-reperfusion injury independent of necroptosis.[111] Therefore, we intended to explore the possible involvement of the MPT pathway in crystal-induced tissue and cell injury. To answer our questions, we focused on four crystalline particles CaOx, MSU, silica and CPPD, all being involved in important diseases. For example, CaOx crystal particles lead to acute oxalate nephropathy and nephrolithiasis[4], MSU prompts gout and urate nephropathy[4], silica particles induce pneumoconiosis and silicosis[4], and CPPD could be involved in pseudogout, chondrocalcinosis, and hemochromatosis.[4] A hallmark of mitochondrial damage is the loss of cristae as well as swollen mitochondria under stress conditions. Thus, we first evaluated the mitochondrial ultrastructure by TEM. L929 cells were exposed to 1 mg/ml CaOx, 1 mg/ml MSU, 0.5 mg/ml SiO2 and 0.5 mg/ml CPPD crystals for 24 hours. As shown in Figure 22, all crystalline-particles induced mitochondrial swelling and loss of cristae in L929 cells (Figure 22), which suggests that mitochondria could be involved in crystalline particle-induced cytotoxicity.

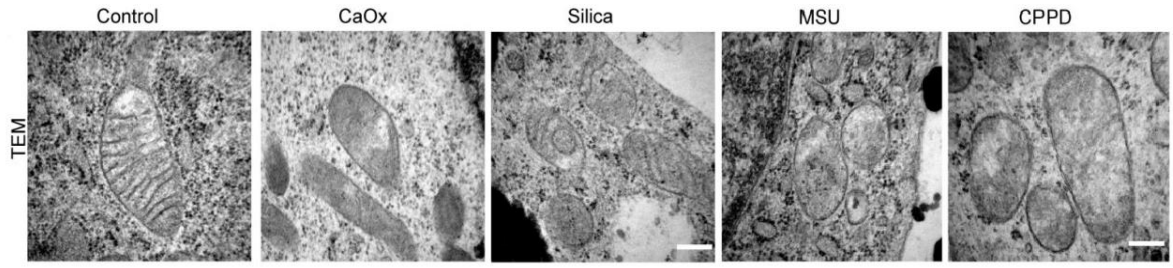

Figure 22. **Transmission electron microscopy images show mitochondrial damage in L929 cells.** L929 cells were stimulated with, MSU, silica, and CPPD crystals for 24 hours. Images collected from TEM show that crystals induce mitochondrial damage as illustrated by a loss of cristae and swollen mitochondria (scale bar 250 nm). **TEM:** Transmission electron microscopy, **CaOx**: calcium oxalate, **MSU**: monosodium urate, CPPD: calcium pyrophosphate dehydrate.

Mulay SR, Honarpisheh MM, et al.[2]

Next, we sought to investigate mitochondrial functions such as ROS production, MOMP and finally, mitochondrial cell death in response to crystals. To do this, we used the dye TMRE to measure the membrane potential, DCFDA to analyze ROS production and calcein/ PI to analyze cell death. L929 cells were incubated with CaOx 1 mg/ml, MSU 1 mg/ml, SiO2 0.5 mg/ml, and CPPD 0.5 mg/ml crystals for 24 hours. We observed that the TMRE positive signal was present in the mitochondria of healthy cells and significantly declined upon exposure to crystals (Figure 23A), indicating loss of membrane potential in mitochondria. Interestingly, we observed an increase in ROS production and cell death upon crystals' exposure to the cells (Figures 23B and 23C). Altogether, we conclude that the cytotoxic effects of crystalline particles are associated with mitochondrial permeability transition.

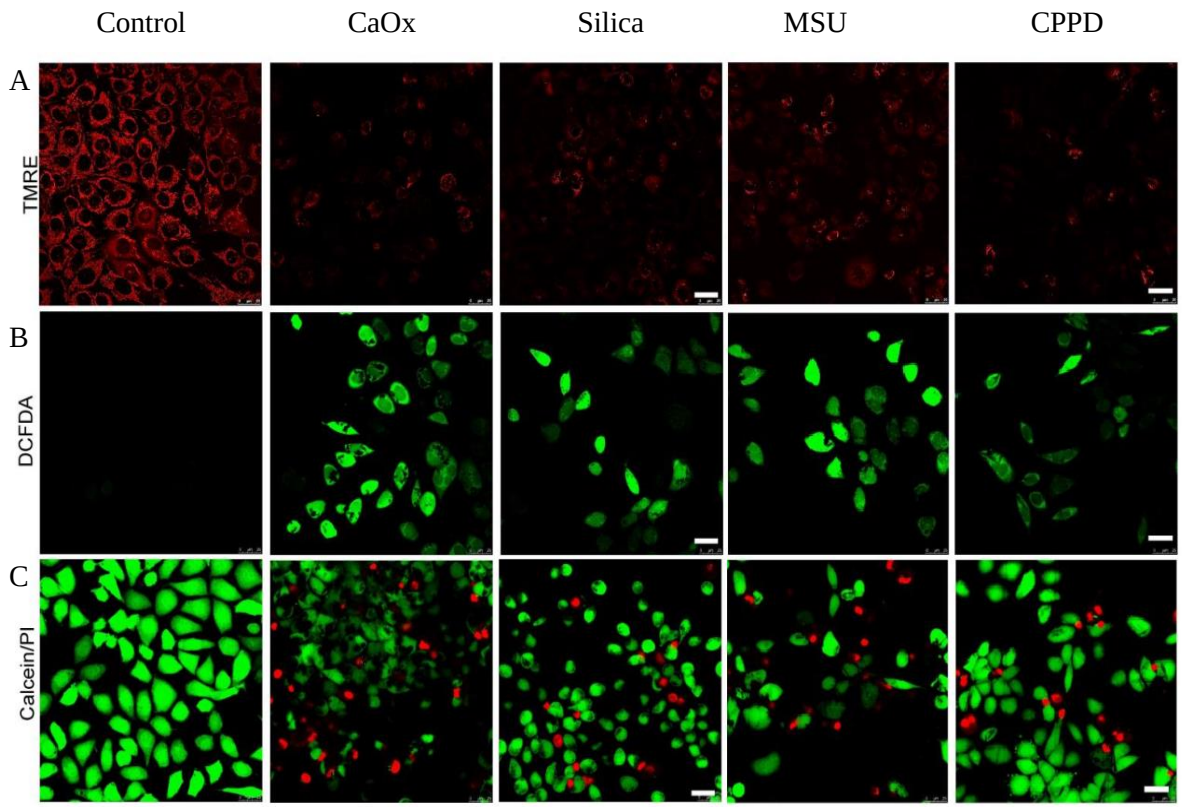

Figure 23. **Live cell staining to visualize mitochondrial membrane potential, ROS production and cell death in L929 cells. (A)** TMRE staining was used to determine MOMP damage. Images show loss of membrane potential after cells were stimulated with 1 mg/ml CaOx, 1 mg/ml MSU, 0.5 mg/ml silica, and 0.5 mg/ml CPPD crystals for 24 hours (scale bar 25 μm). **(B)** DCFDA staining was used to check for ROS production. Images show that stimulation cells with crystals leads to ROS production (scale bar 25 μm). **(C)** Cells were stained with calcein for live cells in green and PI for dead cells in red, and show cellular necrosis after crystal stimulation (scale bar 25 μm). **CaOx**: calcium oxalate, **MSU**: monosodium urate,**CPPD**: calcium pyrophosphate dehydrate **MOMP :** mitochondrial outer membrane potential, **ROS**: reactive oxygen species, **TMRE**: tetramethylrhodamine ethyl ester, **DCFDA**: 2',7'-dichlorodihydrofluorescein diacetate.

Mulay SR, Honarpisheh MM, et al.[2]

4.9. Inhibition of Ppif, a mitochondrial outer membrane protein, and ROS production reduce crystal cytotoxicity

To investigate whether mitochondrial outer membrane proteins and ROS production are involved in crystal cytotoxicity, we blocked mitochondrial membrane protein cyclophilin and ROS production. L929 cells were pre-treated with Ppif inhibitor CsA and ROS inhibitor APDC as for 30 minutes followed by stimulation with CaOx 1 mg/ml, MSU 1 mg/ml, SiO2 0.5 mg/ml and CPPD 0.5 mg/ml crystals for 24 hours. We found that the mitochondrial membrane potential was fully reversed when CsA was added to crystal-stimulated L929 cells (Figure 24). However, the mitochondrial membrane potential was not fully reversed in the presence of

antioxidant APDC (Figure 24), which indicates that ROS production is downstream of losing mitochondrial membrane potential. Interestingly, ROS production and cell death significantly decreased in the presence of CsA and APDC (Figures 25 and 26).

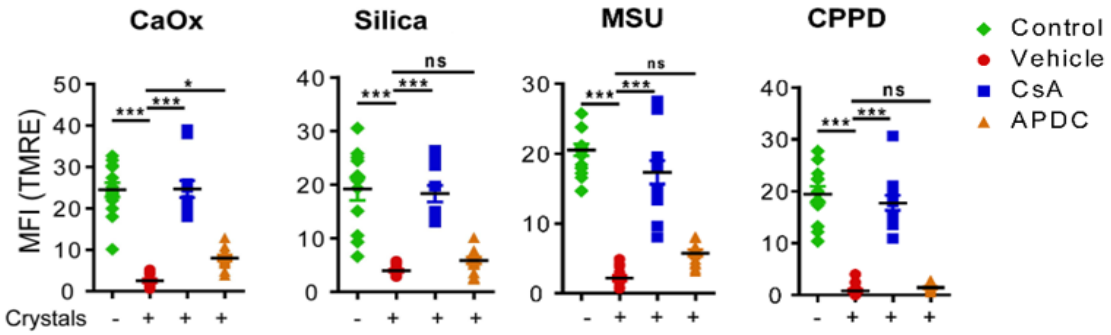

Figure 24. **Quantification of live cell staining in the absence or presence of ROS and Ppif inhibitors to analyze mitochondrial membrane potential in L929 cells.** L929 cells were pre-treated with CsA (1 μM) and (APDC, 200 μM) for 30 minutes prior to stimulation with 1 mg/ml CaOx, 1 mg/ml MSU, 0.5 mg/ml silica, and 0.5 mg/ml CPPD crystals for 24 hours. TMRE staining was used to determine MOMP damage. Results were expressed as MFI (n=10-12). Data are representative of three independent experiments. One-way ANOVA was used to analyze data and are expressed as mean ± SEM. *p<0.05, *** p<0.001. n.s. = not significant vs vehicle. **CaOx**: calcium oxalate, **MSU**: monosodium urate, CPPD: calcium pyrophosphate dehydrate **CsA**: cyclosporine A, **APDC**: antioxidant ammonium pyrrolidine dithiocarbamate,**MOMP**: mitochondrial outer membrane potential, **TMRE**: tetramethylrhodamine ethyl ester, **MFI**: mean fluorescent intensity.

Mulay SR, Honarpisheh MM, et al.[2]

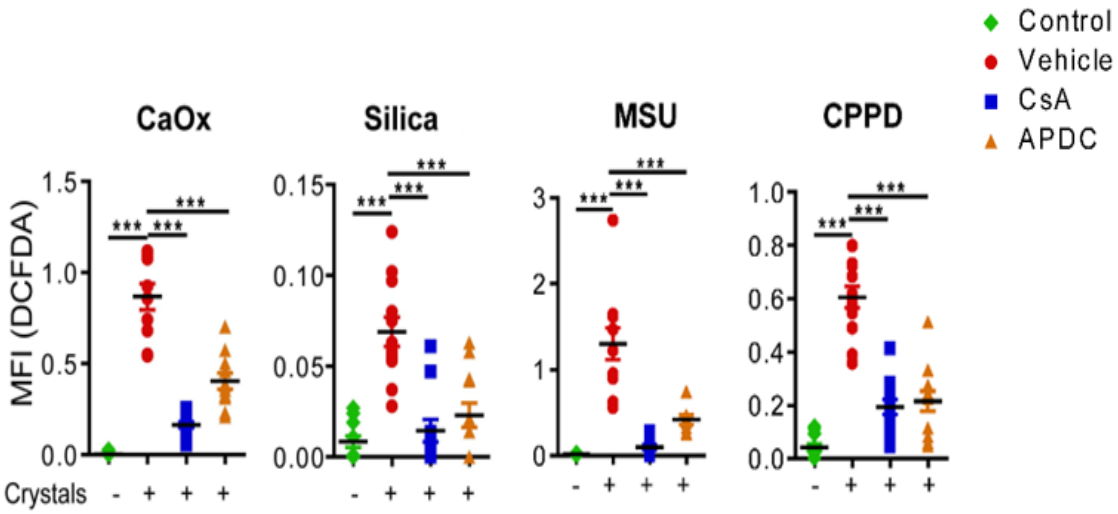

Figure 25. **Quantification of live cell staining in the absence or presence of ROS and Ppif inhibitors to analysis ROS production in L929 cells.** L929 cells were pre-treated with CsA (1 μM) and APDC (200 μM) for 30 minutes prior to stimulation with CaOx 1 mg/ml, MSU 1 mg/ml , SiO2 0.5 mg/ml and CPPD 0.5 mg/ml crystals for 24 hours. DCFDA staining was used to check ROS production and results are expressed as MFI (n=10-12). Data are representative of three independent experiments. One-way ANOVA was used to analyze data and are expressed as mean ± SEM. *p<0.05, *** p<0.001. n.s. = not significant vs vehicle. **CaOx**: calcium oxalate, **MSU**: monosodium urate, **CPPD**: calcium pyrophosphate dehydrate **CsA**: cyclosporine A, **APDC**: antioxidant ammonium pyrrolidine dithiocarbamate, **MFI**: mean fluorescent intensity, **SiO2**: silica. **DCFDA**: 2',7'-dichlorodihydrofluorescein diacetate.

Mulay SR, Honarpisheh MM, et al.[2]

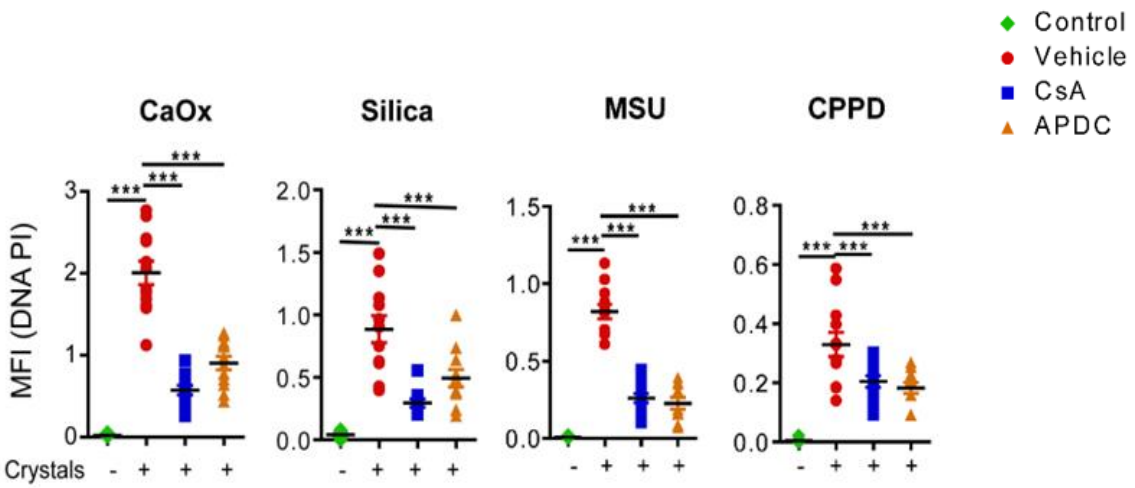

Figure 26. **ROS and Ppif inhibitors reduce cytotoxic effect of crystalline particles in L929 cells.** L929 cells were pre-treated with CsA (1 μM) and APDC (200 μM) for 30 minutes prior to stimulation with CaOx 1 mg/ml, MSU 1 mg/ml, SiO2 0.5 mg/ml and CPPD 0.5 mg/ml crystals for 24 hours. Cells were stained with calcein for live cells (green) and PI for dead cells (red). Data are representative of three independent experiments. One-way ANOVA was used to analyze data and are expressed as mean ± SEM. *p<0.05, *** p<0.001. n.s. = not significant vs vehicle. **CaOx**: calcium oxalate, **MSU**: monosodium urate,**CPPD**: calcium pyrophosphate dehydrate **CsA**: cyclosporine A, **APDC**: antioxidant ammonium pyrrolidine dithiocarbamate, **SiO2**: silica.

Mulay SR, Honarpisheh MM, et al.[2]

To confirm the previous results, we used specific siRNA against *Ppif* as well as isolated primary tubular epithelial cells from wild-type and *Ppif*-deficient mice. We observed that cell death was significantly reduced in *Ppif* siRNA knockdown L929 cells as well as primary tubular epithelial cells isolated from *Ppif*-deficient mice in comparison to scramble or cells from wild-type mice after stimulation with CaOx 1 mg/ml, MSU 1 mg/ml, silica 0.5 mg/ml and CPPD 0.5 mg/ml crystals for 24 hours. (Figure 27A-D). We conclude that crystal cytotoxicity involves MPT , a form of cell death dependent on Ppif protein and ROS release.

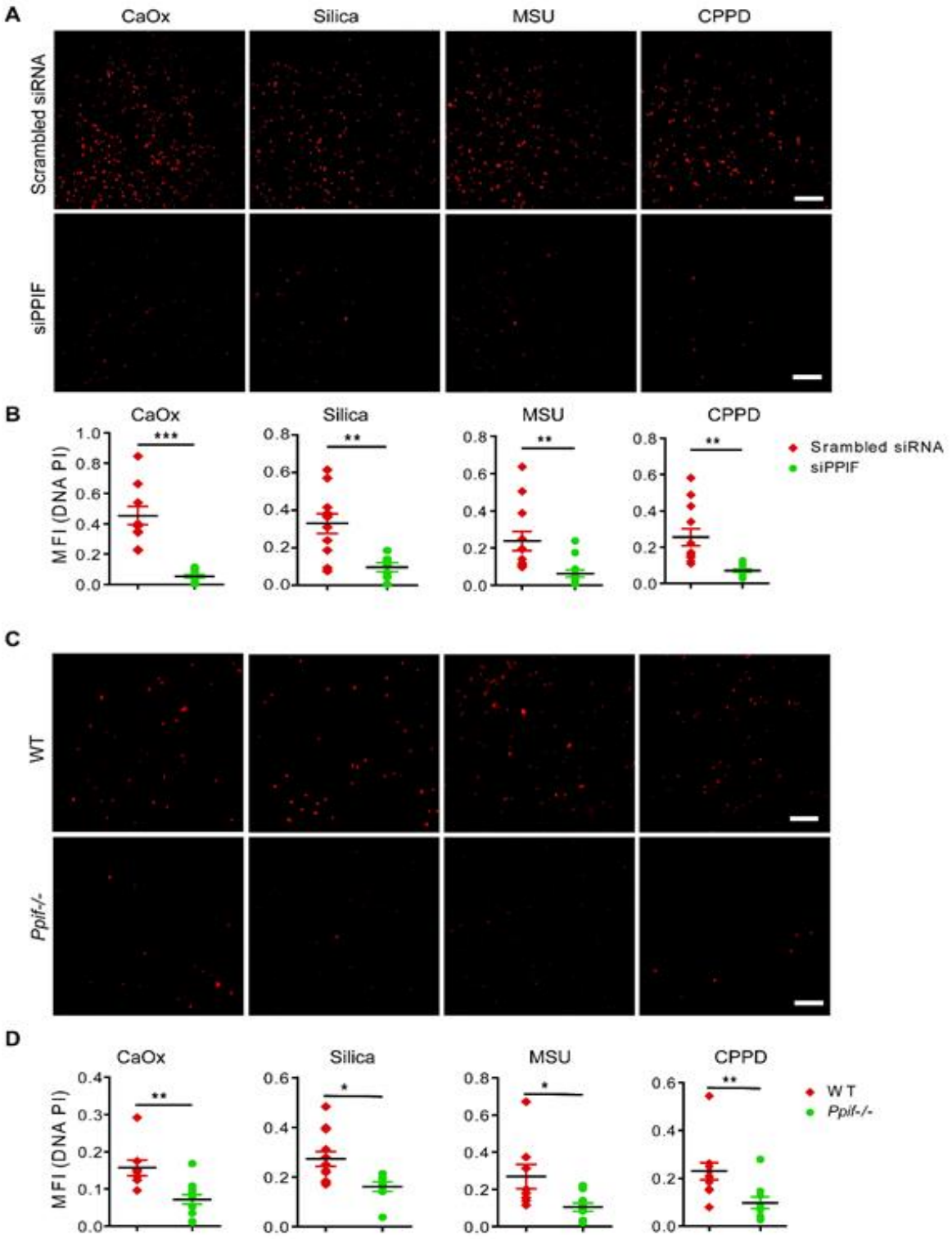

Figure 27. **siRNA-*Ppif* or *Ppif*-deficient cells reduce cell death in L929 cell. (A-B)** L929 cells were transfected with siRNA-*Ppif* or a scrambled control before cells were stimulated with crystals as mentioned above. **(A)** Cells were stained with PI and (**B**) signals were quantified using ImageJ that are expressed as MFI (n=9-12). **(C-D)** Freshly isolated pTECs from *Ppif*-deficient and wild-type mice were stimulated with crystals as mentioned above. **(C)** Cells were stained with PI and **(D)** signals were quantified using ImageJ that are expressed as MFI (n=8-12) **(B).** Data are representative of three independent experiments. One-way ANOVA was used to analyze data and are expressed as mean ± SEM. *p<0.05, **p<0.01, *** p<0.001.

CaOx: calcium oxalate, **MSU**: monosodium urate, **CPPD**: calcium pyrophosphate dehydrate **CsA**: cyclosporine A, **APDC**: antioxidant ammonium pyrrolidine dithiocarbamate, **SiO2**: silica, **MFI**: mean fluorescence intensity, **Ppif**: peptidylprolyl isomerase F.

Mulay SR, Honarpisheh MM, et al.[2]

4.10. Phagocytosis and cathepsin lysosomal leakage precede crystal-induced mitochondrial membrane permeability transition

Previous reports have shown that phagocytosis of CaOx crystals leads to lysosomal destabilization and lysosomal protease leakage such as cathepsins, which are involved in Nlrp3 inflammasome activation in response to CaOx crystals.[47,180,52] Therefore, we asked the questions whether various crystals with different sizes and shapes can trigger lysosomal destabilization and lysosomal cathepsin leakage leading to MPT and cell death. To do so, we applied 2D TEM and 3D SB-EM imaging techniques to visualizes the internalization of crystals by L929 cells. We observed that various crystals (CaOx, silica, MSU and CPPD) are localized within endosomal compartments (Figures 28 and 29A-B) after 24 hours of stimulation. These observations indicate the involvement of lysosome leakage in stimulated cells with various crystals.

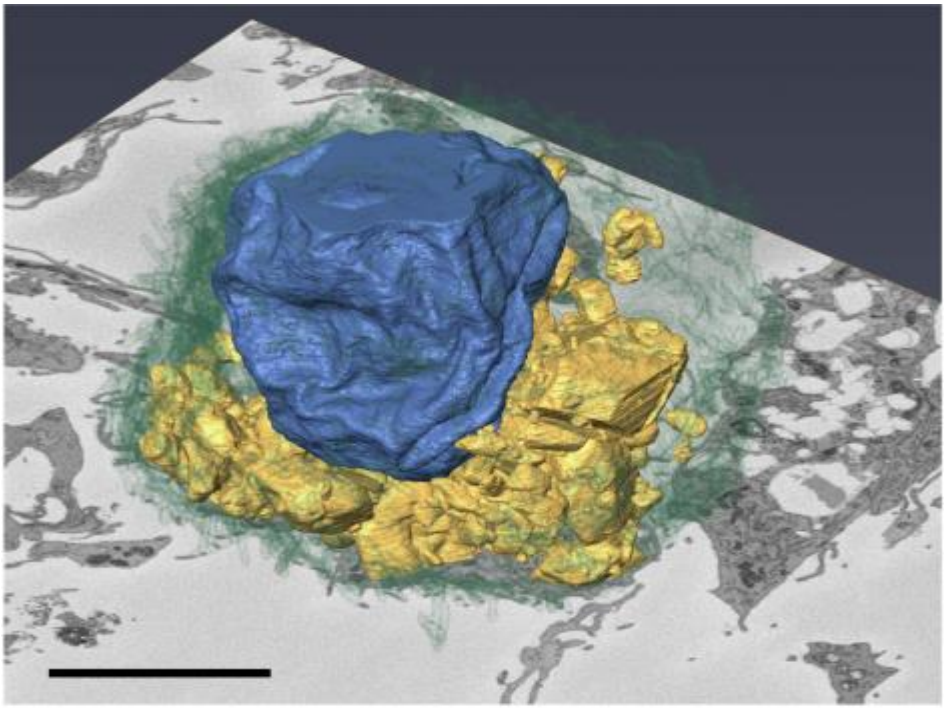

Figure 28. **A 3D reconstruction image.** Images were collected from SB-EM and show internalization of CaOx crystals (yellow) into intracellular compartments, where they fill a major part of the perinuclear cytoplasm. For better visualization, the outer cell membrane is shown in green and the nucleus in blue; scale bar 5 µm. **CaOx**: calcium oxalate.

Mulay SR, Honarpisheh MM, et al.[2]

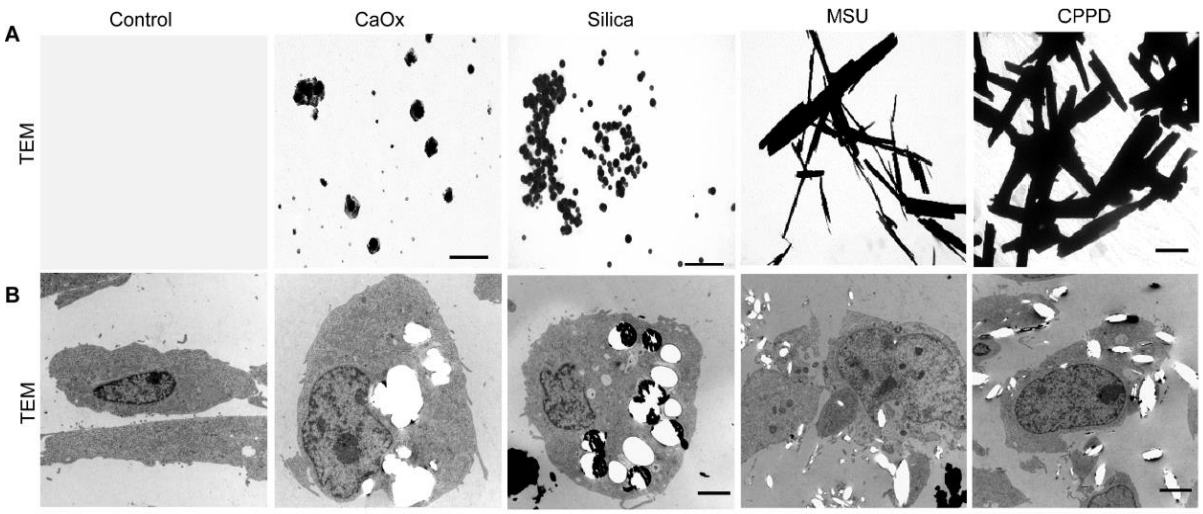

Figure 29. **Transmission electron microscopy images from L929 expose to crystal particles. (A)** 2D images were collected from TEM indicating various sizes and shapes of CaOx (scale bar 250 nm), silica (scale bar 2 μm), MSU, and CPPD crystals (scale bar 500 nm). **(B)** L929 cells were stimulated with crystals of CaOx, silica, MSU, and CPPD with for 24 hours. Images from TEM show crystal phagocytosis. Of note, the crystals present inside the cells were washed out during processing leaving behind voids in the cytosol, whereas silica crystals can still be seen. **CaOx**: calcium oxalate, **MSU**: monosodium urate, **CPPD**: calcium pyrophosphate dehydrate, **TEM**: transmission electron microscopy, **L929**: murine fibroblast cell.

Mulay SR, Honarpisheh MM, et al.[2]

To confirm these observations, we used confocal microscopy and stained L929 cells with calcein (green color to visualize the live cells) and lysopainter (red color to visualize lysosomes within the cell). L929 cells were exposed to CaOx 1 mg/ml, MSU 1 mg/ml, silica 0.5 mg/ml, and CPPD 0.5 mg/ml crystals or left untreated (medium control) for 24 hours. After stimulation, cells were stained with calcein and lysopainter and subjected to confocal microscopy. Unexpectedly, signals were absent in PI positive crystals localized in the lysosomal compartment as illustrated by the lysopainter signals (Figure 30A), which is an indication for the formation of phagolysosome to digest crystals as foreign bodies. To determine the mitochondrial function in the same experiment, we next stained L929 cells with calcein and TMRE (red color to visualize live mitochondrial within cells). We found that stimulation of cells with various crystals for 24 hours resulted in a loss of TMRE signal (Figure 30B). These data suggested that upon phagocytosis of crystals regardless of their sizes, phagolysosomes are formed in order to eliminate crystals, which is associated with a loss of mitochondrial membrane potential and eventually leading to cell death.

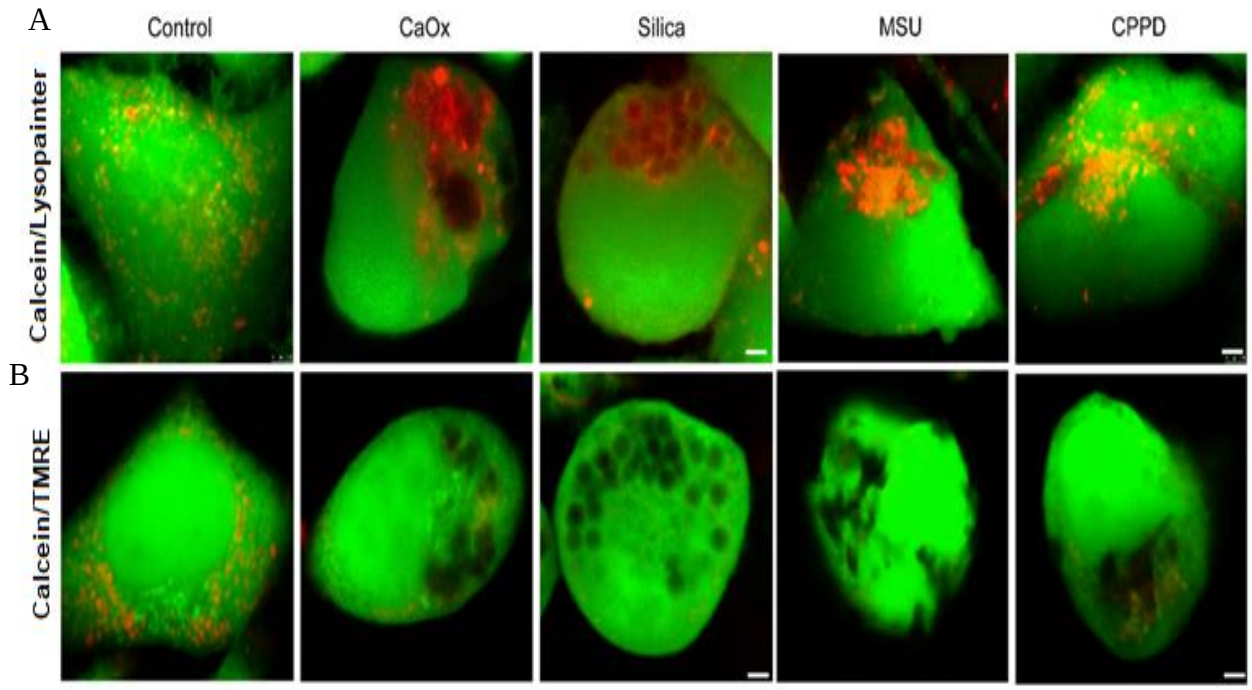

Figure 30. **Confocal images from L929 cells expose to crystal particles.** (A) L292 cells were stimulated with CaOx, silica, MSU and CPPD crystals for 24 hours and cells stained with calcein for live cells and lysopaintaer to visualize lysosome. **(B)** L292 cells were stimulated with CaOx, silica, MSU and CPPD crystals for 24 hours. Afterwards, cells were stained with calcein for live cells and TMRE to visualize the function of mitochondria. **CaOx**: calcium oxalate, **MSU**: monosodium urate, CPPD: calcium pyrophosphate dehydrate.

Mulay SR, Honarpisheh MM, et al.[2]

In addition, we wanted to illustrate lysosome leakage and cell death upon stimulation with crystalline particles. To do this, we used lysotracker (green color to visualize the live lysosomes within cells) and PI (red color to detect DNA and cell death). L929 cells were treated with CaOx 1 mg/ml, MSU 1 mg/ml, silica 0.5 mg/ml, and CPPD 0.5 mg/ml crystals for 24 hours, and stained with lysotracker for confocal microscopy. Interestingly, we found that the lysotracker signals were absent in PI positive cells and lysotracker positive signals as well as no PIs positivity were observed in the medium control (Figure 31), indicating phagolysosome rupture and cell death in response to crystals (PI positive cells).

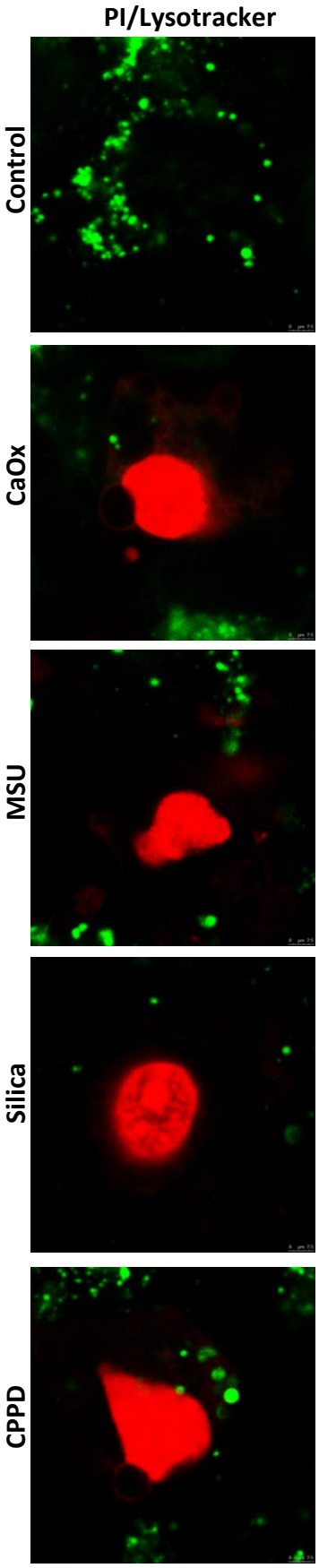

Figure 31. **Confocal images from L929 cells stain with lysotracker and PI.** L292 cells were exposed to CaOx, silica, MSU, and CPPD for 24 hours and cells stained with lysotracker to visualize live lysosomes and PI to show cell death. **CaOx**: calcium oxalate, **MSU**: monosodium urate, **CPPD**: calcium pyrophosphate dehydrate.

Next, we blocked phagocytosis using CytD and cathepsin using CA074Me. We pretreated L929 cells with CytD (5 and 10 µM) or CA074Me (10 and 20 µM) for 30 minutes prior to stimulation with CaOx 1 mg/ml, MSU 1 mg/ml, silica 0.5 mg/ml, and CPPD 0.5 mg/ml crystals for 24 hours. We observed a significant reduction of the PI signals as well as LDH release in stimulated cells pre-treated with CytD or CA074Me in a dose-dependent manner compared to the control group (Figure 32A-D). Taken together, we conclude that crystals are taken up by cells via phagocytosis into intracellular phagolysosome compartments, which leads to lysosomal cathepsin leakage as upstream events to crystal-induced MPT and necroptosis induced-cell death in L929 cells.

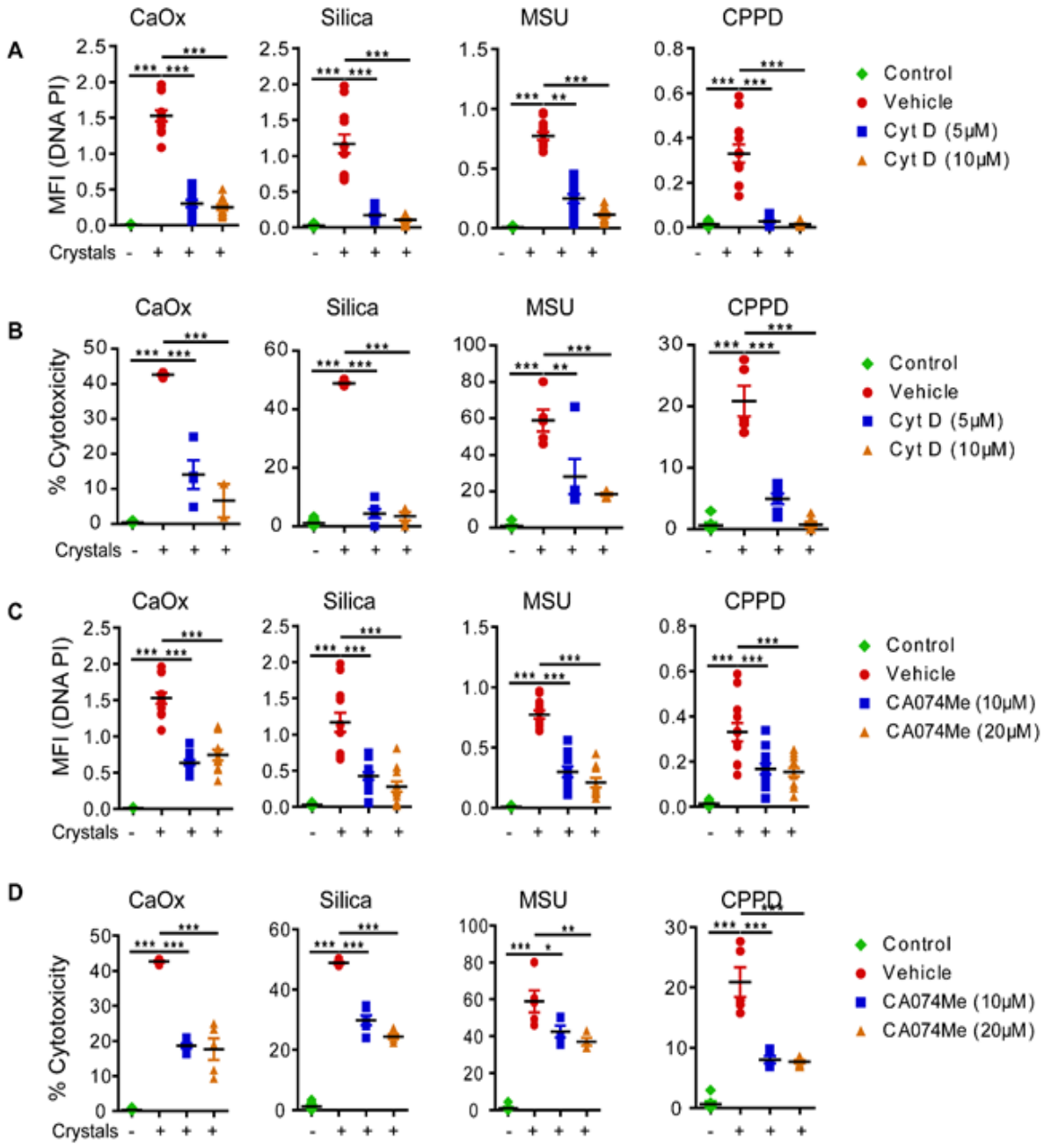

Figure 32. Cell death analysis of L929 cells expose to crystal particles in absence or presence of a cathepsin inhibitor. **A-B**: L929 cells were pre-treated with CytD (5 and 10 µM) prior to stimulation with various crystals. **(A)** Cells were stained with PI and then quantified. Results are expressed as MFI (n=10-12). **(B)** Cell death was measured using a LDH assay kit (n=4-6). (**C-D**) L929 cells were pre-treated with CA074Me (10 and 20 µM) prior to stimulate with crystals. **(C)** Cells were stained with PI and quantified. Results are expressed as MFI (n=10-12). **(D)** LDH assay was used to determined cytotoxicity (n=4-6). Data are representative of three independent experiments. One-way ANOVA was used to analyze data and are expressed as mean ± SEM.*p<0.05, **p<0.001, *** p<0.001 vs vehicle. **CytD**: cytochalasin D, **PI**: propidium iodide, **MFI**: mean fluorescent intensity.

Mulay SR, Honarpisheh MM, et al.[2]

4.11. Mitochondrial damage involves in CaOx crystal-induced acute kidney injury

To confirm our *in-vitro* data also *in-vivo*, we employed an AKI model by injecting sodium oxalate i.p. into mice that leads to intrarenal CaOx crystal deposition and AKI[47,16,181]. After induction of AKI, mice were sacrificed after 24 hours and kidneys fixed and subjected to Pizzolato and H&E staining, as well as *ex-vivo* kidney micro-computed tomography. We observed the formation of tubular plugs due to CaOx crystal deposition within proximal and distal tubules in Pizzolato and H&E staining compared to control mice (Figure 33A-D).

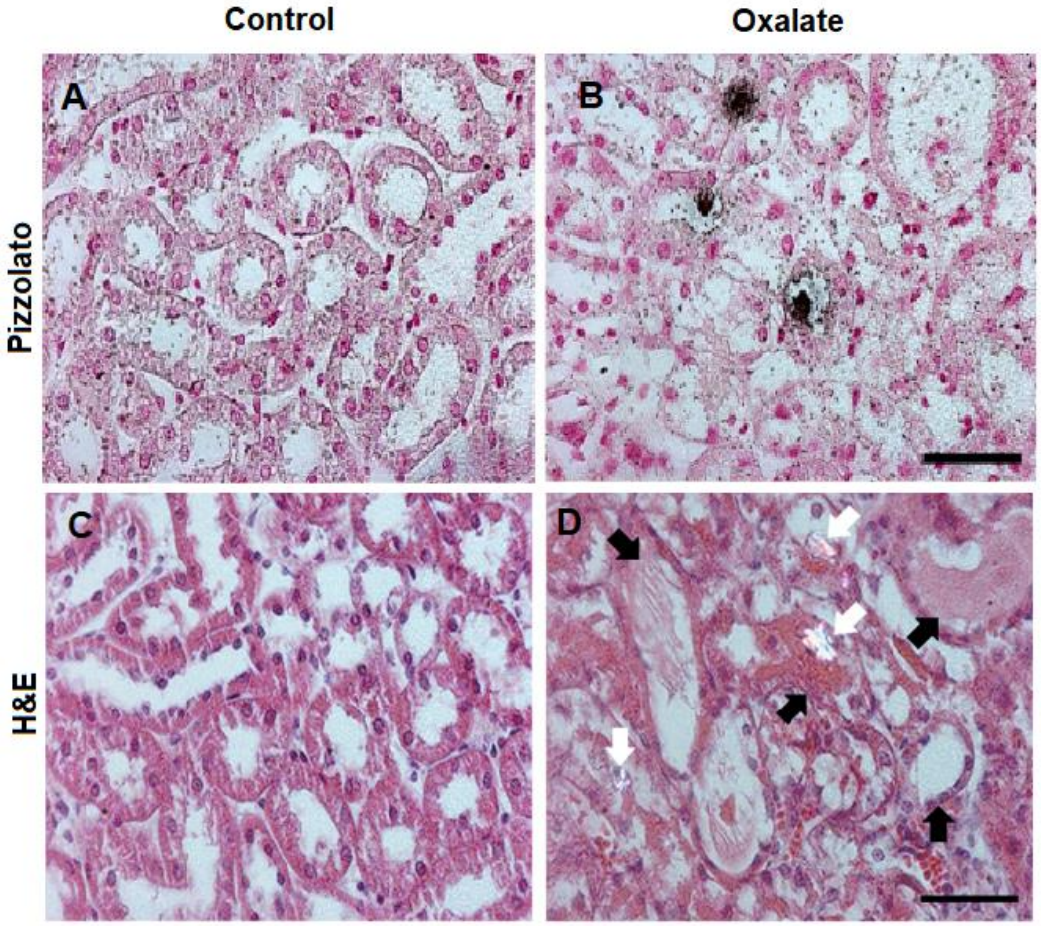

Figure 33. **Deposition of CaOx crystals inside proximal and distal tubules. (A and C)** Pizzolato and H&E staining indicate no crystal deposition in control mice **(B)** but the presence of diffuse intrarenal crystals in mice with acute oxalate nephropathye after 24 hours. **(D)** Crystals (white arrows) can be seen in polarized light background, which is associated with tubule injury (black arrows) in mice with acute oxalate nephropathy after 24 hours. **H&E**: hematoxylin and eosin.

Mulay SR, Honarpisheh MM, et al.[2]

The images collected from SB-EM sections showed large crystal plugs and some smaller crystals inside epithelial cells of the thick ascending limb of the outer medulla (Figure 34A-C). We also investigated mitochondrial morphological abnormalities in injured and unaffected kidneys using TEM. We observed mitochondrial ballooning in renal epithelial cells from AKI mice (Figures 34A-C), whereas tubular segments from healthy mice represented with and normal mitochondria (Figure 34A-C). TEM showed loss of inner membrane cristae ballooning as signs of MPT, water influx, and mitochondrial abnormality in mice with acute oxalate nephropathy (Figure 35A-C).

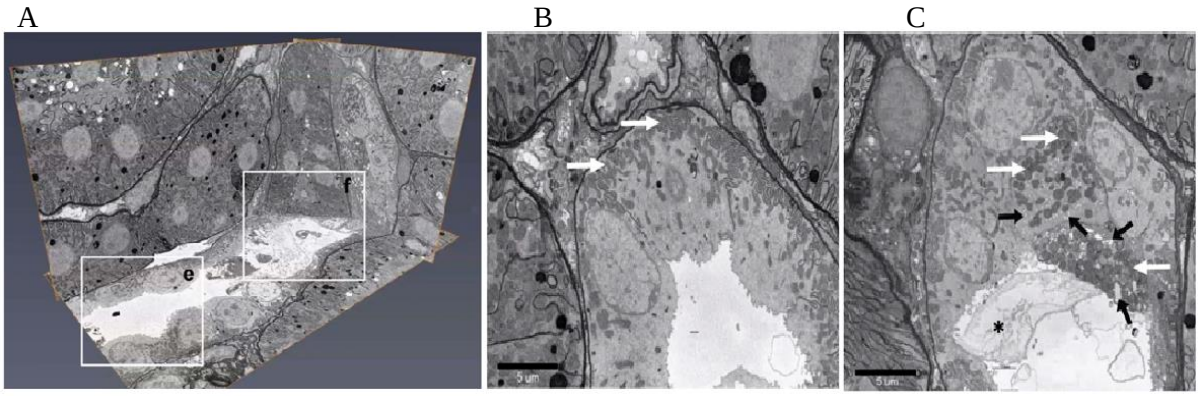

Figure 34. **3D images of the mouse kidney with oxalate nephropathy. (A)** 3D and SB-EM image of the kidney from a mouse with oxalate nephropathy shows a normal segment of a distal tubule (e frame), whereas a segment of the same tubule obstructed with a crystal (f frame). **(B)** Left frame **(e)** with more magnification shows normal and intact mitochondria (white arrows) at the basolateral membrane of distal tubule. **(C)** Right frame with more magnification shows a crystal plug inside the tubular epithelial cells (asterisk) in the tubule lumen and many intracellular crystals (black arrows), which is associatied with mitochondrial damage (white arrows)**.**

Mulay SR, Honarpisheh MM, et al.[2]

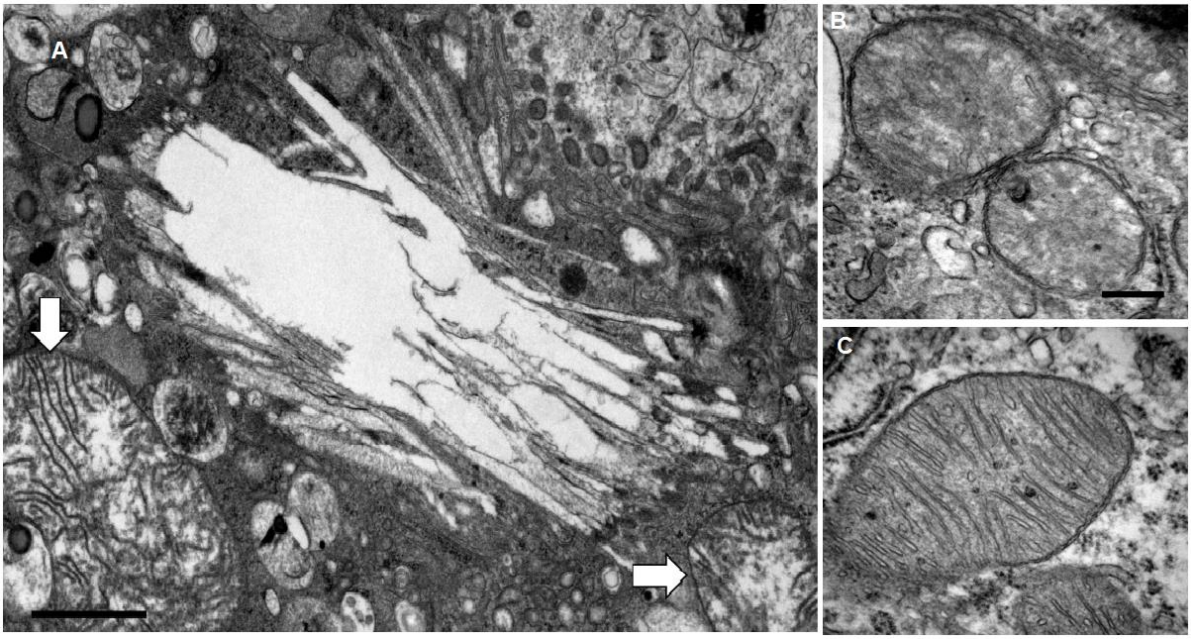

Figure 35. **TEM images from the kidney show mitochondrial damage (A), (C)** Images collected from TEM demonstrate the presence of injured mitochondria as indicate by loss of cristae, the presence of lucent matrix, and swollen mitochondria (white arrows) in proximity to intrarenal crystals in mice with acute oxalate nephropathy. **(B)** Intact mitochondria in control mice. Scale bar A: 1 μm, B-C: 250 nm. **TEM**: transmission electron microscopy.

Mulay SR, Honarpisheh MM, et al.[2]

4.12. *Ppif*-deficiency attenuates CaOx crystal-induced acute kidney injury

The next question was whether Ppif and mitochondrial permeability transition contribute to crystalline AKI. We employed acute oxalate nephropathy in wild-type and *Ppif*-deficient mice. First, we checked crystals deposition in wild-type and *Ppif*-deficient mice and observed that CaOx crystal deposits did not vary between both wild-type and deficient mice (Figure 36A). In addition, we determined functional parameters of crystalline AKI such as plasma creatinine levels, and structural parameters of kidney injury including PAS and TUNEL staining. As shown in Figure 36B-F, tubular injury and necrosis as well as TUNEL positive cells were significantly reduced in *Ppif*-deficient mice compared to wild-type mice (Figure 36B-F). This indicate that CaOx crystal-induced cell death involves *Ppif*-driven MPT-RN in acute oxalate nephropathy.

4.13. Mitochondrial membrane permeability transition-related necrosis and necroptosis both contribute to CaOx crystal cytotoxicity

To check the effect between crystal-induced MPT-RN and necroptosis in oxalate crystal-induced AKI, we induced acute oxalate nephropathy in mice with single versus dual genetic deletion of Ppif and Mlkl. We observed that oxalate exposure induced the same amounts of CaOx crystal deposits in all mouse strains (Figure 36A). *Mlkl*-deficient mice showed similar protection from AKI and tubular damage compared to *Ppif* deficient mice (Figure 36B-F). *Ppif* -and *Mlkl*-double deficient mice showed a significant additive protection on tubular injury compared to either *Ppif* -or *Mlkl*-single deficient mice. However, plasma creatinine levels or the number of TUNEL positive cells did not reduce in double deficiency mice (Figure 36B-F). We conclude that both MPT-RN and necroptosis are involved. Moreover, their partial protective effect in crystalline AKI suggests a interlink of both signaling pathways *in-vivo*.

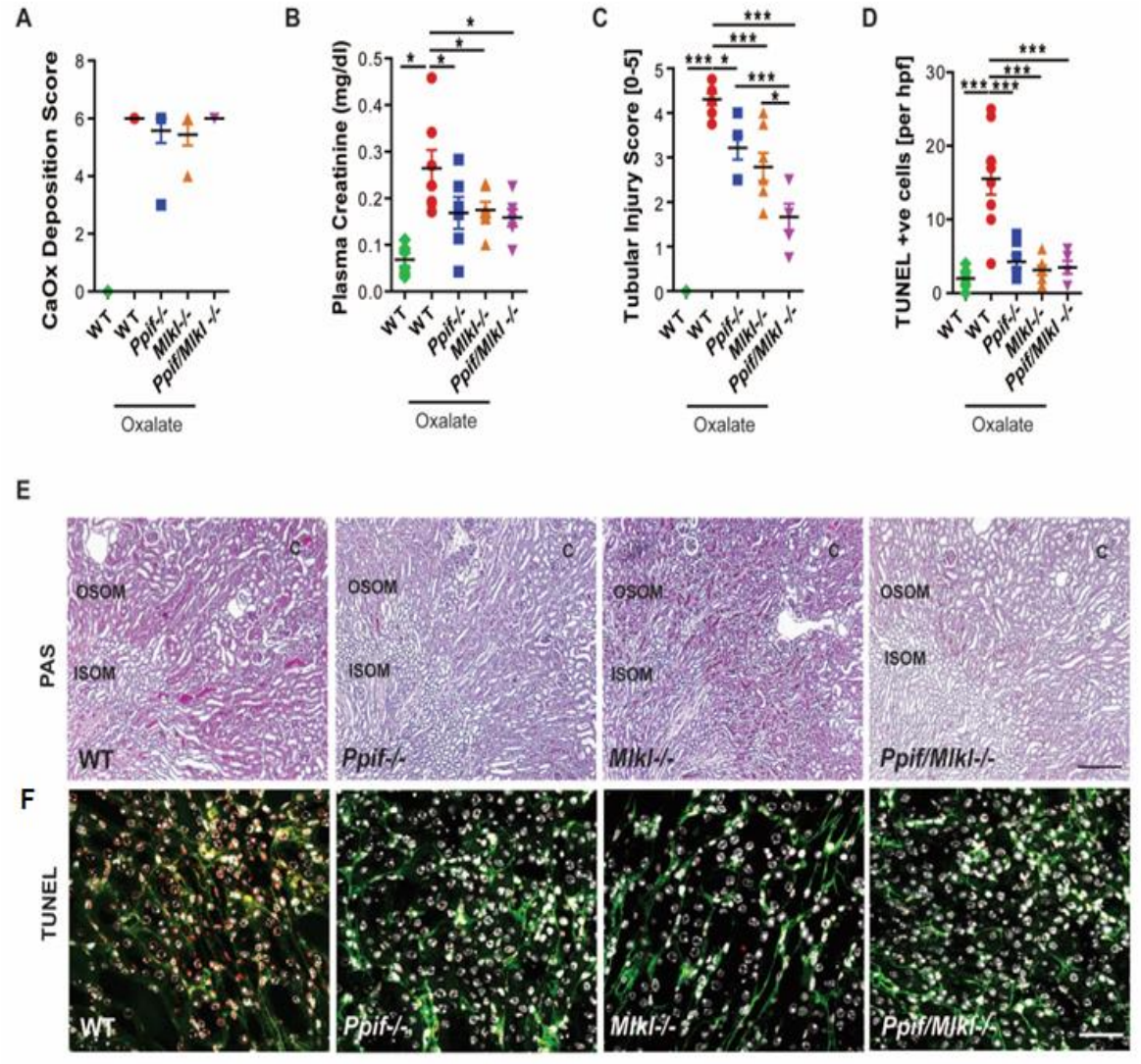

Figure 36. **Acute oxalate nephropathy attenuates in *Ppif*- and *Mlkl*-deficient mice. (A)** Inducing acute oxalate nephropathy in wild-type and *Ppif*- and *Mlkl*-deficient or *Ppif/Mlkl*-double-deficient mice with the same background showed identical amounts of renal CaOx crystal deposition after 24 hours as quantified by morphometry of Pizzolato-stained kidney sections. **B-D**: Plasma creatinine level increased in wild-type mice with acute oxalate nephropathy **(B)**, as well as tubular injury **(C),** and TUNEL positive cells **(D),** which were reduced in the deficient mice. (**E**) PAS staining indicates tubular damage at the corticomedullary junction in wild-type mice. Original image magnification: x100. **(F)** TUNEL staining shows dead cells in red, with counterstaining for laminin in green and cell nuclei DAPI, in white. Original image magnification: x 200. Data are expressed as means ± SEM from 6-9 mice in each group. One-way ANOVA with post-hoc Bonferroni`s correction was used to analyze data. Data are presented as mean ± SEM * $p<0.05$, *** $p<0.001$ versus oxalate-treated wild-type mice. **Ppif**: peptidyl-prolyl cis-trans isomerase, **Mlkl:** mixed lineage kinase domain like pseudokinase, **CaOx**: calcium oxalate, **TUNEL**: Terminal deoxynucleotidyl transferase dUTP nick end labelling. C = cortex, OSOM = outer stripe of the medulla, ISOM = inner stripe of the medulla.

Mulay SR, Honarpisheh MM, et al.[2]

4.14. Mitochondrial membrane permeability transition-related necrosis and necroptosis inhibitors reduce crystalline organ damage

We sought to investigate whether Ppif can be used as therapy for acute oxalate nephropathy and to investigate the potential of inhibiting both MPT-RN and necroptosis. To do so, wild-type mice were injected with the MPTinhibitor CsA and the necroptosis inhibitor Nec1s or both in combination. We observed that inducing acute oxalate nephropathy in mice resulted in equal amounts of CaOx crystal deposition (Figure 37A). Single treatment with CsA and Nec1s showed partial effects in reducing plasma creatinine levels (Figure 37B), a marker of renal function, as well as tubular injury and TUNEL positive cells (Figure 37C-E). However, inhibiting both MPT and necroptosis at the same time had only an effect on the number of TUNEL positive cells but not on renal function and tubular injury compared to the single-treated groups of mice (Figure 37B-F). Our data show that dual inhibition of MPT and necroptosis can have some additional protective effects on crystal-induced organ injury, and suggest the involvement of both cell death pathways *in-vivo*.

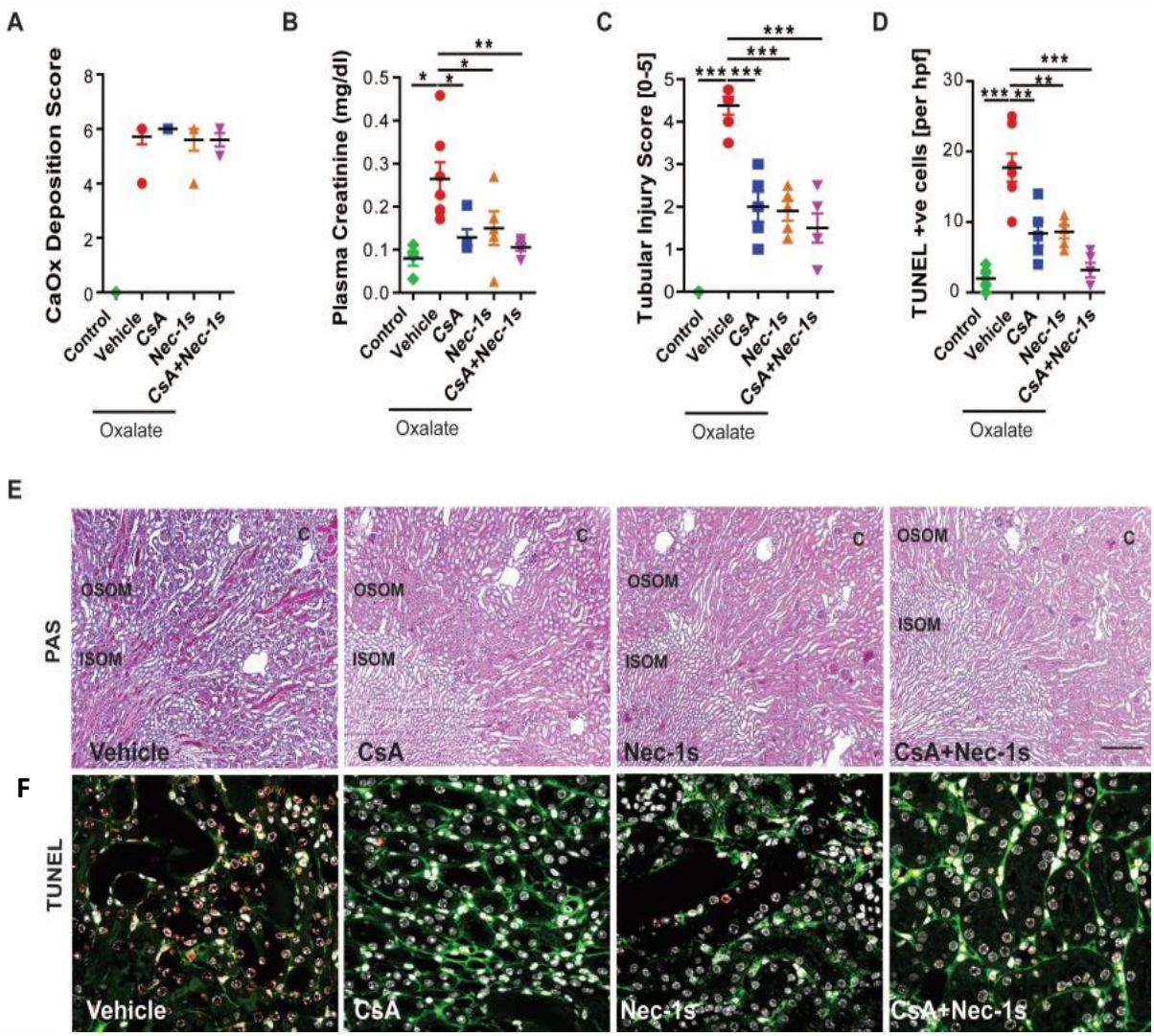

Figure 37. **Nec1s and CsA inhibitors attenuate acute oxalate-induced kidney injury. A-C**: Acute oxalate nephropathy was induced in wild-type mice, which were treated with vehicle, the MPT inhibitor (CsA, 2 mg/kg) or the Rip1 inhibitor Nec1s or in combination of CsA with Nec-1s. Pizzolato-staining revealed the same amounts of CaOx crystal deposition after 24 hours **(A)**. Treatment with the single inhibitors or dual blockade significantly reduced the plasma creatinine levels **(B**) and tubular injury **(C)**, as well as showed less TUNEL positive cells in kidney samples **(D).** PAS staining showed tubular injury at the corticomedullary junction in wild-type mice. Original image magnification: x100 (E upper panel). **(F)** TUNEL staining visualized dead cells in red, with counterstaining for laminin in green and cell nuclei DAPI, in white. Original image magnification: x200 (E lower panel). Data are presented as means ± SEM from 5-7 mice in each group. One-way ANOVA with post-hoc Bonferroni`s correction was used to analyze data. * $p<0.05$, ** $p<0.01$, *** $p<0.001$ versus vehicle-treated mice. **CsA**: cyclosporine A, **MPT**: membrane permeability transition, **Nec1s**: necrostatin-1s, **CaOx**: calcium oxalate, **TUNEL**: Terminal deoxynucleotidyl transferase dUTP nick end labelling. C = cortex, OSOM = outer stripe of the medulla, ISOM = inner stripe of the medulla.

Mulay SR, Honarpisheh MM, et al.[2]

4.15. Involvement of MPT in human tubular cells

To confirm and validate our mouse results in human cells, we used HK2 and CD24/CD133+ epithelial progenitor cells, which were isolated from healthy human kidneys that are known to contribute to the turnover of tubular epithelial cells and their regeneration after acute injury.[182,183] HK2 cells were pre-treated with the MPT inhibitor CsA, the ROS inhibitor APDC, the phagocytosis inhibitor CytD and the cathepsin inhibitor CAO74Me for 30 minutes prior to stimulation with CaOx, silica, MSU, and CPPD crystals for 24 hours. We saw a significant reduction of PI positive signals in treated cells compared to the vehicle group (Figure 38A-D). These data indicate that MPT is also involved in crystal cytotoxicity in human cells. Furthermore, we used CD24/CD133+ epithelial progenitor cells and pre-treated them with the MPT inhibitor CsA, the ROS inhibitor APDC, the phagocytosis inhibitor CytD and the cathepsin inhibitor CAO74Me for 30 minutes prior to stimulation with CaOx, silica, MSU, and CPPD crystals for 24 hours. We observed a significant reduction in PI positive signals after pre-treating cells with various inhibitors. We conclude that the MPT pathway is involved in crystal-induced cell death and injury in human cells (Figure 39A-D).

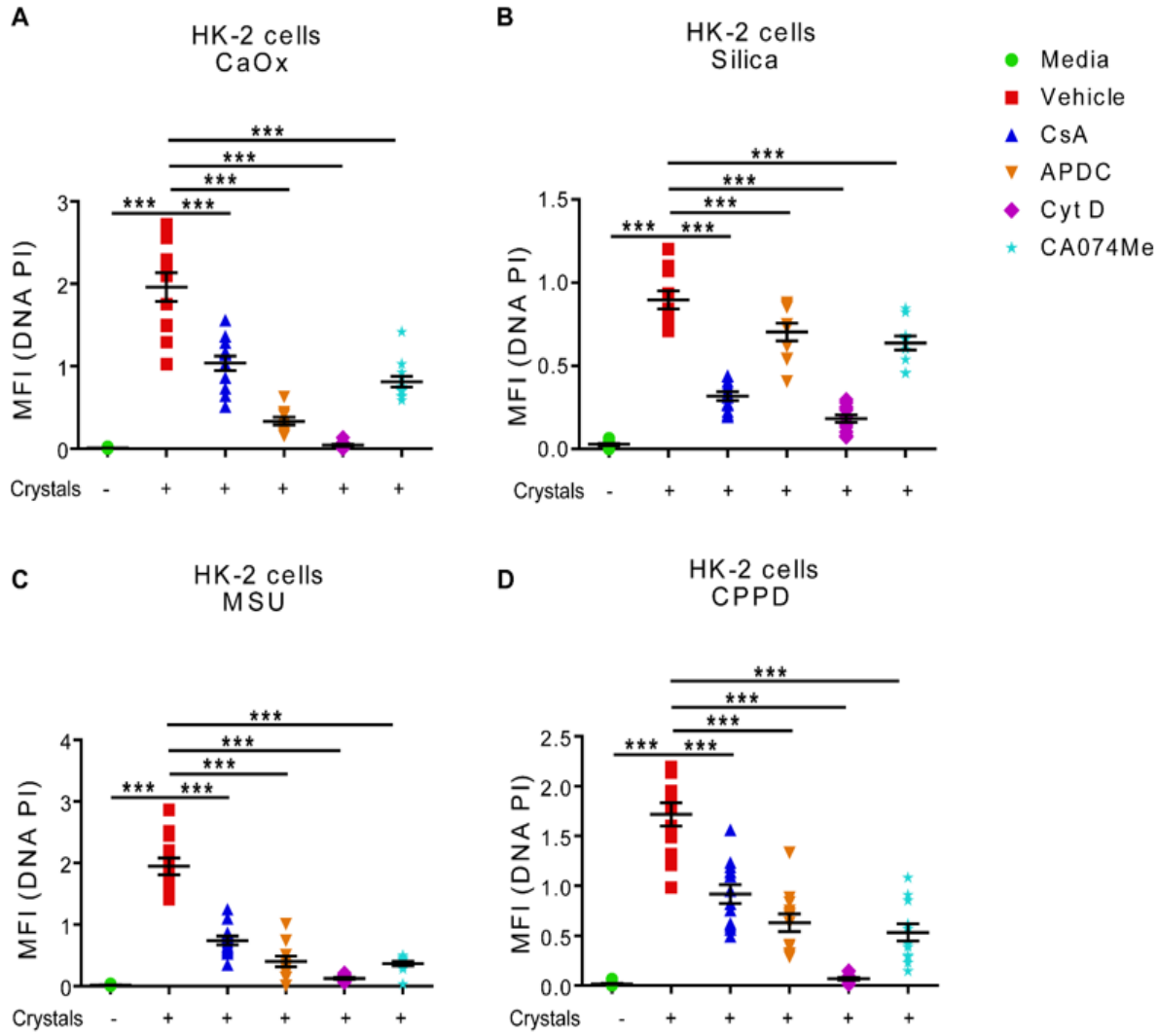

Figure 38. **Cell death analysis of HK2 cells stimulated with crystalline particles in the presence of various inhibitors. (A-D)** HK2 cells were pre-treated with different inhibitors as mentioned before and stimulation with 1 mg/ml CaOx, 0.5 mg/ml silica, 0.5 mg/ml MSU and 0.5 mg/ml CPPD crystals. Cells were stained with the dye PI. Results were quantified and expressed as MFI (n =10-12). Data are representative of three independent experiments. One-way ANOVA was used to analyze data and are presented as mean SEM. *** $p<0.001$ vs vehicle. **CaOx**: calcium oxalate, **MSU**: monosodium urate, **CPPD**: calcium pyrophosphate dehydrate. **MFI**: mean fluorescent intensity.

Mulay SR, Honarpisheh MM, et al.[2]

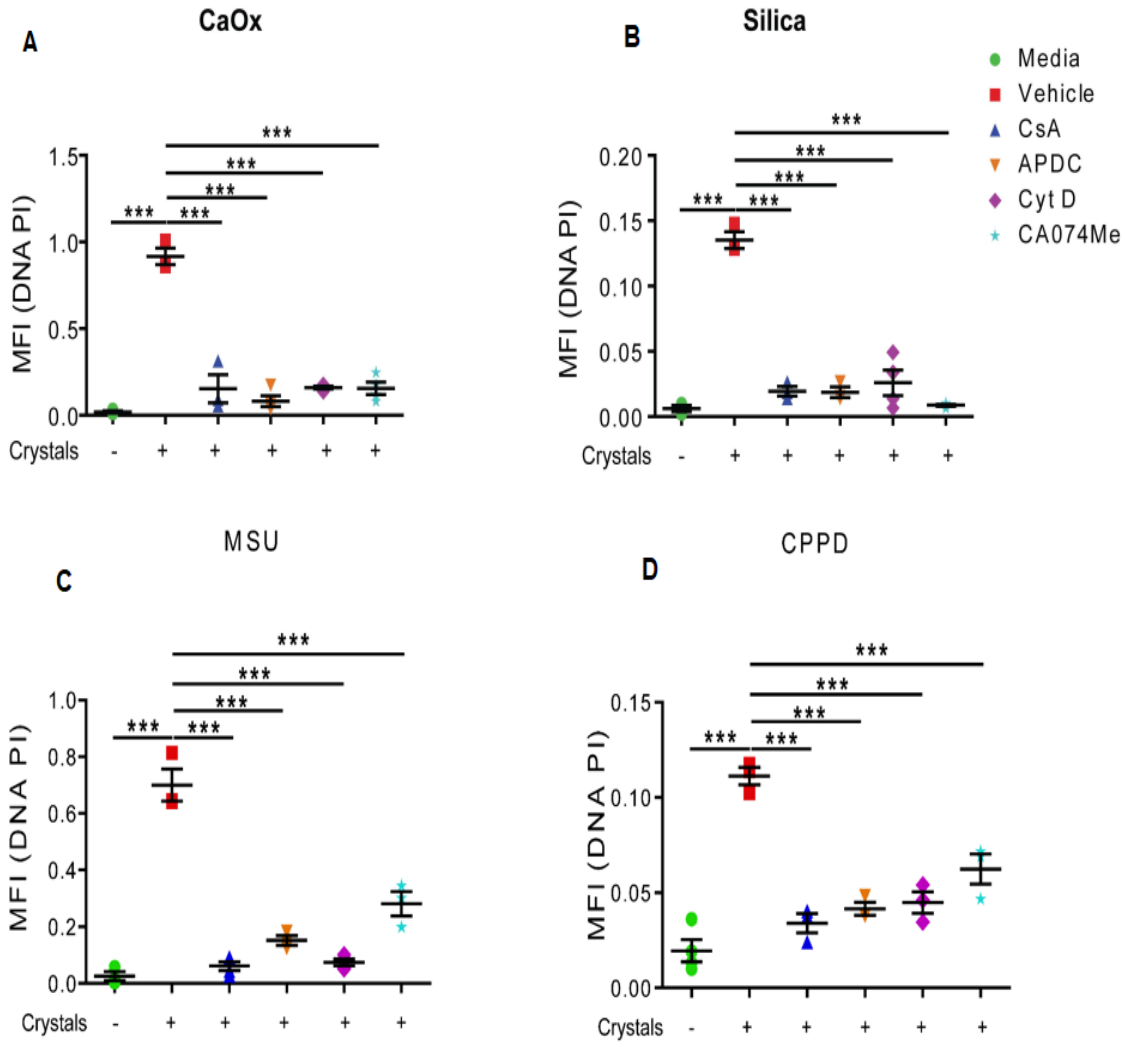

Figure 39. **Cell death analysis of primary human renal progenitor cells stimulated with crystal particles. (A-D)** Primary renal human progenitor cells were pre-treated with vehicle, CsA (1 µM), APDC (200 µM), CytD (10 µM), and CA074Me (20 µM) prior to stimulation with 1 mg/ml CaOx, 0.25 mg/ml silica, 0.5 mg/ml MSU and 0.5 mg/ml CPPD crystals. Cells were stained with PI andiImages were quantified and expressed as MFI (n=3-4). Data is representative from three independent experiments. One-way ANOVA was used to analyze data and are presented as mean ± SEM. *** p<0.001 vs vehicle. **CaOx**: calcium oxalate, **MSU**: monosodium urate, **CPPD**: calcium pyrophosphate dehydrate, **APDC**: (2R,4R)-4-aminopyrrolidine-2,4-dicarboxylate; **CytD**: Cytochalasin D, **CsA**: cyclosporin A.

Mulay SR, Honarpisheh MM, et al.[2]

5. Discussion

In this thesis project we had hypothesized that:

1. Acute tissue injury leading to progressive organ damage is associated with increased expression of necroptosis-related genes.

2. Environmental and metabolic crystals, regardless of their shape and size induce necroptosis in primary and immortalize human and mouse renal tubular cells.

3. Crystalline particles induce MPT as an alternative form of cell death and drive organ injury *in vivo*.

The molecular events of kidney injury are associated with cell death and inflammation, i.e. necroinflammation. Cell death pathways can be distinguished by morphology or caspase activity. For example, apoptosis is a non-immunogenic cell death pathway due to the formation of apoptotic bodies and their removal by immune cells, whereas regulated necrosis pathways are highly immunogenic and able to trigger inflammation. Necrosis was thought to be an uncontrolled form of cell death but meanwhile many studies show that necrosis is usually highly regulated [117]Necrotic cells release DAMPs, which induce the secretion of inflammatory cytokines. In turn, cytokines can induce regulated-necrosis, which results in an autoamplification loop named necroinflammation. Necroinflammation is the main event in AKI. [16, 108, 184, 47] Our data now show that the mRNA expression levels of Ripk3, Mlkl, and cIAP1/2 are significantly increased in three different models of AKI. These observations, regardless of the different inducer of injury, raise the question whether the necroptosis pathway is involved in renal tubular damage or not. However, we saw different patterns of expression levels of regulated-necrosis-related genes, including, *Tnfr1*, *Ripk1*, *Casp8*, *Fadd*, *Ppif (CypD)*, *Casp1*, *Nlrp3*, and *Parp1*. For example, *Nlrp3* and *Casp1* are significantly increased in IRI and cisplatin, whereas they did not induce acute oxalate nephropathy. Although *Nlrp3*- and *Casp1*-deficient mice show less injury compared to wild-type mice. Interestingly, Ppif (CypD) did not change in IRI and acute oxalate mice, but was significantly down-regulated in cisplatin model. *Ppif* -deficient mice were protected from IRI. In spite of that, Linkermann, *et al*, demonstrated that *Ppif* -deficient mice showed significantly prolonged survival in a lethal IRI model compared to wild-type mice.[111] In addition, *Ppif*-deficient mice exhibited improvement of renal function and less kidney damage.[111] Moreover, *Gpx4* mRNA expression did not change in all three AKI models. Although in previous studies, the inhibition of ferroptosis with a new

generation of a third-generation ferrostatin (SRS16-86) drug as well as *Ppif*-deficient mice showed less kidney injury.[159, 160] Furthermore, we observed that *Parp1*, a mediator of the parthanatos pathway, did not change in any of the AKI models. Little is known about the association of the parthanatos with kidney injury. However, one study showed that Parp1 reduced graft rejection in kidney transplantation patients and could serve as a serum biomarker[185]. It is worth mentioning that, the two major proteins Ripk3 and Mlkl are highly induced in renal IRI, acute oxalate nephropathy, and cisplatin models at mRNA and the protein level using RT-PCR and immunohistochemistry. However, the contribution of cell death and inflammation in CKD is not very clear since chronic tissue injuries are represented by a low grade of continuous inflammation as well as more chronic wound healing mechanisms, often resulting in tissue atrophy and scaring. Our data now show that *Ripk3* and *Mlkl* transcripts significantly increased on day 7 and 14 compared to the control group in chronic oxalate nephropathy; however, *Mlkl* expression levels decreased on day 21 but not Ripk3. These observations suggested that firstly the necroptosis pathway could be involved in CKD following IRI.

Secondly, necroptosis inhibitors may give maximal protection during early phase of injury. Although functional studies are needed to check the role of necroptosis in CKD. Interestingly, *Nlrp3* and *Casp1* were highly induced at day 7, 14, and 21. These high expression levels could be due to macrophage infiltration and different state of these specialized immune cells. Indeed, our group showed that the Nlrp3 inhibitor b-hydroxybutyrate, as well as lack of *Nlrp3*, attenuated nephrocalcinosis-related CKD in mice[186]. Meanwhile, *Ppif (CypD)* mRNA is significantly down-regulated at all three-time points, which could serve as a negative regulator of the MPT pathway in chronic oxalate nephropathy but functional studies are required to confirm the present data. Nonetheless, it is noticeable that only mRNA profiling studies may not represent the functional role of each gene in the process of the diseases with high complexity as well as multi-interaction pathway responses to a particular injury. However, our data showed a new sight into how regulated-necrosis-related genes respond to tissue injury, and it could be useful to develop a novel therapy for the tissue and organ injury but not limited to only kidney related-diseases.

Crystals or crystalline particles induce NLRP3 inflammasome complex formation; hence activate inflammation and the necroinflammation loop[187]. Cholesterol crystals phagocyte by human monocyte and macrophage activate NLRP3 result in IL-1β secretion.[188] In addition, Duewell, *et al*. showed that cholesterol crystals contribute to the development of

atherosclerosis in mice.[189] The deposition of MSU and CPPD crystals associated with gout and pseudogout, respectively, trigger Nlrp3 inflammasome activation, resulting in acute and chronic inflammation.[180] CaOx crystals have been described to be involved in acute kidney damage through activation of the NLRP3 inflammasome in renal dendritic cells, which is associated with the release of IL-1β and inflammation.[47] A similar mechanism has been shown for other crystals including silica, asbestos.[52,190], TiO2[191], and CaP[192] although inflammasome formation can also lead to activation of Casp1, which could result in activation of the pyroptosis pathway.[193, 194] However, our data now show that blocking caspases did not prevent cytotoxicity of crystalline particles. These observations indicate that crystal or crystalline particles induced-cell death is independent of caspase activity. In addition, FACS analysis showed the involvement of primary necrosis as predominant form of cell death in crystal or crystalline particles cytotoxicity. Our group recently reported that crystal or crystalline particle induced-cell death occurs through activation of the necroptosis pathway in primary mouse tubular epithelial cells.[16] Furthermore, the involvement of necroptosis in acute oxalate nephropathy was confirmed using *Mlkl*-deficient mice.[16] Our data now reveal that blocking core proteins of the necroptosis pathway results in partial protection in crystal or crystalline particle cytotoxicity regardless of their sizes, shapes and origin (Figure 40). RIPK1 is an upstream kinase protein of RIPK3 of the necroptosis signaling pathway, which is considered to be the initiator of this pathway by inducing RIPK3 phosphorylation (Figure 40). The main reason why RIPK1 activity is believed to be needed for necroptosis activation is that blocking RIPK1 with Nec1s could effectively prevents necroptosis and shows a protective effect in various animal disease models.[195,196,197,198,199] Interestingly, Conor J. Kearney, *et al.* demonstrated that silencing *Ripk1* using siRNA at mRNA level does not suppress but activates necroptosis in L929 cells treated with TNF-α and zVAD, which means that RIPK1 can act as an inhibitor rather than an initiator of necroptosis.[200] Moreover, enzymatic post-translational modifications of RIPK1 play a crucial role in the suppression of necroptosis. For example, ubiquitination of RIPK1 prevented necroptosis.[201] These data strongly suggested that RIPK1 can behave completely different depending on the biological conditions. However, our data revealed that inhibition of RIPK1 using Nec1s results in the reduction of crystal or crystalline particle cytotoxicity in renal human tubular cells (Figure 40). However, it would be interesting to study different aspects of RIPK1 in crystalline particle cytotoxicity. In addition, we saw that pretreatment of cells with the RIPK3 inhibitor dabrafenib prevented crystal or crystalline particle-induced cell death (Figure 40). Moreover, silencing *RIPK3* using specific siRNA showed the same trends of protection. MLKL is a crucial protein in the necroptosis signalling

pathway, which is also responsible for the execution of necroptosis-dependent cell death.[202] It was reported that MLKL gets phosphorylated through RIPK3 activation.[103] Furthermore, upon necroptosis activation, conformational switching of the pseudokinase domain triggers human MLKL tetramerization, which is needed for the execution of cell death.[203] Interestingly, MLKL activation can trigger NLRP3 inflammasome activation and release of IL-1β in macrophages.[204] Our data show that depletion of MLKL with NSA or *Mlkl*-deficient mice partially prevented crystalline particle-induced cell death (Figure 40). Furthermore, many studies showed that sizes and shapes of particles are critical in responding to inflammatory signals, for example, nanoparticles with different sizes and shapes can have broad cytotoxicity effects in various cell types as well as animal models.[205] Interestingly, silica particles with a range of 30 nm to 1000 nm show more cytotoxic effect on cells, including lysosomal destabilization, cell death, and IL-1β secretion compared to larger 3000 nm - 10000 nm particles.[206] Muñoz LE, *et al*. showed that nanoparticles lead to neutrophil NETosis dependent on the size of particles.[173] The authors in this study used nanodiamonds ranging between 10 nm to 1000 nm and polystyrene ranging between 40 nm to 1000 nm. They observed that aggregated NETs formation happens only in response to small sized nanoparticles. Besides that, human epithelial (HeLa) cells exposed to small nanodiamond particles (10 nm) showed the most cytotoxic effect associated with vacuolization and formation of structures resembling apoptotic subcellular microvesicles. In addition, they observed that nuclear material released into ACMV like blebs, whereas nanodiamond particles with more than 50 nm did not have a cytotoxic effect. However, zVAD-FMK, a pan-caspase inhibitor, did not abolish the cytotoxic effects of small sized nanoparticles (10 nm). The authors concluded that nanoparticles directly damage the plasma membrane without activation of apoptosis in epithelial cells.[173] However, it is well-established that apoptosis does not lead to plasma membrane damage or rupture. Therefore, it is not yet clear whether small nanodiamond particles induce cell death through only cell membrane damage or whether they can activate the programmed cell death pathways. CaP bioceramics have been used as bone substitutes for several years. HA particles are dispersed within an amorphous CaP matrix and CaP particles can be released during remodeling of bone and lead to inflammation. Of note, HA particles with different sizes can have diverse effects on inflammatory markers.[207,208] In the present study, we used crystals or crystalline particles with significantly differences in their sizes as well as shapes. Interestingly, we saw that regardless of their sizes and shapes, all crystalline particles induced necroptosis in human and mouse renal tubular epithelial cells but induced different effects of protection. These observations strongly suggested that other forms of cell death could be involved in

crystal or crystalline particle-induced cell death. Furthermore, we saw that the inhibition of actin polymerization significantly reduced the cytotoxic effects of crystalline particles indicating that phagocytosis is required for crystalline particle-induced cell death (Figure 40). Our data demonstrate that crystal or crystalline particles irrespective of origin (environmental or metabolic), sizes, and shapes are associated with necroptosis. These findings show that RIPK1, RIPK3, and MLKL could serve as potential molecular targets to limit tissue damage in silicosis, TiO2-induced lung injury, CaP-related bone implantation as in occupational-related diseases, and cholesterol embolism, gout, pseudogout, and oxalate nephropathy, as in metabolic-related disorders.

As mentioned earlier, our data show that crystal- or crystalline particle-induced cell death involves caspase independent mechanisms; however, inhibition of necroptosis showed only a partial protective effect. Therefore, we had hypothesized that other regulated necrosis pathways might be involved in crystal cytotoxicity. Indeed, reports have shown that CaOx crystal particles can alter the mitochondrial membrane potential, and a process that can be reversed by using the Ppif inhibitor CsA.[209] In addition, CsA injected into hyperoxaluric rats reduced calcium crystallization compared to healthy rats.[209] Moreover, MPT-RN is involved in renal IRI as well as cisplatin-induced kidney injury.[210] Indeed, *Ppif*-deficient mice showed less kidney injury in acute oxalate nephropathy compared to wild-type mice. Besides that, CsA injected into wild-type mice showed similar protection. In addition, proteins located on the outer and inner mitochondrial membranes play an important role in inflammation and cell death.[211, 117, 212] MPT appears to be controlled by Ppif protein, which can promote opening of pores during the activation of MPT.[213] In addition, Ppif can drive the breakdown of MOMP, water influx, mitochondrial swelling, loss of cristae, ROS production, and eventually, mitochondrial and cellular rupture[211,117] In particular, Ppif-dependent mitochondrial damage is associated with proximal tubules function after hypoxic and ischemic injury.[214] Our data show that phagocytosis of CaOx crystals can have a direct Ppif-driven cytotoxic effect and lead to MPT-RN in freshly isolated primary tubular epithelial cells (Figure 40). Furthermore, the same mechanism of regulated-cell death contributes to acute oxalate nephropathy. Interestingly, we did not observe any differences in crystal deposition in *Ppif*-deficient mice compared to wild-type mice. These findings suggested that Ppif does not play a role in crystals deposition in acute oxalate nephropathy. However, a previous study has reported that inhibition of Ppif in rats could limit the renal calcium crystallization[215], although ethylene glycol had been used to induce calcium crystallization but this might be due to different mechanisms. It is worth

mentioning that a recent study reported that genetic differences in the background of C57BL/6 mouse substrains could have diverse effects on kidney crystal depositions.[216] The molecular mechanisms of crystal or crystalline particle-induced MPT-RN have not been completely understood. Our data on 2D TEM as well as 3D reconstruction revealed that renal epithelial tubular cells can phagocytose crystalline particles, which leads to formation of phagolysosomes (Figure 40). Since crystalline particles are difficult to digest inside phagolysosome, they rather induce lysosomal leakage and trigger the release of cathepsins (Figure 40). It is known that cathepsins are released as a consequence of lysosomal damage and are associated with crystal-induced activation of the NLRP3 inflammasome.[33,47] Indeed, our data demonstrate that blocking cathepsins using a chemical inhibitor partially reduced crystal- or crystalline particle-induced MPT-RN (Figure 40). However, reports have shown that cathepsins can reduce regulated-necrosis in mouse macrophages through Rip1 kinase cleavage. Since different cathepsins have been described, further studies are needed to rule out the function of each cathepsin. Interestingly, preventing the internalization of crystalline particles in renal epithelial tubular cells significantly reduced ROS production and cell necrosis, as well as an improved MOMP. These findings suggested that phagocytosis of crystals is an essential step in crystal or crystalline particle-induced MPT-RN. In line with previous reports, ROS production is a critical step in MPT-related regulated necrosis.[211,117] Our data now reveal that blocking ROS production can effectively reduce crystal-induced MPT-related regulated necrosis as well as loss of MOMP (Figure 40). Interestingly, blocking Ppif with CsA as well as specific siRNA against Ppif at mRNA level significantly reduced crystal-induced MPT-related regulated necrosis, ROS production, and loss of MOMP. Since our previous data indicate the involvement of necroptosis in crystal or crystalline particle-induced cell death, we were interested in checking what could be the potential contribution of MLKL in MPT-RN. It was reported that widespread mitochondrial depletion does not affect RIPK3-dependent necroptotic cell death.[217] However, recent studies showed the involvement of the necroptosis pathway through mitochondrial function in different conditions.[218,219] Interestingly, one study showed that pMLKL translocates to the mitochondrial membrane and contributes to cell death.[220] Our data now show that *Ppif* -and *Mlkl*-deficient mice did not give consistent results in acute oxalate nephropathy. These findings indicate that both necroptosis and MPT-RN contribute to crystal or crystalline particle-induced tissue injury in the context of AKI. One recent study showed that activation of necroptosis through the TNF-α signaling pathway in mouse microvascular endothelial cells leads to cell death and transplant rejection in mice, which could be attenuated by inhibiting Ppif.[221] However, the role of cathepsins was not considered in this study despite

their important role in crystal-induced cell death and necroptosis. In addition, MPT activation in crystal or crystalline particles-induced cell death is completely different from TNFa signalling; therefore it might lead to different results and observations. Our data now show the contribution of both necroptosis and MPT-RN in crystal-induced cell death and organ injury. These finding could contribute to the development of novel therapies in crystal or crystalline particle-induced cell death as well as organ injury.

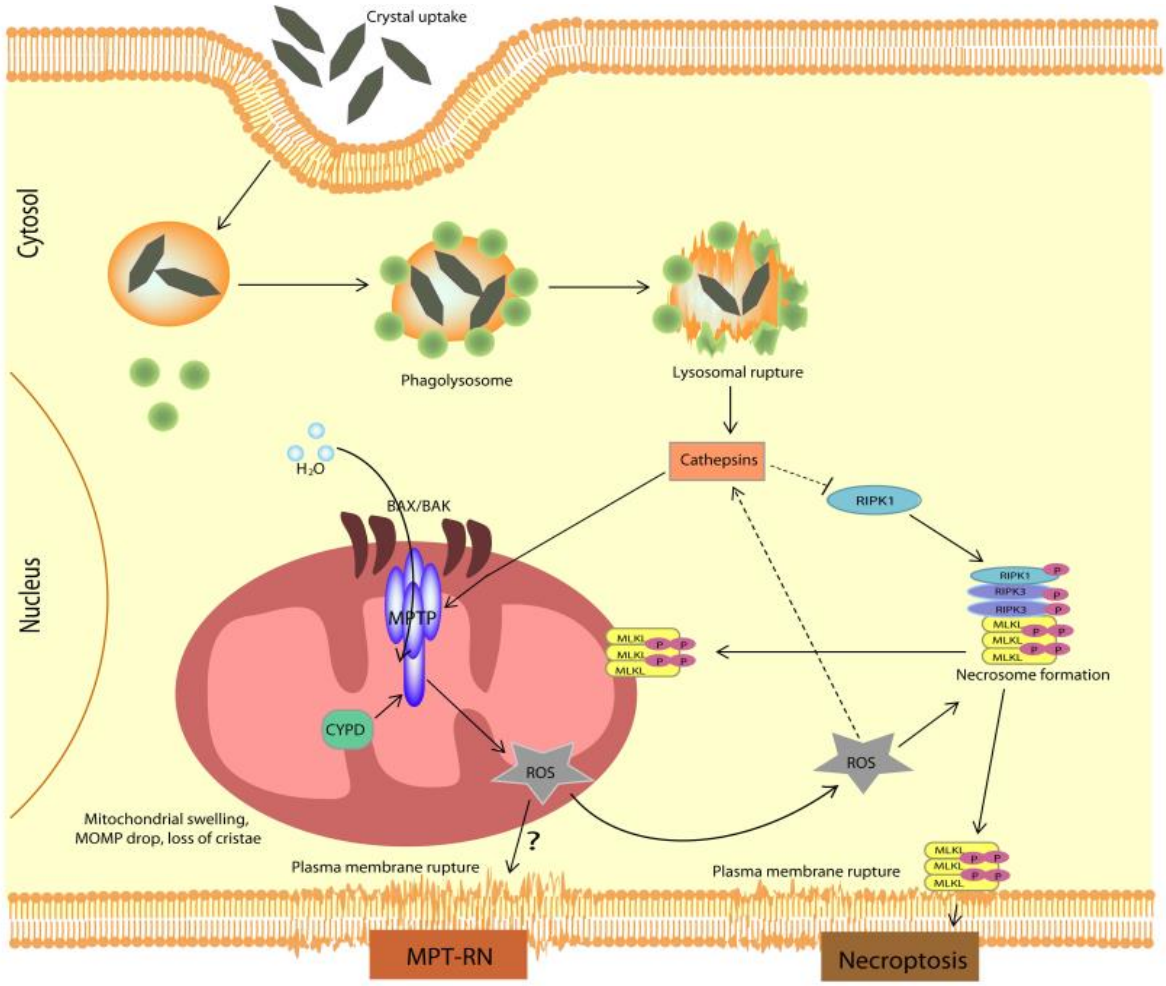

Figure 40**. Schematic synthesis of necroptosis and MPT pathways.** Crystal particles are taken up by renal epithelial cells and form phagolysosomes, which then rupture due to a lack of capacity of the epithelial cell to digest the crystalline particles. Cathepsins could release from lysosomal rupture into the cytosol and regulate mitochondrial permeability transition as well as necroptosis. Upon RIPK and RIPK3 phosphorylation, MLKL is activated and translocates to the plasma membrane and mitochondrial membrane resulting in cell rupture and regulated necrosis. On the other hand, crystalline particles can activate the MPT pathway leading to cell death. In this process, ROS production due to mitochondrial damage promotes the formation of the necrosome. **MPT**: membrane permeability transition, **RIPK1/3**: receptor-interacting serine/threonine-protein kinase 1/3, **MLKL**: mixed lineage kinase domain like pseudokinase **ROS**: reactive oxygen species.

6. Study limitations

We have encountered various limitations in the present study. Since we used two systems *in-vitro* and *in-vivo* to confirm our results, we had limitations related to both methods.

One part of the study was aimed to determine the cytotoxic effects of crystalline particles *in-vitro*. The list of limitations are as follow:

- We could only study a small range of different concentrations of crystal particles due to their physical properties. This means that if we would have used higher concentrations crystal particles would have covered all cells and eventually resulted in physical and unwanted damage.
- In our *in-vitro* study, we only used human or mouse non-immune cells in the concept of kidney injury. However, it would be useful to also confirm the data in a broader range of cell types.
- Due to the high cytotoxic effects of crystalline particles, we could only perform all experiments within 24 hours, which may not optimally mimic crystal-induced tissue injury under physiological conditions *in-vivo*.

One of the main limitations of the *in-vivo* system was that we could perform only a single mouse model of acute oxalate nephropathy, which allows us to check the involvement of Ppif and Mlkl proteins in the concept of CaOx-dependent kidney damage.We were unable to carry out other mouse disease models for related to the above mentioned types of crystalline particles such as acute gouty arthritis, silicosis, and cholesterol crystal embolism; therefore we focussed more on *in-vitro* experiments. For example, MSU, CPPD, silica, TiO2, and cholesterol would have been equally interesting to study *in-vivo* but would have required other ethical agreements, which were not available. Another major limitation was that we could not use other human samples to show the importance of our findings in human diseases.

Despite these limitations, we performed all experiments on primary human and mouse cells as well as cell lines to show the involvement of necroptosis as well as MPT-RN in crystal or crystalline particles cytotoxicity.

7. Conclusion

Our data provide new insights into the pathomechanism of crystalline particles in organ failure as well as tissue injury.

The findings of our study have the following potential implications as listed below:

- The regulated necrosis-related genes, particularly Ripk1, Ripk3, and Mlkl, were highly induced in mouse models of AKI as well as CKD, which provided a rationale to test for their causal contribution to tissue injury and organ failure.
- Caspase-dependent cell death pathways do not contribute to crystal-induced cytotoxicity.
- Environmental and metabolite crystalline particles induce necroptosis.
- Crystalline particles require internalization into the cells via phagocytosis to initiate cell death processes.
- Mitochondrial damage contributes to crystalline particles cytotoxicity.
- Ppif mediates mitochondrial damage and promotes crystal cytotoxicity.
- Neutralizing MPT and targeting necroptosis abrogate acute oxalate nephropathy.

Since the cytotoxic effects of crystal or crystalline particles can lead to acute inflammation, cell death, and eventually severe organ failure, understanding the molecular mechanisms of crystal-induced tissue injury is crucial. Indeed, our data now reveal that metabolic and environmental crystalline particles can activate necroptosis and MPT-RN, and that blocking these two cell death pathways can limit the cytotoxicity effect of crystal-induced kidney failure. It is likely that the same mechanism is involved in crystal-induced injury in other organs as our *in-vitro* studies with different crystalline microparticles demonstrate. Besides that, our data on human progenitor cells showed the same molecular mechanisms on the crystal or crystalline particle-induced cell death.

Taken together, our research highlights the importance of MPT-RN and necroptosis in organ and tissue injury in mouse as well as human cells. Potentially, our data could be useful to develop a novel target therapy for occupational job related-diseases as well as metabolic crystalline particle-related diseases.

Zusammenfassung

Unterschiedliche Kristalle und kristalline Partikel sind mit Krankheitskomplikationen assoziiert. Eine unkontrollierte Bildung kristalliner Partikel im Körper führt zur Zell- und Organschädigung am betroffenen Ort. Unter anderem führen z.B. Harnsäurekristall (MSU)-Ablagerungen in Gelenken zur Gichtarthritis sowie Inhalation von Silikonstäuben zur Silikose und Cholesterinplaques zur Progression von Atherosklerose. Kristalle führen durch Aktivierung der NLR-Familie, NLRP3 und Inflammasom-Formation, welche wiederum IL-1β und IL18 Sekretion induzieren, zu Entzündungsprozessen in Geweben. Daten haben gezeigt, dass Silikonpartikel in Makrophagen zu Apoptose führen. Unsere Arbeitsgruppe zeigte, dass Kristalle zu RIPK1, RIP3 und MLKL vermittelten Nekroptose beitragen. In dieser Studie wurden vier unterschiedliche metabolische Kristalle (z.B. Kalziumoxalat (CaOx), MSU, Calcium Pyrophosphat Dihydrat (CPPD), und Cystein) genutzt um die zyototoxischen Effekte an Zellen und Organen zu untersuchen. Zwei Fragen blieben jedoch unklar: 1. Können Kristallpartikel aus der Umwelt zu Zellnekroptose führen? und 2. Ist ein anderer Zelltodmechanismus am Kristall-induzierten Zelltod beteiligt? Zur Beantwortung der ersten Frage selektierten wir unterschiedliche Kristalle und kristalline Partikel, darunter Silikone, Titanium Oxide, Cholesterol und Calcium Phosphat als Umwelt-assoziierte Kristalle, sowie MSU, CaOx, Cholesterol und Calcium Phosphat als metabolische Kristalle.

Zunächst untersuchten wir die Expression von Zelltod-regulierenden Genen in unterschiedlichen Tiermodellen. Wir beobachteten, dass RIK3 und MLKL sowohl im chronischen Modell der Oxalat-Nephropathie sowie akut-chronischem Ischemie-Reperfusion-Modell stark hochreguliert waren. Im Anschluss wurde in einer Reihe von Experimenten, die Beteiligung des Nekroptose-Signalwegs an Kristall-induziertem Zelltod evaluiert. Pharmakologische Inhibition der wichtigsten Proteine (RIPK1, RIPK3, MLKL) der Nekroptose resultierte in Zelltodverringerung. Passend zu diesen Beobachtungen konnte gezeigt werden, dass *Mlkl*-Knockdown und RIPK3-Runterregulierung mittels siRNA in primären Tubularzellen ebenfalls Zelltod reduziert. Um zu überprüfen, ob die intrazelluläre Aufnahme von Kristallen erforderlich ist, um den nekrotischen Zelltod zu induzieren, haben wir die Phagozytose mit CytD blockiert.Interessanterweise haben wir gesehen, dass die Hemmung der Phagozytose den Zelltod als Reaktion auf Kristalle signifikant verringert. Die gezielte Inhibierung der Nekroptose führte jedoch nicht zu einem vollständigen Blockade des Kristall-induzierten Zelltod. Aus diesem Grund spekulierten wir, dass ein anderer Zelltodweg

beteiligt ist. Frühere Studien zeigten eine mögliche Beteiligung für den mitochondrial Permiabilität-vermittelten (MPT) Zelltod-Signalweg.. Wir stellten die Hypothese auf, dass der MPT Zelltod eine Rolle bei der Kristall-induzierten Zytotoxizität spielen könnte. In der Tat bestätigen die Daten, dass MPT am durch Kristallpartikel-induzierten Zelltod beteiligt ist. Zusammenfassend zeigen unsere Ergebnisse, dass Nekroptose und MPT-RN eine wichtige Rolle beim durch Kristall- oder Kristallpartikel-induzierten Zelltod in vitro sowie bei der akuten Oxalatnephropathie in vivo spielen. Diese Ergebnisse könnten bei der Entwicklung neuer Therpaien für Erkrankungen im Zusammenhang mit Kristallen oder kristallinen Partikeln hilfreich sein.

Summary

Various crystals or crystalline particles are associated with clinical complications. The formation of crystalline particles within the wrong place of the body can result in cell injury and organ failure. For example, monosodium urate (MSU) deposition within joints cause gouty arthritis, deposition of CaOx in renal tubular compartment results in kidney injury, silica dust inhalation is associated with silicosis, and cholesterol promotes plaque and atherosclerosis progression. It is well-known that crystals can induce inflammation through activation of the NLR family, pyrin domain containing 3 (NLRP3), and inflammasome formation, which trigger interleukin 1 beta (IL-1β) and interleukin 18 (IL18) secretion. It has been shown that silica particles trigger apoptosis in macrophages. Although, our group showed that crystals cause necroptosis driven by receptor-interacting protein kinase 1 (RIPK1), receptor-interacting protein kinase 3 (RIPK3), and mixed lineage kinase domain-like pseudokinase (MLKL) proteins. In this study, four different metabolic crystals, including calcium oxalate (CaOx), MSU, calcium pyrophosphate dihydrate (CPPD), and cystine were used to show the cytotoxic effects on cells and organs. However, two main questions remained unclear; 1. Do environmental crystal particles induce necroptosis? And 2. Is another cell death pathway involved in crystal-induced cell death? To answer the first question, different crystal or crystalline particles such as silica, titanium dioxide (TiO2), cholesterol, and calcium phosphate (CaP) as environmental and MSU, CaOx, cholesterol, and CaP as metabolic crystalline particles were selected. Firstly, the expression level of regulated necrosis-related genes in different models was determined. We observed that Ripk3 and Mlkl were highly upregulated in acute and chronic oxalate nephropathy as well as acute and chronic ischemia-reperfusion injury as expected. Next, in a series of in-*vitro* and *in-vivo* experiments, the involvement of necroptosis was evaluated in response to environmental and metabolic crystalline particles. Pharmacological inhibition of Ripk1, Ripk3, and Mlkl prevented necroptosis cell death. In line with this finding using *Mlkl*-deficient primary renal tubular cells as well as siRNA against Ripk3 can reduce cell death and confirm the previous results. To check whether phagocytosis of crystals is required for inducing necroptotic cell death, we blocked phagocytosis using CytD.

Interestingly, we saw that inhibiting phagocytosis significantly decreased cell death in response to crystals. However, targeting necroptosis did not result in a complete protection crystal-induced cell death. Therefore, we speculated that another cell death pathway involved. Previous studies showed a potential role for the MPT cell death pathway. Therefore, we hypothesized that the MPT pathway could play a role in crystal induce cytotoxicity. Indeed, the data confirm

that MPT is involved in crystal particle-induced cell death. Taken together, our findings indicate that necroptosis and MPT-RN play an important role in crystal- or crystalline particle-induced cell death *in-vitro* as well as acute oxalate nephropathy *in-vivo*. These findings could be useful in developing new therapies for crystal- or crystalline particle-related diseases.

References

1. Honarpisheh, M.*, et al.* Phagocytosis of environmental or metabolic crystalline particles induces cytotoxicity by triggering necroptosis across a broad range of particle size and shape. *Sci Rep* **7**, 15523 (2017).
2. Mulay, S.R.*, et al.* Mitochondria Permeability Transition versus Necroptosis in Oxalate-Induced AKI. *J Am Soc Nephrol* **30**, 1857-1869 (2019).
3. Honarpisheh, M.*, et al.* Regulated necrosis-related molecule mRNA expression in humans and mice and in murine acute tissue injury and systemic autoimmunity leading to progressive organ damage, and progressive fibrosis. *Biosci Rep* **36**(2016).
4. Mulay, S.R. & Anders, H.J. Crystallopathies. *N Engl J Med* **374**, 2465-2476 (2016).
5. Pawar, A.S.*, et al.* Incidence and characteristics of kidney stones in patients with horseshoe kidney: A systematic review and meta-analysis. *Urol Ann* **10**, 87-93 (2018).
6. Messner, B. & Bernhard, D. Smoking and cardiovascular disease: mechanisms of endothelial dysfunction and early atherogenesis. *Arterioscler Thromb Vasc Biol* **34**, 509-515 (2014).
7. Herrington, W., Lacey, B., Sherliker, P., Armitage, J. & Lewington, S. Epidemiology of Atherosclerosis and the Potential to Reduce the Global Burden of Atherothrombotic Disease. *Circ Res* **118**, 535-546 (2016).
8. Ruan, Y.*, et al.* Cardiovascular disease (CVD) and associated risk factors among older adults in six low-and middle-income countries: results from SAGE Wave 1. *BMC Public Health* **18**, 778 (2018).
9. Sangani, R.G. & Ghio, A.J. Lung injury after cigarette smoking is particle related. *Int J Chron Obstruct Pulmon Dis* **6**, 191-198 (2011).
10. Stayner, L., Dankovic, D., Smith, R. & Steenland, K. Predicted lung cancer risk among miners exposed to diesel exhaust particles. *Am J Ind Med* **34**, 207-219 (1998).
11. Ezzati, M. & Kammen, D. Indoor air pollution from biomass combustion and acute respiratory infections in Kenya: an exposure-response study. *Lancet* **358**, 619-624 (2001).
12. Zhang, J.J. Introduction to JTD Air Pollution Section. *J Thorac Dis* **9**, 3410-3411 (2017).
13. Brockmeyer, S. & D'Angiulli, A. How air pollution alters brain development: the role of neuroinflammation. *Transl Neurosci* **7**, 24-30 (2016).
14. Mulay, S.R., Shi, C., Ma, X. & Anders, H.J. Novel Insights into Crystal-Induced Kidney Injury. *Kidney Dis (Basel)* **4**, 49-57 (2018).
15. Quinones, A. & Saric, M. The cholesterol emboli syndrome in atherosclerosis. *Curr Atheroscler Rep* **15**, 315 (2013).
16. Mulay, S.R.*, et al.* Cytotoxicity of crystals involves RIPK3-MLKL-mediated necroptosis. *Nat Commun* **7**, 10274 (2016).
17. Doshi, M.*, et al.* Paraprotein-Related Kidney Disease: Kidney Injury from Paraproteins-What Determines the Site of Injury? *Clin J Am Soc Nephrol* **11**, 2288-2294 (2016).
18. Motwani, S.S.*, et al.* Paraprotein-Related Kidney Disease: Glomerular Diseases Associated with Paraproteinemias. *Clin J Am Soc Nephrol* **11**, 2260-2272 (2016).
19. Klinkhammer, B.M.*, et al.* Cellular and Molecular Mechanisms of Kidney Injury in 2,8-Dihydroxyadenine Nephropathy. *J Am Soc Nephrol* (2020).
20. Coe, F.L., Evan, A. & Worcester, E. Kidney stone disease. *J Clin Invest* **115**, 2598-2608 (2005).
21. Chaudhary, A., Singla, S.K. & Tandon, C. In vitro Evaluation of Terminalia arjuna on Calcium Phosphate and Calcium Oxalate Crystallization. *Indian J Pharm Sci* **72**, 340-345 (2010).
22. Alelign, T. & Petros, B. Kidney Stone Disease: An Update on Current Concepts. *Adv Urol* **2018**, 3068365 (2018).
23. Bensatal, A. & Ouahrani, M.R. Inhibition of crystallization of calcium oxalate by the extraction of Tamarix gallica L. *Urol Res* **36**, 283-287 (2008).

24. Dal Moro, F., Mancini, M., Tavolini, I.M., De Marco, V. & Bassi, P. Cellular and molecular gateways to urolithiasis: a new insight. *Urol Int* **74**, 193-197 (2005).
25. Mulay, S.R. & Anders, H.J. Crystal nephropathies: mechanisms of crystal-induced kidney injury. *Nat Rev Nephrol* **13**, 226-240 (2017).
26. Sayer, J.A. Progress in Understanding the Genetics of Calcium-Containing Nephrolithiasis. *J Am Soc Nephrol* **28**, 748-759 (2017).
27. Worcester, E.M. & Coe, F.L. Clinical practice. Calcium kidney stones. *N Engl J Med* **363**, 954-963 (2010).
28. Roncal-Jimenez, C.*, et al.* Heat Stress Nephropathy From Exercise-Induced Uric Acid Crystalluria: A Perspective on Mesoamerican Nephropathy. *Am J Kidney Dis* **67**, 20-30 (2016).
29. Miller, D.C. & Wolf, J.S., Jr. Acute renal colic. *N Engl J Med* **350**, 2422-2423; author reply 2422-2423 (2004).
30. Oliviero, F., Scanu, A. & Punzi, L. Metabolism of crystals within the joint. *Reumatismo* **63**, 221-229 (2012).
31. Tsujihata, M. Mechanism of calcium oxalate renal stone formation and renal tubular cell injury. *Int J Urol* **15**, 115-120 (2008).
32. Fazen, L.E., Linde, B. & Redlich, C.A. Occupational lung diseases in the 21st century: the changing landscape and future challenges. *Curr Opin Pulm Med* **26**, 142-148 (2020).
33. Franklin, B.S., Mangan, M.S. & Latz, E. Crystal Formation in Inflammation. *Annu Rev Immunol* **34**, 173-202 (2016).
34. Baranowska-Wojcik, E., Szwajgier, D., Oleszczuk, P. & Winiarska-Mieczan, A. Effects of Titanium Dioxide Nanoparticles Exposure on Human Health-a Review. *Biol Trace Elem Res* **193**, 118-129 (2020).
35. Shin, S.W., Song, I.H. & Um, S.H. Role of Physicochemical Properties in Nanoparticle Toxicity. *Nanomaterials (Basel)* **5**, 1351-1365 (2015).
36. Liu, R.*, et al.* Small-sized titanium dioxide nanoparticles mediate immune toxicity in rat pulmonary alveolar macrophages in vivo. *J Nanosci Nanotechnol* **10**, 5161-5169 (2010).
37. Acar, M.S.*, et al.* Titanium dioxide nanoparticles induce cytotoxicity and reduce mitotic index in human amniotic fluid-derived cells. *Hum Exp Toxicol* **34**, 74-82 (2015).
38. Hu, R.*, et al.* Molecular mechanism of hippocampal apoptosis of mice following exposure to titanium dioxide nanoparticles. *J Hazard Mater* **191**, 32-40 (2011).
39. Wang, Y.*, et al.* Susceptibility of young and adult rats to the oral toxicity of titanium dioxide nanoparticles. *Small* **9**, 1742-1752 (2013).
40. Maurer, K.H. & Schumacher, H.R. Hydroxyapatite phagocytosis by human polymorphonuclear leucocytes. *Ann Rheum Dis* **38**, 84-88 (1979).
41. Suzuki, Y. & Churg, J. Structure and development of the asbestos body. *Am J Pathol* **55**, 79-107 (1969).
42. Archer, V.E. Carcinogenicity of fibers and films: a theory. *Med Hypotheses* **5**, 1257-1262 (1979).
43. Broz, P. & Dixit, V.M. Inflammasomes: mechanism of assembly, regulation and signalling. *Nat Rev Immunol* **16**, 407-420 (2016).
44. Leung, C.C., Yu, I.T. & Chen, W. Silicosis. *Lancet* **379**, 2008-2018 (2012).
45. Donaldson, K., Murphy, F.A., Duffin, R. & Poland, C.A. Asbestos, carbon nanotubes and the pleural mesothelium: a review of the hypothesis regarding the role of long fibre retention in the parietal pleura, inflammation and mesothelioma. *Part Fibre Toxicol* **7**, 5 (2010).
46. Tall, A.R. & Yvan-Charvet, L. Cholesterol, inflammation and innate immunity. *Nat Rev Immunol* **15**, 104-116 (2015).
47. Mulay, S.R.*, et al.* Calcium oxalate crystals induce renal inflammation by NLRP3-mediated IL-1beta secretion. *J Clin Invest* **123**, 236-246 (2013).
48. Nakayama, M. Macrophage Recognition of Crystals and Nanoparticles. *Front Immunol* **9**, 103 (2018).

49. Mulay, S.R. Multifactorial functions of the inflammasome component NLRP3 in pathogenesis of chronic kidney diseases. *Kidney Int* **96**, 58-66 (2019).
50. Amaral, E.P.*, et al.* Lysosomal Cathepsin Release Is Required for NLRP3-Inflammasome Activation by Mycobacterium tuberculosis in Infected Macrophages. *Front Immunol* **9**, 1427 (2018).
51. Yang, Y., Wang, H., Kouadir, M., Song, H. & Shi, F. Recent advances in the mechanisms of NLRP3 inflammasome activation and its inhibitors. *Cell Death Dis* **10**, 128 (2019).
52. Hornung, V.*, et al.* Silica crystals and aluminum salts activate the NALP3 inflammasome through phagosomal destabilization. *Nat Immunol* **9**, 847-856 (2008).
53. He, Y., Hara, H. & Nunez, G. Mechanism and Regulation of NLRP3 Inflammasome Activation. *Trends Biochem Sci* **41**, 1012-1021 (2016).
54. Dostert, C.*, et al.* Malarial hemozoin is a Nalp3 inflammasome activating danger signal. *PLoS One* **4**, e6510 (2009).
55. Orlowski, G.M.*, et al.* Multiple Cathepsins Promote Pro-IL-1beta Synthesis and NLRP3-Mediated IL-1beta Activation. *J Immunol* **195**, 1685-1697 (2015).
56. Munoz-Planillo, R.*, et al.* K(+) efflux is the common trigger of NLRP3 inflammasome activation by bacterial toxins and particulate matter. *Immunity* **38**, 1142-1153 (2013).
57. Refsnes, M.*, et al.* Different particle determinants induce apoptosis and cytokine release in primary alveolar macrophage cultures. *Part Fibre Toxicol* **3**, 10 (2006).
58. Ewence, A.E.*, et al.* Calcium phosphate crystals induce cell death in human vascular smooth muscle cells: a potential mechanism in atherosclerotic plaque destabilization. *Circ Res* **103**, e28-34 (2008).
59. Wang, L.*, et al.* Nano-hydroxyapatite particles induce apoptosis on MC3T3-E1 cells and tissue cells in SD rats. *Nanoscale* **4**, 2894-2899 (2012).
60. Iyer, R., Hamilton, R.F., Li, L. & Holian, A. Silica-induced apoptosis mediated via scavenger receptor in human alveolar macrophages. *Toxicol Appl Pharmacol* **141**, 84-92 (1996).
61. Desai, J.*, et al.* PMA and crystal-induced neutrophil extracellular trap formation involves RIPK1-RIPK3-MLKL signaling. *Eur J Immunol* **46**, 223-229 (2016).
62. Desai, J.*, et al.* Particles of different sizes and shapes induce neutrophil necroptosis followed by the release of neutrophil extracellular trap-like chromatin. *Sci Rep* **7**, 15003 (2017).
63. Tait, S.W., Ichim, G. & Green, D.R. Die another way--non-apoptotic mechanisms of cell death. *J Cell Sci* **127**, 2135-2144 (2014).
64. Green, D.R. & Llambi, F. Cell Death Signaling. *Cold Spring Harb Perspect Biol* **7**(2015).
65. Kerr, J.F., Wyllie, A.H. & Currie, A.R. Apoptosis: a basic biological phenomenon with wide-ranging implications in tissue kinetics. *Br J Cancer* **26**, 239-257 (1972).
66. D'Arcy, M.S. Cell death: a review of the major forms of apoptosis, necrosis and autophagy. *Cell Biol Int* **43**, 582-592 (2019).
67. Ashkenazi, A. & Salvesen, G. Regulated cell death: signaling and mechanisms. *Annu Rev Cell Dev Biol* **30**, 337-356 (2014).
68. Zong, W.X. & Thompson, C.B. Necrotic death as a cell fate. *Genes Dev* **20**, 1-15 (2006).
69. Laster, S.M., Wood, J.G. & Gooding, L.R. Tumor necrosis factor can induce both apoptic and necrotic forms of cell lysis. *J Immunol* **141**, 2629-2634 (1988).
70. Goossens, V., Grooten, J., De Vos, K. & Fiers, W. Direct evidence for tumor necrosis factor-induced mitochondrial reactive oxygen intermediates and their involvement in cytotoxicity. *Proc Natl Acad Sci U S A* **92**, 8115-8119 (1995).
71. Holler, N.*, et al.* Fas triggers an alternative, caspase-8-independent cell death pathway using the kinase RIP as effector molecule. *Nat Immunol* **1**, 489-495 (2000).
72. Degterev, A.*, et al.* Chemical inhibitor of nonapoptotic cell death with therapeutic potential for ischemic brain injury. *Nat Chem Biol* **1**, 112-119 (2005).
73. Degterev, A.*, et al.* Identification of RIP1 kinase as a specific cellular target of necrostatins. *Nat Chem Biol* **4**, 313-321 (2008).

74. Alnemri, E.S*., et al.* Human ICE/CED-3 protease nomenclature. *Cell* **87**, 171 (1996).
75. Pistritto, G*., et al.* Expression and transcriptional regulation of caspase-14 in simple and complex epithelia. *Cell Death Differ* **9**, 995-1006 (2002).
76. Czabotar, P.E., Lessene, G., Strasser, A. & Adams, J.M. Control of apoptosis by the BCL-2 protein family: implications for physiology and therapy. *Nat Rev Mol Cell Biol* **15**, 49-63 (2014).
77. Brumatti, G., Salmanidis, M. & Ekert, P.G. Crossing paths: interactions between the cell death machinery and growth factor survival signals. *Cell Mol Life Sci* **67**, 1619-1630 (2010).
78. Tait, S.W. & Green, D.R. Mitochondria and cell death: outer membrane permeabilization and beyond. *Nat Rev Mol Cell Biol* **11**, 621-632 (2010).
79. Galluzzi, L., Kepp, O. & Kroemer, G. Mitochondrial regulation of cell death: a phylogenetically conserved control. *Microb Cell* **3**, 101-108 (2016).
80. Cain, K*., et al.* Apaf-1 oligomerizes into biologically active approximately 700-kDa and inactive approximately 1.4-MDa apoptosome complexes. *J Biol Chem* **275**, 6067-6070 (2000).
81. Adrain, C., Slee, E.A., Harte, M.T. & Martin, S.J. Regulation of apoptotic protease activating factor-1 oligomerization and apoptosis by the WD-40 repeat region. *J Biol Chem* **274**, 20855-20860 (1999).
82. Fulda, S. & Debatin, K.M. Extrinsic versus intrinsic apoptosis pathways in anticancer chemotherapy. *Oncogene* **25**, 4798-4811 (2006).
83. Locksley, R.M., Killeen, N. & Lenardo, M.J. The TNF and TNF receptor superfamilies: integrating mammalian biology. *Cell* **104**, 487-501 (2001).
84. Ashkenazi, A. & Dixit, V.M. Death receptors: signaling and modulation. *Science* **281**, 1305-1308 (1998).
85. Rubio-Moscardo, F*., et al.* Characterization of 8p21.3 chromosomal deletions in B-cell lymphoma: TRAIL-R1 and TRAIL-R2 as candidate dosage-dependent tumor suppressor genes. *Blood* **106**, 3214-3222 (2005).
86. Suliman, A., Lam, A., Datta, R. & Srivastava, R.K. Intracellular mechanisms of TRAIL: apoptosis through mitochondrial-dependent and -independent pathways. *Oncogene* **20**, 2122-2133 (2001).
87. Chicheportiche, Y*., et al.* TWEAK, a new secreted ligand in the tumor necrosis factor family that weakly induces apoptosis. *J Biol Chem* **272**, 32401-32410 (1997).
88. Peter, M.E. & Krammer, P.H. Mechanisms of CD95 (APO-1/Fas)-mediated apoptosis. *Curr Opin Immunol* **10**, 545-551 (1998).
89. Goldar, S., Khaniani, M.S., Derakhshan, S.M. & Baradaran, B. Molecular mechanisms of apoptosis and roles in cancer development and treatment. *Asian Pac J Cancer Prev* **16**, 2129-2144 (2015).
90. Zaman, S., Wang, R. & Gandhi, V. Targeting the apoptosis pathway in hematologic malignancies. *Leuk Lymphoma* **55**, 1980-1992 (2014).
91. Liu, H*., et al.* Improvement of Pharmacokinetic Profile of TRAIL via Trimer-Tag Enhances its Antitumor Activity in vivo. *Sci Rep* **7**, 8953 (2017).
92. Boldin, M.P*., et al.* A novel protein that interacts with the death domain of Fas/APO1 contains a sequence motif related to the death domain. *J Biol Chem* **270**, 7795-7798 (1995).
93. Fu, Q*., et al.* Structural Basis and Functional Role of Intramembrane Trimerization of the Fas/CD95 Death Receptor. *Mol Cell* **61**, 602-613 (2016).
94. Varfolomeev, E*., et al.* c-IAP1 and c-IAP2 are critical mediators of tumor necrosis factor alpha (TNFalpha)-induced NF-kappaB activation. *J Biol Chem* **283**, 24295-24299 (2008).
95. Li, H., Kobayashi, M., Blonska, M., You, Y. & Lin, X. Ubiquitination of RIP is required for tumor necrosis factor alpha-induced NF-kappaB activation. *J Biol Chem* **281**, 13636-13643 (2006).
96. Brenner, D., Blaser, H. & Mak, T.W. Regulation of tumour necrosis factor signalling: live or let die. *Nat Rev Immunol* **15**, 362-374 (2015).

97. Liu, Z.G., Hsu, H., Goeddel, D.V. & Karin, M. Dissection of TNF receptor 1 effector functions: JNK activation is not linked to apoptosis while NF-kappaB activation prevents cell death. *Cell* **87**, 565-576 (1996).
98. Green, D.R. Cell death and the immune system: getting to how and why. *Immunol Rev* **277**, 4-8 (2017).
99. Vercammen, D., Vandenabeele, P., Beyaert, R., Declercq, W. & Fiers, W. Tumour necrosis factor-induced necrosis versus anti-Fas-induced apoptosis in L929 cells. *Cytokine* **9**, 801-808 (1997).
100. Kaiser, W.J*., et al.* Toll-like receptor 3-mediated necrosis via TRIF, RIP3, and MLKL. *J Biol Chem* **288**, 31268-31279 (2013).
101. Upton, J.W., Kaiser, W.J. & Mocarski, E.S. Virus inhibition of RIP3-dependent necrosis. *Cell Host Microbe* **7**, 302-313 (2010).
102. Linkermann, A. & Green, D.R. Necroptosis. *N Engl J Med* **370**, 455-465 (2014).
103. Sun, L*., et al.* Mixed lineage kinase domain-like protein mediates necrosis signaling downstream of RIP3 kinase. *Cell* **148**, 213-227 (2012).
104. Newton, K*., et al.* Cleavage of RIPK1 by caspase-8 is crucial for limiting apoptosis and necroptosis. *Nature* **574**, 428-431 (2019).
105. Cho, Y.S*., et al.* Phosphorylation-driven assembly of the RIP1-RIP3 complex regulates programmed necrosis and virus-induced inflammation. *Cell* **137**, 1112-1123 (2009).
106. Zhang, Y*., et al.* RIP1 autophosphorylation is promoted by mitochondrial ROS and is essential for RIP3 recruitment into necrosome. *Nat Commun* **8**, 14329 (2017).
107. Conos, S.A*., et al.* Active MLKL triggers the NLRP3 inflammasome in a cell-intrinsic manner. *Proc Natl Acad Sci U S A* **114**, E961-E969 (2017).
108. Mulay, S.R., Linkermann, A. & Anders, H.J. Necroinflammation in Kidney Disease. *J Am Soc Nephrol* **27**, 27-39 (2016).
109. Choi, M.E., Price, D.R., Ryter, S.W. & Choi, A.M.K. Necroptosis: a crucial pathogenic mediator of human disease. *JCI Insight* **4**(2019).
110. Weinlich, R., Oberst, A., Beere, H.M. & Green, D.R. Necroptosis in development, inflammation and disease. *Nat Rev Mol Cell Biol* **18**, 127-136 (2017).
111. Linkermann, A*., et al.* Two independent pathways of regulated necrosis mediate ischemia-reperfusion injury. *Proc Natl Acad Sci U S A* **110**, 12024-12029 (2013).
112. Luedde, M*., et al.* RIP3, a kinase promoting necroptotic cell death, mediates adverse remodelling after myocardial infarction. *Cardiovasc Res* **103**, 206-216 (2014).
113. Lau, A*., et al.* RIPK3-mediated necroptosis promotes donor kidney inflammatory injury and reduces allograft survival. *Am J Transplant* **13**, 2805-2818 (2013).
114. Galluzzi, L., Kepp, O., Chan, F.K. & Kroemer, G. Necroptosis: Mechanisms and Relevance to Disease. *Annu Rev Pathol* **12**, 103-130 (2017).
115. Hunter, D.R. & Haworth, R.A. The Ca2+-induced membrane transition in mitochondria. I. The protective mechanisms. *Arch Biochem Biophys* **195**, 453-459 (1979).
116. Izzo, V., Bravo-San Pedro, J.M., Sica, V., Kroemer, G. & Galluzzi, L. Mitochondrial Permeability Transition: New Findings and Persisting Uncertainties. *Trends Cell Biol* **26**, 655-667 (2016).
117. Vanden Berghe, T., Linkermann, A., Jouan-Lanhouet, S., Walczak, H. & Vandenabeele, P. Regulated necrosis: the expanding network of non-apoptotic cell death pathways. *Nat Rev Mol Cell Biol* **15**, 135-147 (2014).
118. Baines, C.P*., et al.* Loss of cyclophilin D reveals a critical role for mitochondrial permeability transition in cell death. *Nature* **434**, 658-662 (2005).
119. Schinzel, A.C*., et al.* Cyclophilin D is a component of mitochondrial permeability transition and mediates neuronal cell death after focal cerebral ischemia. *Proc Natl Acad Sci U S A* **102**, 12005-12010 (2005).

120. Clarke, S.J., McStay, G.P. & Halestrap, A.P. Sanglifehrin A acts as a potent inhibitor of the mitochondrial permeability transition and reperfusion injury of the heart by binding to cyclophilin-D at a different site from cyclosporin A. *J Biol Chem* **277**, 34793-34799 (2002).
121. Warne, J.*, et al.* Selective Inhibition of the Mitochondrial Permeability Transition Pore Protects against Neurodegeneration in Experimental Multiple Sclerosis. *J Biol Chem* **291**, 4356-4373 (2016).
122. Cung, T.T.*, et al.* Cyclosporine before PCI in Patients with Acute Myocardial Infarction. *N Engl J Med* **373**, 1021-1031 (2015).
123. Piot, C.*, et al.* Effect of cyclosporine on reperfusion injury in acute myocardial infarction. *N Engl J Med* **359**, 473-481 (2008).
124. Linkermann, A., Konstantinidis, K. & Kitsis, R.N. Catch me if you can: targeting the mitochondrial permeability transition pore in myocardial infarction. *Cell Death Differ* **23**, 1-2 (2016).
125. Devalaraja-Narashimha, K., Diener, A.M. & Padanilam, B.J. Cyclophilin D gene ablation protects mice from ischemic renal injury. *Am J Physiol Renal Physiol* **297**, F749-759 (2009).
126. Vaseva, A.V.*, et al.* p53 opens the mitochondrial permeability transition pore to trigger necrosis. *Cell* **149**, 1536-1548 (2012).
127. Karch, J. & Molkentin, J.D. Is p53 the long-sought molecular trigger for cyclophilin D-regulated mitochondrial permeability transition pore formation and necrosis? *Circ Res* **111**, 1258-1260 (2012).
128. Kim, J.S., He, L. & Lemasters, J.J. Mitochondrial permeability transition: a common pathway to necrosis and apoptosis. *Biochem Biophys Res Commun* **304**, 463-470 (2003).
129. Karch, J.*, et al.* Inhibition of mitochondrial permeability transition by deletion of the ANT family and CypD. *Sci Adv* **5**, eaaw4597 (2019).
130. Vorobjeva, N.*, et al.* Mitochondrial permeability transition pore is involved in oxidative burst and NETosis of human neutrophils. *Biochim Biophys Acta Mol Basis Dis* **1866**, 165664 (2020).
131. Fatokun, A.A., Dawson, V.L. & Dawson, T.M. Parthanatos: mitochondrial-linked mechanisms and therapeutic opportunities. *Br J Pharmacol* **171**, 2000-2016 (2014).
132. Virag, L., Robaszkiewicz, A., Rodriguez-Vargas, J.M. & Oliver, F.J. Poly(ADP-ribose) signaling in cell death. *Mol Aspects Med* **34**, 1153-1167 (2013).
133. David, K.K., Andrabi, S.A., Dawson, T.M. & Dawson, V.L. Parthanatos, a messenger of death. *Front Biosci (Landmark Ed)* **14**, 1116-1128 (2009).
134. Cookson, B.T. & Brennan, M.A. Pro-inflammatory programmed cell death. *Trends Microbiol* **9**, 113-114 (2001).
135. Bergsbaken, T., Fink, S.L. & Cookson, B.T. Pyroptosis: host cell death and inflammation. *Nat Rev Microbiol* **7**, 99-109 (2009).
136. Zychlinsky, A., Prevost, M.C. & Sansonetti, P.J. Shigella flexneri induces apoptosis in infected macrophages. *Nature* **358**, 167-169 (1992).
137. Shi, J., Gao, W. & Shao, F. Pyroptosis: Gasdermin-Mediated Programmed Necrotic Cell Death. *Trends Biochem Sci* **42**, 245-254 (2017).
138. Doitsh, G.*, et al.* Cell death by pyroptosis drives CD4 T-cell depletion in HIV-1 infection. *Nature* **505**, 509-514 (2014).
139. Adamczak, S.E.*, et al.* Pyroptotic neuronal cell death mediated by the AIM2 inflammasome. *J Cereb Blood Flow Metab* **34**, 621-629 (2014).
140. Chung, S.D., Lai, T.Y., Chien, C.T. & Yu, H.J. Activating Nrf-2 signaling depresses unilateral ureteral obstruction-evoked mitochondrial stress-related autophagy, apoptosis and pyroptosis in kidney. *PLoS One* **7**, e47299 (2012).
141. Krautwald, S. & Linkermann, A. The fire within: pyroptosis in the kidney. *Am J Physiol Renal Physiol* **306**, F168-169 (2014).
142. Aachoui, Y., Sagulenko, V., Miao, E.A. & Stacey, K.J. Inflammasome-mediated pyroptotic and apoptotic cell death, and defense against infection. *Curr Opin Microbiol* **16**, 319-326 (2013).

143. Wang, Y.*, et al.* Chemotherapy drugs induce pyroptosis through caspase-3 cleavage of a gasdermin. *Nature* **547**, 99-103 (2017).
144. Brough, D. & Rothwell, N.J. Caspase-1-dependent processing of pro-interleukin-1beta is cytosolic and precedes cell death. *J Cell Sci* **120**, 772-781 (2007).
145. Franchi, L., Eigenbrod, T., Munoz-Planillo, R. & Nunez, G. The inflammasome: a caspase-1-activation platform that regulates immune responses and disease pathogenesis. *Nat Immunol* **10**, 241-247 (2009).
146. Kayagaki, N.*, et al.* Non-canonical inflammasome activation targets caspase-11. *Nature* **479**, 117-121 (2011).
147. Yang, J., Zhao, Y. & Shao, F. Non-canonical activation of inflammatory caspases by cytosolic LPS in innate immunity. *Curr Opin Immunol* **32**, 78-83 (2015).
148. Ng, T.M. & Monack, D.M. Revisiting caspase-11 function in host defense. *Cell Host Microbe* **14**, 9-14 (2013).
149. Kip, E.*, et al.* Impact of caspase-1/11, -3, -7, or IL-1beta/IL-18 deficiency on rabies virus-induced macrophage cell death and onset of disease. *Cell Death Discov* **3**, 17012 (2017).
150. Kayagaki, N.*, et al.* Caspase-11 cleaves gasdermin D for non-canonical inflammasome signalling. *Nature* **526**, 666-671 (2015).
151. Shi, J.*, et al.* Cleavage of GSDMD by inflammatory caspases determines pyroptotic cell death. *Nature* **526**, 660-665 (2015).
152. Ding, J.*, et al.* Pore-forming activity and structural autoinhibition of the gasdermin family. *Nature* **535**, 111-116 (2016).
153. Liu, X.*, et al.* Inflammasome-activated gasdermin D causes pyroptosis by forming membrane pores. *Nature* **535**, 153-158 (2016).
154. Sborgi, L.*, et al.* GSDMD membrane pore formation constitutes the mechanism of pyroptotic cell death. *EMBO J* **35**, 1766-1778 (2016).
155. Dixon, S.J. Ferroptosis: bug or feature? *Immunol Rev* **277**, 150-157 (2017).
156. Yang, W.S. & Stockwell, B.R. Ferroptosis: Death by Lipid Peroxidation. *Trends Cell Biol* **26**, 165-176 (2016).
157. Yagoda, N.*, et al.* RAS-RAF-MEK-dependent oxidative cell death involving voltage-dependent anion channels. *Nature* **447**, 864-868 (2007).
158. Dixon, S.J.*, et al.* Ferroptosis: an iron-dependent form of nonapoptotic cell death. *Cell* **149**, 1060-1072 (2012).
159. Linkermann, A.*, et al.* Synchronized renal tubular cell death involves ferroptosis. *Proc Natl Acad Sci U S A* **111**, 16836-16841 (2014).
160. Friedmann Angeli, J.P.*, et al.* Inactivation of the ferroptosis regulator Gpx4 triggers acute renal failure in mice. *Nat Cell Biol* **16**, 1180-1191 (2014).
161. Yang, W.S.*, et al.* Regulation of ferroptotic cancer cell death by GPX4. *Cell* **156**, 317-331 (2014).
162. Dixon, S.J.*, et al.* Pharmacological inhibition of cystine-glutamate exchange induces endoplasmic reticulum stress and ferroptosis. *Elife* **3**, e02523 (2014).
163. Timmerman, L.A.*, et al.* Glutamine sensitivity analysis identifies the xCT antiporter as a common triple-negative breast tumor therapeutic target. *Cancer Cell* **24**, 450-465 (2013).
164. Woo, J.H.*, et al.* Elucidating Compound Mechanism of Action by Network Perturbation Analysis. *Cell* **162**, 441-451 (2015).
165. Seiler, A.*, et al.* Glutathione peroxidase 4 senses and translates oxidative stress into 12/15-lipoxygenase dependent- and AIF-mediated cell death. *Cell Metab* **8**, 237-248 (2008).
166. Imai, H.*, et al.* Early embryonic lethality caused by targeted disruption of the mouse PHGPx gene. *Biochem Biophys Res Commun* **305**, 278-286 (2003).
167. Carlson, B.A.*, et al.* Glutathione peroxidase 4 and vitamin E cooperatively prevent hepatocellular degeneration. *Redox Biol* **9**, 22-31 (2016).
168. Martin-Sanchez, D.*, et al.* Ferroptosis, but Not Necroptosis, Is Important in Nephrotoxic Folic Acid-Induced AKI. *J Am Soc Nephrol* **28**, 218-229 (2017).

169. Do Van, B.*, et al.* Ferroptosis, a newly characterized form of cell death in Parkinson's disease that is regulated by PKC. *Neurobiol Dis* **94**, 169-178 (2016).
170. Murphy, J.M.*, et al.* The pseudokinase MLKL mediates necroptosis via a molecular switch mechanism. *Immunity* **39**, 443-453 (2013).
171. Mulay, S.R.*, et al.* Oxalate-induced chronic kidney disease with its uremic and cardiovascular complications in C57BL/6 mice. *Am J Physiol Renal Physiol* **310**, F785-F795 (2016).
172. Xu, Y.*, et al.* A Role for Tubular Necroptosis in Cisplatin-Induced AKI. *J Am Soc Nephrol* **26**, 2647-2658 (2015).
173. Munoz, L.E.*, et al.* Nanoparticles size-dependently initiate self-limiting NETosis-driven inflammation. *Proc Natl Acad Sci U S A* **113**, E5856-E5865 (2016).
174. Munoz, L.E.*, et al.* Colourful death: six-parameter classification of cell death by flow cytometry--dead cells tell tales. *Autoimmunity* **46**, 336-341 (2013).
175. Hagemann, J.H., Haegele, H., Muller, S. & Anders, H.J. Danger control programs cause tissue injury and remodeling. *Int J Mol Sci* **14**, 11319-11346 (2013).
176. Suarez-Alvarez, B., Liapis, H. & Anders, H.J. Links between coagulation, inflammation, regeneration, and fibrosis in kidney pathology. *Lab Invest* **96**, 378-390 (2016).
177. Sziksz, E.*, et al.* Fibrosis Related Inflammatory Mediators: Role of the IL-10 Cytokine Family. *Mediators Inflamm* **2015**, 764641 (2015).
178. Wynn, T.A. & Vannella, K.M. Macrophages in Tissue Repair, Regeneration, and Fibrosis. *Immunity* **44**, 450-462 (2016).
179. Kanlaya, R., Sintiprungrat, K., Chaiyarit, S. & Thongboonkerd, V. Macropinocytosis is the major mechanism for endocytosis of calcium oxalate crystals into renal tubular cells. *Cell Biochem Biophys* **67**, 1171-1179 (2013).
180. Martinon, F., Petrilli, V., Mayor, A., Tardivel, A. & Tschopp, J. Gout-associated uric acid crystals activate the NALP3 inflammasome. *Nature* **440**, 237-241 (2006).
181. Khan, S.R. Nephrocalcinosis in animal models with and without stones. *Urol Res* **38**, 429-438 (2010).
182. Angelotti, M.L.*, et al.* Characterization of renal progenitors committed toward tubular lineage and their regenerative potential in renal tubular injury. *Stem Cells* **30**, 1714-1725 (2012).
183. Lazzeri, E.*, et al.* Endocycle-related tubular cell hypertrophy and progenitor proliferation recover renal function after acute kidney injury. *Nat Commun* **9**, 1344 (2018).
184. Marschner, J.A., Schafer, H., Holderied, A. & Anders, H.J. Optimizing Mouse Surgery with Online Rectal Temperature Monitoring and Preoperative Heat Supply. Effects on Post-Ischemic Acute Kidney Injury. *PLoS One* **11**, e0149489 (2016).
185. Srivastava, M.*, et al.* Reduced PARP1 as a Serum Biomarker for Graft Rejection in Kidney Transplantation. *J Proteomics Bioinform* **8**, 031-038 (2015).
186. Anders, H.J.*, et al.* The macrophage phenotype and inflammasome component NLRP3 contributes to nephrocalcinosis-related chronic kidney disease independent from IL-1-mediated tissue injury. *Kidney Int* **93**, 656-669 (2018).
187. Linkermann, A., Stockwell, B.R., Krautwald, S. & Anders, H.J. Regulated cell death and inflammation: an auto-amplification loop causes organ failure. *Nat Rev Immunol* **14**, 759-767 (2014).
188. Rajamaki, K.*, et al.* Cholesterol crystals activate the NLRP3 inflammasome in human macrophages: a novel link between cholesterol metabolism and inflammation. *PLoS One* **5**, e11765 (2010).
189. Duewell, P.*, et al.* NLRP3 inflammasomes are required for atherogenesis and activated by cholesterol crystals. *Nature* **464**, 1357-1361 (2010).
190. Dostert, C.*, et al.* Innate immune activation through Nalp3 inflammasome sensing of asbestos and silica. *Science* **320**, 674-677 (2008).
191. Winter, M.*, et al.* Activation of the inflammasome by amorphous silica and TiO2 nanoparticles in murine dendritic cells. *Nanotoxicology* **5**, 326-340 (2011).

192. Ea, H.K., So, A., Liote, F. & Busso, N. Basic calcium phosphate crystals induce NLRP3 inflammasome activation: the in vitro and in vivo face to face. *Proc Natl Acad Sci U S A* **108**, E1361; author reply E1362 (2011).
193. de Vasconcelos, N.M. & Lamkanfi, M. Recent Insights on Inflammasomes, Gasdermin Pores, and Pyroptosis. *Cold Spring Harb Perspect Biol* (2019).
194. Dubois, H.*, et al.* Nlrp3 inflammasome activation and Gasdermin D-driven pyroptosis are immunopathogenic upon gastrointestinal norovirus infection. *PLoS Pathog* **15**, e1007709 (2019).
195. Zhao, H.*, et al.* Role of necroptosis in the pathogenesis of solid organ injury. *Cell Death Dis* **6**, e1975 (2015).
196. Tonnus, W.*, et al.* The clinical relevance of necroinflammation-highlighting the importance of acute kidney injury and the adrenal glands. *Cell Death Differ* **26**, 68-82 (2019).
197. Degterev, A. & Linkermann, A. Generation of small molecules to interfere with regulated necrosis. *Cell Mol Life Sci* **73**, 2251-2267 (2016).
198. Zhou, W. & Yuan, J. Necroptosis in health and diseases. *Semin Cell Dev Biol* **35**, 14-23 (2014).
199. Smith, C.C. & Yellon, D.M. Necroptosis, necrostatins and tissue injury. *J Cell Mol Med* **15**, 1797-1806 (2011).
200. Kearney, C.J., Cullen, S.P., Clancy, D. & Martin, S.J. RIPK1 can function as an inhibitor rather than an initiator of RIPK3-dependent necroptosis. *FEBS J* **281**, 4921-4934 (2014).
201. Zhang, X.*, et al.* Ubiquitination of RIPK1 suppresses programmed cell death by regulating RIPK1 kinase activation during embryogenesis. *Nat Commun* **10**, 4158 (2019).
202. Remijsen, Q.*, et al.* Depletion of RIPK3 or MLKL blocks TNF-driven necroptosis and switches towards a delayed RIPK1 kinase-dependent apoptosis. *Cell Death Dis* **5**, e1004 (2014).
203. Petrie, E.J.*, et al.* Conformational switching of the pseudokinase domain promotes human MLKL tetramerization and cell death by necroptosis. *Nat Commun* **9**, 2422 (2018).
204. Gutierrez, K.D.*, et al.* MLKL Activation Triggers NLRP3-Mediated Processing and Release of IL-1beta Independently of Gasdermin-D. *J Immunol* **198**, 2156-2164 (2017).
205. Wang, J. & Fan, Y. Lung injury induced by TiO2 nanoparticles depends on their structural features: size, shape, crystal phases, and surface coating. *Int J Mol Sci* **15**, 22258-22278 (2014).
206. Kusaka, T.*, et al.* Effect of silica particle size on macrophage inflammatory responses. *PLoS One* **9**, e92634 (2014).
207. Laquerriere, P.*, et al.* Importance of hydroxyapatite particles characteristics on cytokines production by human monocytes in vitro. *Biomaterials* **24**, 2739-2747 (2003).
208. Grandjean-Laquerriere, A., Laquerriere, P., Guenounou, M., Laurent-Maquin, D. & Phillips, T.M. Importance of the surface area ratio on cytokines production by human monocytes in vitro induced by various hydroxyapatite particles. *Biomaterials* **26**, 2361-2369 (2005).
209. Niimi, K.*, et al.* Mitochondrial permeability transition pore opening induces the initial process of renal calcium crystallization. *Free Radic Biol Med* **52**, 1207-1217 (2012).
210. Martin-Sanchez, D.*, et al.* Targeting of regulated necrosis in kidney disease. *Nefrologia* **38**, 125-135 (2018).
211. Galluzzi, L.*, et al.* Molecular mechanisms of cell death: recommendations of the Nomenclature Committee on Cell Death 2018. *Cell Death Differ* **25**, 486-541 (2018).
212. Mao, F.*, et al.* Mesenchymal stem cells and their therapeutic applications in inflammatory bowel disease. *Oncotarget* **8**, 38008-38021 (2017).
213. Porter, G.A., Jr. & Beutner, G. Cyclophilin D, Somehow a Master Regulator of Mitochondrial Function. *Biomolecules* **8**(2018).
214. Park, J.S., Pasupulati, R., Feldkamp, T., Roeser, N.F. & Weinberg, J.M. Cyclophilin D and the mitochondrial permeability transition in kidney proximal tubules after hypoxic and ischemic injury. *Am J Physiol Renal Physiol* **301**, F134-150 (2011).
215. Niimi, K.*, et al.* Novel effect of the inhibitor of mitochondrial cyclophilin D activation, N-methyl-4-isoleucine cyclosporin, on renal calcium crystallization. *Int J Urol* **21**, 707-713 (2014).

216. Usami, M.*, et al.* Genetic differences in C57BL/6 mouse substrains affect kidney crystal deposition. *Urolithiasis* **46**, 515-522 (2018).
217. Tait, S.W.*, et al.* Widespread mitochondrial depletion via mitophagy does not compromise necroptosis. *Cell Rep* **5**, 878-885 (2013).
218. Sureshbabu, A.*, et al.* RIPK3 promotes sepsis-induced acute kidney injury via mitochondrial dysfunction. *JCI Insight* **3**(2018).
219. Sun, W.*, et al.* Cytosolic calcium mediates RIP1/RIP3 complex-dependent necroptosis through JNK activation and mitochondrial ROS production in human colon cancer cells. *Free Radic Biol Med* **108**, 433-444 (2017).
220. Karch, J.*, et al.* Necroptosis Interfaces with MOMP and the MPTP in Mediating Cell Death. *PLoS One* **10**, e0130520 (2015).
221. Gan, I.*, et al.* Mitochondrial permeability regulates cardiac endothelial cell necroptosis and cardiac allograft rejection. *Am J Transplant* **19**, 686-698 (2019

Declaration

I hereby declare that all of the present work embodied in this thesis was carried out by me from 04/2014 until 02/2018 under the supervision of Prof. Dr. Hans Joachim Anders, Nephrologisches Zentrum, Medizinische Klinik und Poliklinik IV, Innenstadt Klinikum der Universität München. This work has not been submitted in part or full to any other university or institute for any degree or diploma.

Part of the work was supported by others, as mentioned below:

1. Prof. Peter Boor (Division of Nephrology, Institute of Pathology, Rheinisch-Westfälische Technische Hochschule University of Aachen, Germany) and Dr. Bastian Popper (Biomedical Center, Core Facility Animal Models, Ludwig Maximilian University, Planegg Martinsried, Germany)

They performed the Transmission Electron Microscopy (TEM) from the *in-vitro* and *in-vivo* studies.

2. Ilya Belevich, and Eija Jokitalo (Electron Microscopy Unit, Institute of Biotechnology, University of Helsinki, Helsinki, Finland).

They performed Serial Block Face Scanning Electron Microscopy (SB-EM) from the *in-vitro* study.

3. Prof. Rostyslav Bilyy (Department of Histology, Cytology, and Embryology, Danylo Halytsky Lviv National Medical University, Lviv, Ukraine).

They carried out the micro-computed tomography (µCT) studies from the *in-vivo* study.

Part of the work presented here has been published in

1. Mulay SR*, **Honarpisheh MM***, Foresto-Neto O*, Shi C, Desai J, Zhao ZB, Marschner JA, Popper B, Buhl EM, Boor P, Linkermann A, Liapis H, Bilyy R, Herrmann M, Romagnani P, Belevich I, Jokitalo E, Becker JU, Anders HJ. **Mitochondria Permeability Transition versus Necroptosis in Oxalate-Induced AKI**. J Am Soc Nephrol. 2019 Jul 11. pii: ASN.2018121218. doi: 10.1681/ASN.2018121218. (* equal contribution)

2. **Honarpisheh M**, Foresto-Neto O, Desai J, Steiger S, Gómez LA, Popper B, Boor P, Anders HJ, Mulay SR. **Phagocytosis of environmental or metabolic crystalline particles induces cytotoxicity by triggering necroptosis across a broad range of particle size and shape**. Sci Rep. 2017 Nov 14;7(1):15523.

3. **Honarpisheh M**, Desai J, Marschner JA, Weidenbusch M, Lech M, Vielhauer V, Anders HJ, Mulay SR. **Regulated necrosis-related molecule mRNA expression in humans and mice and in murine acute tissue injury and systemic autoimmunity leading to progressive organ damage, and progressive fibrosis**. Biosci Rep. 2016 Dec 9;36(6). pii: e00425.

Date: 08.03.2020 Signature: ……..

Place: Munich, Germany

Acknowledgment

Many people have helped and inspired me during my doctoral study, and I would like to convey my gratitude to all of them.

I take this opportunity to thank my mentor & guide, Prof. Hans-Joachim Anders. He patiently provided the vision, encouragement and advice necessary for me to proceed through the doctoral program. Thanks a lot for giving me this opportunity to work here at the research laboratories of the Renal Division at LMU, instilling the confidence in me and your help with the transition to a new professional perspective. I would also like to thank Prof. Volker Vielhauer, PD Bruno Luckow, and Prof. Peter Nelson for their constant encouragement of my research work and constructive suggestions throughout my stay at LMU.

I thank all my lab friends, especially Shrikant, for helping a lot during my study and writing my thesis, as well as Steffi, Dana, Maciej, Santhosh, Simone, and all medical students for the wonderful time we had together. Especially to Dana, for sharing your skills and knowledge helped me a lot and will always be remembered. Chain of gratitude would be incomplete if I forget to thank Dan, Jana, Nuru and Ewa for providing skillful technical assistance to carry out the research work successfully. I am also indebted to my other friends Mortiz, Jyaysi, Orestes, & others; thanks for your love & support. One of the most important reasons why I love Munich is having all you guys being around. Thank you all for giving me the life long memories, engraved in my heart.

There are no words to express my feeling, love and affectionate gratitude to my family, my father, mother, my sister, my brother, for their faith, love, inspiration, selfless sacrifices and constant encouragement throughout my life.

I am grateful to Elham, my wife who was there for me in all my difficult times and encourage me not to fail and continue fighting.

I am grateful to everybody who has been part of my life and helped in some way or other, but if I failed to mention their names, thank you all.

It is my duty to express my tearful acknowledgement to the animals, which have been sacrificed for the betterment of human being.